FAA-RD-77-29

AIRFRAME NOISE PREDICTION METHOD

MARTIN R. FINK

MARCH 1977

FINAL REPORT

Prepared for

U.S. DEPARTMENT OF TRANSPORTATION
FEDERAL AVIATION ADMINISTRATION
Systems Research & Development Service
Washington, D.C. 20590

NOTICE

Technical Report Documentation Page

1. Report No.	2. Government Accession No.	3. Recipient's Catalog No.
FAA-RD-77-29		

4. Title and Subtitle	5. Report Date
Airframe Noise Prediction Method	March 1977
	6. Performing Organization Code
7. Author(s) R. Fink	8. Performing Organization Report No. R77-912697-11
9. Performing Organization Name and Address United Technologies Research Center Silver Lane E. Hartford, CT. 06108	10. Work Unit No. (TRAIS) 11. Contract or Grant No. DOT-FA76WA-3821
12. Sponsoring Agency Name and Address Federal Aviation Administration 800 Independence Avenue, S.W. Washington, D.C. 20591	13. Type of Report and Period Covered Contractor Final Report (June 1976 - April 1977) 14. Sponsoring Agency Code ARD-550

15. Supplementary Notes

H. C. True, DOT/FAA Technical Monitor

16. Abstract

A noise component method is presented for calculating airframe noise. Noise from clean wing and tail surface is represented as trailing edge noise caused by the turbulent boundary layer. Landing gear noise is given by an empirical representation of model data. Trailing edge flap noise is modeled as a lift dipole normal to the deflected flap, with amplitude and spectrum given by a correlation of flyover data.

Measured flyover data for the Prue-2 sailplane, Aero Commander Shirke general aviation airplane, Lockheed JetStar business jet, Boeing 707 commercial jet, and Convair F-106B delta wing airplane are used as test cases. These spectra are compared with predictions by this method and the NASA ANOPP total aircraft method and drag element method.

Methods for reducing various components of airframe noise are examined and evaluated.

17. Key Words	18. Distribution Statement
Noise, airframe noise, edge noise, wing noise, trailing edge flap noise, landing gear noise, noise reduction.	Document is available to the public through the National Technical Information Service, Springfield, VA. [illegible]

19. Security Classif. (of this report)	20. Security Classif. (of this page)	21. No. of Pages	22. Price
Unclassified	Unclassified	140	

Form DOT F 1700.7 (8-72) Reproduction of completed page authorized

METRIC CONVERSION FACTORS

Approximate Conversions to Metric Measures

Symbol	When You Know	Multiply by	To Find	Symbol
		LENGTH		
in	inches	2.5	centimeters	cm
ft	feet	30	centimeters	cm
yd	yards	0.9	meters	m
mi	miles	1.6	kilometers	km
		AREA		
in^2	square inches	6.5	square centimeters	cm^2
ft^2	square feet	0.09	square meters	m^2
yd^2	square yards	0.8	square meters	m^2
mi^2	square miles	2.6	square kilometers	km^2
	acres	0.4	hectares	ha
		MASS (weight)		
oz	ounces	28	grams	g
lb	pounds	0.45	kilograms	kg
	short tons (2000 lb)	0.9	tonnes (1000 kg)	t
		VOLUME		
tsp	teaspoons	5	milliliters	ml
tbsp	tablespoons	15	milliliters	ml
fl oz	fluid ounces	30	milliliters	ml
c	cups	0.24	liters	l
pt	pints	0.47	liters	l
qt	quarts	0.95	liters	l
gal	gallons	3.8	liters	l
ft^3	cubic feet	0.03	cubic meters	m^3
yd^3	cubic yards	0.76	cubic meters	m^3
		TEMPERATURE (exact)		
°F	Fahrenheit temperature	5/9 (after subtracting 32)	Celsius temperature	°C

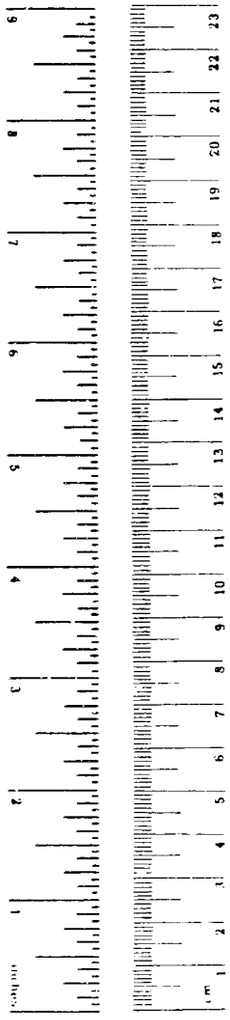

Approximate Conversions from Metric Measures

Symbol	When You Know	Multiply by	To Find	Symbol
		LENGTH		
mm	millimeters	0.04	inches	in
cm	centimeters	0.4	inches	in
m	meters	3.3	feet	ft
m	meters	1.1	yards	yd
km	kilometers	0.6	miles	mi
		AREA		
cm^2	square centimeters	0.16	square inches	in^2
m^2	square meters	1.2	square yards	yd^2
km^2	square kilometers	0.4	square miles	mi^2
ha	hectares (10,000 m^2)	2.5	acres	
		MASS (weight)		
g	grams	0.035	ounces	oz
kg	kilograms	2.2	pounds	lb
t	tonnes (1000 kg)	1.1	short tons	
		VOLUME		
ml	milliliters	0.03	fluid ounces	fl oz
l	liters	2.1	pints	pt
l	liters	1.06	quarts	qt
l	liters	0.26	gallons	gal
m^3	cubic meters	35	cubic feet	ft^3
m^3	cubic meters	1.3	cubic yards	yd^3
		TEMPERATURE (exact)		
°C	Celsius temperature	9/5 (then add 32)	Fahrenheit temperature	°F

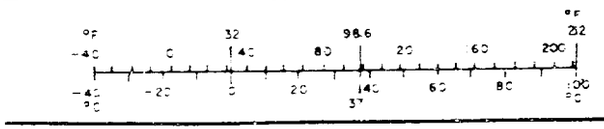

TABLE OF CONTENTS

1.0 INTRODUCTION

Noise emission from current airplanes is dominated by propulsion-system noise. Certification levels for aircraft noise, as specified under Federal Air Regulation (FAR) 36, have been achieved by use of either existing high bypass ratio turbofan engines or existing low bypass ratio turbofan engines plus noise-attenuating nacelles. Systems studies of noise levels for future advanced-technology transports (e.g., Ref. 1) have concluded that engine noise levels 10 effective perceived noise decibels (EPNdB) lower than those of FAR 36 could be achieved with early 1970's technology high bypass ratio turbofan engines combined with extensive inlet and discharge duct acoustic suppression. An additional 5 EPNdB noise reduction was predicted for advanced (1985) acoustic liners. Still another 5 EPNdB (that is, 20 EPNdB below FAR 36) was predicted by use of special noise abatement procedures combined with advanced liner technology. More recently, acoustic tests have been conducted with full-scale high bypass ratio turbofan engine hardware (Ref. 2). These tests demonstrated that noise levels corresponding to 12 EPNdB below FAR 36 at approach and sideline, and 9 EPNdB below at takeoff, can be achieved with 1975-technology acoustic liners and sonic inlets. However, these reductions of propulsion-system noise would not cause equal reductions of total aircraft noise at the certification points. Airframe noise, generated by motion of aircraft external surfaces through the air, is believed (Ref. 3) to be only 10 to 15 dB below FAR 36. Airframe noise may impose a fundamental noise floor roughly equal to the demonstrated noise from high bypass ratio turbofans with extensive inlet and exhaust acoustic suppression. Future certification levels must be based on what can be achieved with economically viable airframes and propulsion systems. Thus it is necessary to understand the fundamental processes of airframe noise radiation.

Several methods for predicting airframe noise had been examined by NASA under their Aircraft Noise Prediction Program (ANOPP). Two airframe noise prediction methods, the clean aircraft method (also called total aircraft method) and the drag element method, were recommended (Ref. 4) and were

[1]Brines, G. L.: Studies for Determining the Optimum Propulsion System Characteristics for Use in a Long Range Transport Aircraft. NASA CR-120950, July 1972.

[2]Sofrin, T. G. and Riloff, N. Jr.: Two-Stage, Low-Noise Advanced Technology Fan. V. Acoustic Final Report. NASA CR-134831, Sept. 1975.

[3]Morgan, H. G. and Hardin, J. C.: Airframe Noise - The Next Aircraft Noise Barrier. Journal of Aircraft, Vol. 12, No. 7, July 1975, pp 622-624.

[4]Hardin, J. C., Fratello, D. J., Hayden, R. E., Kadman, Y., and Africk, S.: Prediction of Airfreme Noise. NASA TN D-7821, Feb. 1975.

subsequently programmed by NASA Langley Research Center. Verification by comparisons with measured airframe noise spectra have not been published for the clean aircraft method and were available for only a few cases for the drag element method. A lengthier component analysis method was described in Ref. 4 but its predictions were not compared with data. For several airframe components, differences exist between the dominant noise mechanism assumed by the drag element method, the component analysis method, and other investigations.

This program was conducted to (Task I) identify airframe noise generation mechanisms and sources, and develop both a graphical method and a digital computer program for predicting noise from each source, (Task II) verify the resulting airframe noise model by comparing its predictions and those of the NASA ANOPP airframe noise models with data for a wide range of aircraft type and size, flight speed, flap and landing gear position, and wing planform, (Task III) identify concepts for airframe noise reduction, and (Task IV) develop a program plan to verify empirically the assumed airframe noise generating mechanisms and potential suppression concepts. Results of the first three Tasks are reported herein.

2.0 SYMBOLS

Symbol	Description
A	Reference area
A(M)	Convective amplification factor defined by Eq. (A-14)
b	Span of wing, horizontal tail, or vertical tail
c_a	Atmospheric speed of sound
c_F	Trailing edge flap gross chord
D	Landing gear wheel (tire) diameter
$D(\theta,\phi)$	Normalized directivity factor defined by Eq. (A-8)
f	One-third octave band center frequency, Hz
f_{max}	One-third octave band center frequency at which sound pressure level is maximum, Hz
G_1-G_5	Empirical functions of Strouhal number in Eqs. (11) through (20) for landing gear noise
G_6,G_7	Empirical functions of Strouhal number in Eqs. (21) through (28) for trailing edge flap noise
h	Altitude
H	Length of landing gear strut exposed beneath wing or fuselage
I	Acoustic intensity
$\overline{p^2}$	Mean square acoustic pressure
P	Acoustic power
r	Distance from airplane to observer, evaluated at retarded time
S	Planform area
$S(f_n)$	Normalized one-third octave spectrum function

Symbol	Description
t	Time
V	Airspeed
α	Root mean square normalized turbulence intensity
Λ_{TE}	Sweepback angle at trailing edge
δ_F	Trailing edge flap deflection, deg
δ_W	Turbulent boundary layer thickness at wing trailing edge as calculated for a flat plate
θ	Azimuth angle in plane defined by flight path and observer position, evaluated at retarded time and measured from approach direction
ν	Kinematic viscosity of air
ρ_a	Atmospheric density
ϕ	Direction angle from vertical plane through flight path, evaluated at retarded time
ω	Angular frequency

Subscripts

E	Edge noise
f	Evaluated within one frequency band
F	Trailing edge flap
G	Landing gear noise
ℓ	Lower
L	Lift fluctuation noise
u	Upper
W	Wing (extended to centerline)

3.0 DEVELOPMENT OF AIRFRAME NOISE PREDICTION METHOD

3.1 Clean Wing and Tail Surfaces

3.1.1 Overall Sound Pressure level

The basic concept of the method developed herein for clean airframes was first presented in Ref. 5. An updated description is given here. Noise radiation from clean airframes is assumed to be caused by convection of the wing and tail turbulent boundary layers past the trailing edges of those surfaces. The resulting trailing edge noise radiation has been studied analytically (e.g., Refs. 6 and 7). Functional dependence given by those analyses has been verified experimentally (Ref. 8). It is assumed that noise caused by an upper-surface and a lower-surface boundary layer is randomly phased so that separately calculated acoustic intensities can be directly added. Far-field acoustic pressure then has the dependence

$$\overline{p^2} \sim \alpha^2(\delta b/r^2)V^5\cos^2\Lambda_{TE}\cos^2\phi\cos^2(\theta/2) \qquad (1)$$

where α and δ are the boundary layer turbulence intensity and scale length, respectively. Maximum overall sound pressure level would occur in the fly-over plane where sideline angle ϕ is zero and far-field distance r is related to altitude h by

$$h = r\sin\theta \qquad (2)$$

[5] Fink, M. R.: Approximate Prediction of Airframe Noise. Journal of Aircraft, Vol. 13, No. 11, Nov. 1976, pp 843-834. Also, AIAA Paper 76-526, July 1976.

[6] Ffowcs Williams, J. and Hall, L. H.: Aerodynamic Sound Generation by Turbulent Flow in the Vicinity of a Scattering Half Plane. Journal of Fluid Mechanics, Vol. 40, Part 4, March 1970, pp 657-670.

[7] Chase, D. M.: Sound Radiated by Turbulent Flow Off a Rigid Half Plane as Obtained From a Wavevector Spectrum of Hydrodynamic Pressure. Journal of Acoustical Society of America, Vol. 52, No. 3, Part 2, Sept. 1972, pp 1011-1023.

[8] Fink, M. R.: Experimental Evaluation of Theories for Trailing Edge and Incidence Fluctuation Noise. AIAA Journal, Vol. 13, No. 11, Nov. 1975.

Also, most airplane wings have small trailing edge sweepback angles Λ_{TE} so the dependence of far-field acoustic pressure on flight conditions and direction angle during a constant-altitude flyover is

$$\overline{p^2} \sim \alpha^2 (\delta b/h^2) V^5 \sin^2\theta \cos^2(\theta/2) \qquad (3)$$

The angle from the approach horizontal direction, θ, is measured at the retarded time (the time when the measured sound had left the airframe). Source motion effects are temporarily neglected because of the low subsonic Mach numbers of interest. Maximum far-field acoustic pressure due to trailing edge noise then occurs when this angle is approximately 71°, that is, 19° before the trailing edge is overhead. Depending on flight Mach number, the wing position when this maximum noise reaches the observer could be ahead or behind the overhead direction. This result agrees with available data. In contrast, if a lift dipole directivity is assumed, maximum noise measured by a fixed observer would leave the airframe at the overhead position and would always reach the observer when the airframe was considerably past that position. Such directivity has not been reported.

Next, it was noted that turbulence intensity within a turbulent boundary layer is approximately independent of Reynolds number for conditions typical of aircraft wings. Boundary layer thickness varies with chord to the 0.8 power and velocity to the -0.2 power. For simplicity, those exponents were approximated in Ref. 4 by the closest integers. Far-field maximum acoustic pressure would then be expected to be proportional to the product of wing chord and span (the wing area, S) divided by altitude squared, and to vary with flyover velocity to the fifth power.

This approximation was checked by adjusting a large number of measured maximum overall sound pressure levels as OASPL-10 log (S/h^2) and plotting this quantity against velocity. An updated version of this comparison is given in Figure 1 for sixteen aerodynamically clean airframes. The data from Table 2 of Ref. 9 are levels for the idealized (smoothed) spectra rather than composite (actual) spectra. This smoothing process was described in Ref. 9 as intended to "...isolate those effects due solely to the general aerodynamic noise rather than being peculiar to any individual aircraft". Noise from the feathered propellers, and low-frequency ground reflections, were the major irregularities removed from most spectra. In the case of the

[9] Heely, G. J.: Measurement and Analysis of Aircraft Far-Field Aerodynamic Noise. NASA CR-2377, Dec. 1974.

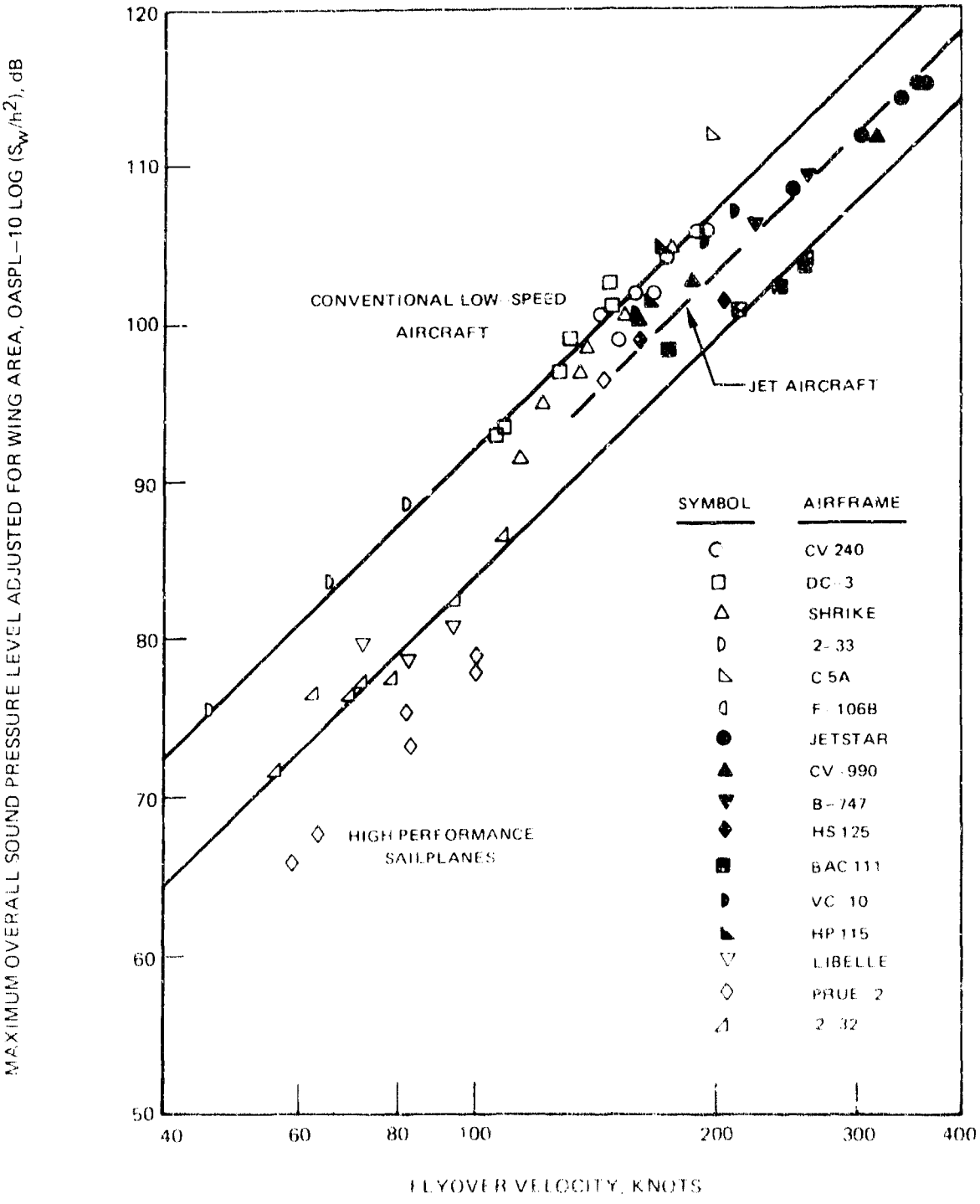

FIGURE 1 - MAXIMUM OVERALL SOUND PRESSURE LEVEL FOR CLEAN AIRFRAMES, NORMALIZED WITH RESPECT TO WING AREA

Prue-2 sailplane, not only tones caused by laminar boundary layer instability (Ref. 10) but the entire low-frequency part of the spectrum below 200 Hz had been removed by the smoothing process. The resulting smoothed adjusted levels for this airframe probably are too low. In contrast, composite (actual) levels were used in the NASA ANOPP correlation given in Ref. 4. Data for the Cessna 150 from the Ref. 9 study are not shown in Figure 1 because that airframe had a fixed landing gear. Additional data shown by open symbols were taken from Tables I and III of Ref. 4. Only about half the tabulated data points for the Schweizer 2-32 sailplane are plotted; the others were dominated by laminar instability tones.

All data points plotted as open symbols were measured with microphones mounted on posts or tripods 4 ft above the ground, as specified for noise certification measurements conducted under FAR 36. Resulting one-third octave spectra tend to be oscillatory at low frequencies because of sound wave cancellation and reinforcement. At higher frequencies the directly-radiated flyover noise, and flyover noise reflected from the ground to the microphone, combine to give a measured level approximately 3 dB above directly-radiated noise. Spectrum irregularities caused by phase differences between directly-radiated and ground-reflected waves can be eliminated by use of microphones mounted flush with the ground. For frequencies of practical interest, the direct and reflected waves should be in phase, causing measured levels to be 6 dB above directly-radiated noise. Airframe noise data published by NASA Dryden Flight Research Center (e.g., Ref. 11) and Royal Aircraft Establishment (Ref. 12) have been measured with flush-mounted microphones. These data, decreased 3 dB to allow direct comparison with data measured for certification purposes, are plotted in Figure 1 as solid symbols.

The data symbols generally fall within three groups. Adjusted OASPL for two of the three high-performance sailplanes, the F-106B jet interceptor, and the BAC 1-11 jet transport, are closely matched by a solid line given by

[10]Fink, M. R.: Prediction of Airfoil Tone Frequencies. Journal of Aircraft, Vol. 12, No. 2, Feb. 1975, pp 118-120.

[11]Putnam, T. W., Lasagna, P. L., and White, K. C.: Measurements and Analyses of Aircraft Airframe Noise. Aeroacoustics: STOL Noise; Airframe and Airfoil Noise, Vol. 45, Progress in Aeronautics and Astronautics, M.I.T. Press, Cambridge, Mass., 1976, p 363-378. Also, AIAA Paper 75-510, March 1975.

[12]Fethney, P.: An Experimental Study of Airframe Self-Noise. Aeroacoustics: STOL Noise; Airframe and Airfoil Noise, Vol. 45, Progress in Aeronautics and Astronautics, M.I.T. Press, Cambridge, Mass., 1976, pp 377-403. Also AIAA Paper 75-511, Mar. 1975.

$$OASPL = 50 \log(V/100\,kt) + 10\log(S/h^2) + 84\,dB \qquad (4)$$

Note that aspect ratio does not occur in this equation, and that aspect ratio for the Libelle and F-106B differ by a factor of more than ten. In contrast, prediction equations given in Refs. 3 and 9 include a variation with aspect ratio to the -2 and -4 powers, respectively.

Data for conventional low-speed aircraft such as three retractable-landing-gear propeller-driven aircraft of Ref. 9 and the Schweizer 2-33 strut-braced training sailplane fall on a line 8 dB above that given by Eq. (4). Also matched by this line are data for the Handley Page HP 115 slender delta-wing research airplane, which has small streamlined fixed landing gear. This airplane has an aspect ratio of 0.9, and equations which predict a dependence of noise on induced drag or aspect ratio greatly overpredict (Ref. 12) its measured noise. Data for jet aircraft generally lie between these two curves. A reasonable prediction for business jets (JetStar and HS 125) and large commercial jets (B-747 and CV-990) is 4 dB above the level given by Eq. (4).

These aircraft and flight conditions correspond to a factor of about 40 in Reynolds number and therefore a factor of two in the ratio of flat plate turbulent boundary layer thickness to wing chord. The calculation method for noise of clean airframes as developed in this report assumes that the noise intensity is proportional to the product of flat-plate turbulent boundary layer thickness and wing span, as expressed in Eq. (3). This thickness was calculated for a chord length equal to the wing gross geometric chord (ratio of gross wing area to gross wing span). This parameter was chosen because these two quantities are more readily available than the wing mean aerodynamic chord, exposed area, or exposed span. Turbulent boundary layer thickness was taken as

$$\delta_W = 0.37(S_W/b_W)(VS_W/b_W\nu)^{-0.2} \qquad (5)$$

Measured maximum flyover values of OASPL for the same data that were used in Ref. 1, but adjusted for a dependence on the product of boundary layer thickness δ_W and wing span b_W divided by altitude square, are plotted in Figure 2. Data symbols for jet aircraft are displaced higher relative to the smaller low-speed aircraft. This occurs because the larger size and higher flight speed of the jet airplanes yields relatively larger Reynolds numbers and smaller ratios of boundary layer thickness to wing chord. Data for aerodynamically clean high-performance sailplanes can be approximated by

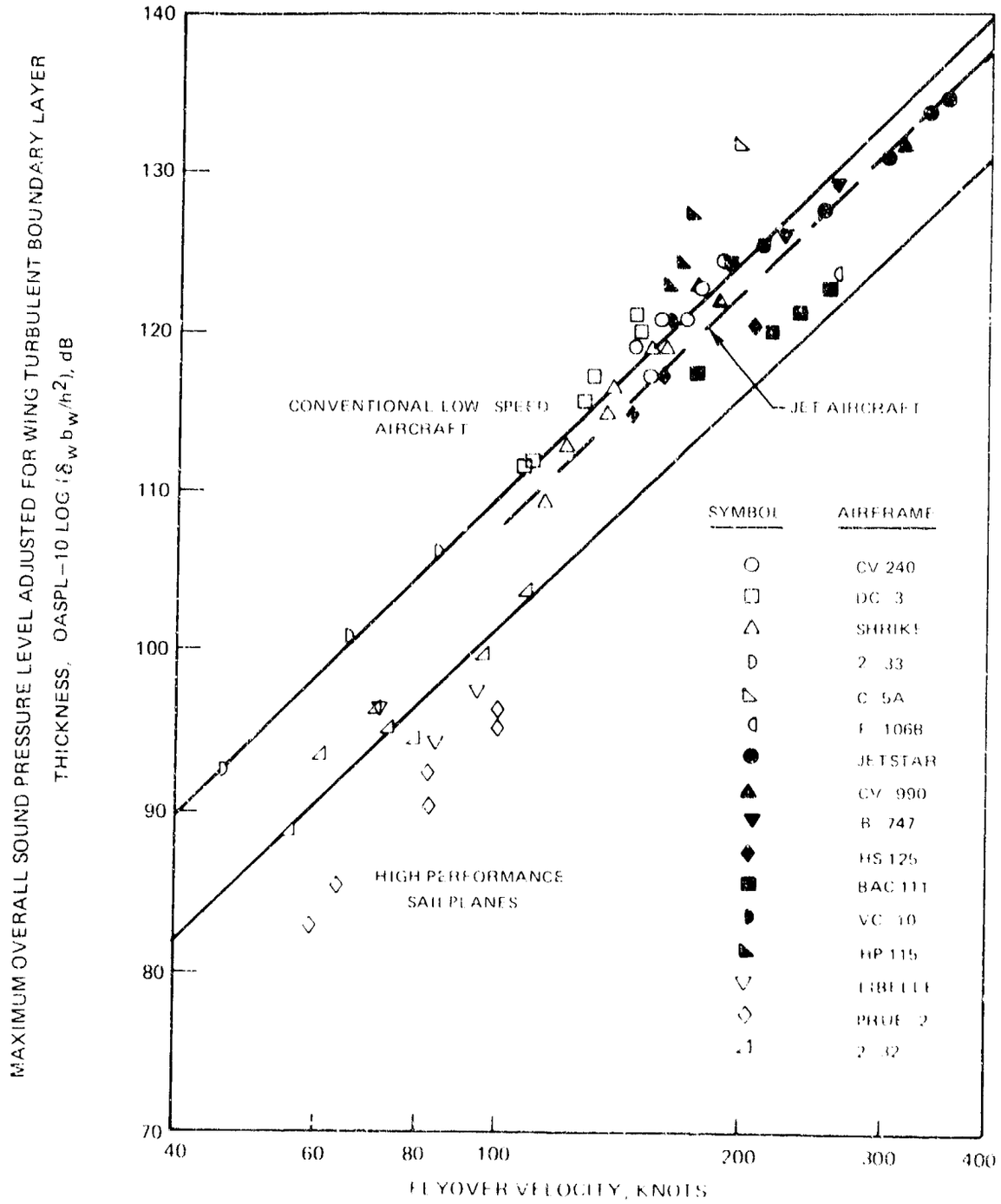

FIGURE 7 - MAXIMUM OVERALL SOUND PRESSURE LEVEL FOR CLEAN AIRFRAMES, NORMALIZED WITH RESPECT TO PRODUCT OF WING SPAN AND WING TRAILING EDGE BOUNDARY LAYER THICKNESS

$$OASPL = 50 \log (V/100\,kt) + 10 \log (\delta_w b_w / h^2) + 101.5\,dB \qquad (6)$$

Data for conventional low-speed aircraft were 8 dB higher as before, but data for jet aircraft had an average value roughly 6 dB above the line for aerodynamically clean sailplanes. Of course, the ultimate test of this prediction method is not the agreement with measured OASPL but the agreement between predicted and measured spectra. The actual equation used for calculating trailing edge noise is given in the discussion of directivity, after the discussion of spectrum shape.

3.1.2 Spectrum Shape for Trailing Edge Noise

If the major noise generation mechanism for airframe noise of aerodynamically clean airframes is trailing edge noise, the spectrum shape for airframe noise should be given by the existing solutions for trailing edge noise. A semiempirical equation for normalized spectral density of trailing edge noise from externally blown flaps was given as Eq. (12) of Ref. 13. This equation had been found to predict the noise spectra of upper surface blown flaps for measurement directions, exhaust velocities, and frequency ranges where such noise was not dominated by directly-radiated quadrupole noise from the deflected jet. Converting from normalized spectral density and Strouhal number based on jet diameter to third-octave sound pressure level $SPL_{1/3}$ relative to overall sound pressure level OASPL and center frequency f relative to the center frequency f_{max} which yields maximum $SPL_{1/3}$,

$$SPL_{1/3} - OASPL = 10 \log \left\{ 0.613 (f/f_{max})^4 \left[(f/f_{max})^{3/2} + 0.5 \right]^{-4} \right\} \qquad (7)$$

The spectrum shape given by this equation is compared in Figure 3 with the nondimensional airframe noise spectrum recommended for use with the NASA ANOPP Total Aircraft Analysis (Figure 4 of Ref. 4). The two dotted curves are boundaries of smoothed nondimensional spectra from twenty-eight flights of five different airplanes tested by Healy (Ref. 9). The solid curve drawn between these boundaries was taken from Ref. 4. The open symbols calculated from Eq. (7) are within ±1 dB of the solid data-average curve for frequency

[13] Fink, M. R.: Prediction of Externally Blown Flap Noise and Turbomachinery Exit Noise. NASA CR-134882, Aug. 1975.

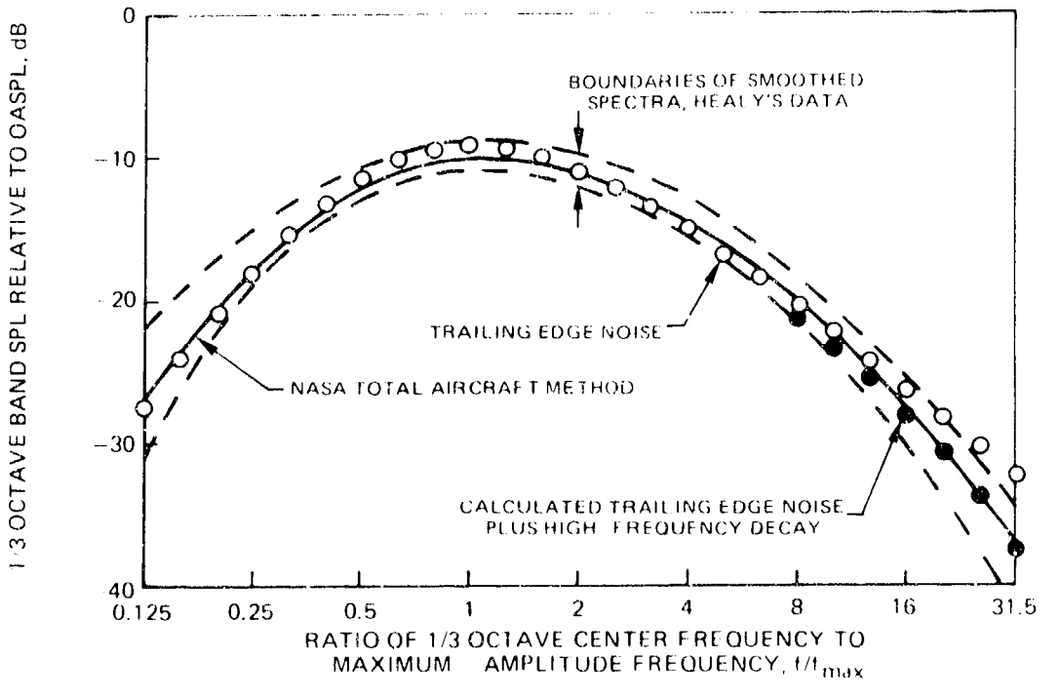

FIGURE 3 - AIRFRAME NOISE NORMALIZED SPECTRA CALCULATED BY SEVERAL METHODS

ratios up to 8. At larger frequency ratios they decay less rapidly than the data. The measured rapid spectrum decay at large frequency ratios might be a real property of the noise mechanism but more likely was caused by atmospheric attenuation of the radiated flyover noise.

This difficulty in predicting the measured spectra at large frequency ratios had been encountered by Revell (Ref. 14). His semiempirical drag analysis within the NASA ANOPP method (Ref. 4, pp 33-36) approximates the normalized airframe noise spectrum shown in Figure 3 by four straight lines multiplied by an exponential decay of mean square acoustic pressure. Without that added decay, his equation for frequency ratios greater than 4 gives a spectrum shape that varies inversely with frequency ratio squared. The asymptote of Eq. (7) at large frequency ratios has the same variation. Revell's correction factor can be expressed as an added term

$$\Delta SPL_{1/3} = -0.02\left|(f/f_{max}-1)\right|^{3/2}\log e \qquad (8)$$

Agreement with the solid curve in Figure 3 would be improved if approximately 3.5 times this correction were added to Eq. (7). The resulting normalized spectrum given by

$$SPL_{1/3} - OASPL = 10\log\left\{0.613(f/f_{max})^4\left[(f/f_{max})^{3/2}+0.5\right]^{-4}\right\} - 0.03\left|(f/f_{max}-1)\right|^{3/2} \qquad (9)$$

is shown in Figure 3 as solid symbols. They are within 0.1 dB of Eq. (7) for frequency ratios less than 3 and closely approximate the measured spectrum decay at large frequency ratios. For far-field distances much different from 500 ft, use of tabulated atmospheric attenuation properties rather than this simple approximation is recommended.

The nondimensional spectrum given by Eq. (9) should be valid only for an untapered (constant-chord) wing. To determine the effect of wing taper ratio on spectrum shape, this equation was applied to calculating the acoustic

[14]Revell, J. D., Healy, G. J., and Gibson, J. S.: Methods for the Prediction of Airframe Aerodynamic Noise. Aeroacoustics: Acoustic Wake Propagation; Aircraft Noise Prediction; Aeroacoustic Instrumentation, Vol. 46, Progress in Aeronautics and Astronautics, M.I.T. Press, Cambridge, Mass., 1976, pp 139-154. Also, AIAA Paper 75-539, Mar. 1975.

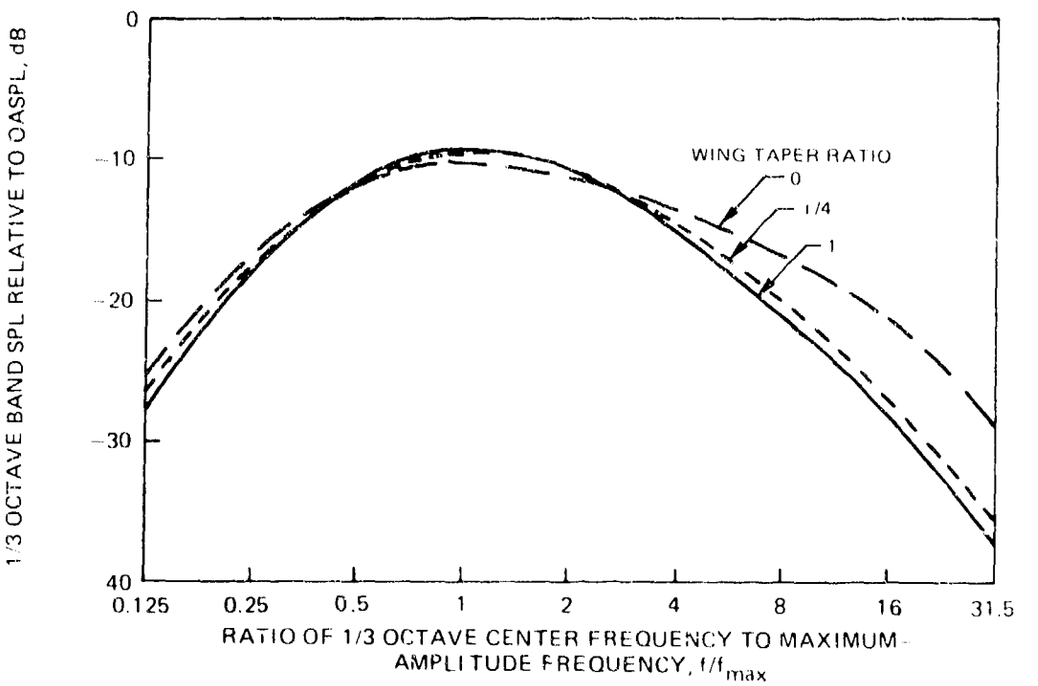

FIGURE 4 - CALCULATED EFFECT OF WING TAPER RATIO ON NORMALIZED 1/3 OCTAVE AIRFRAME NOISE SPECTRUM

spectrum from each of a large number of spanwise segments comprising tapered wings. Spectra were calculated for wings having the same mean geometric chord (ratio of wing area to wing span) and flight conditions. Resulting nondimensional spectra are plotted in Figure 4 for taper ratios of 0, 1/4, and 1. The spectrum for a taper ratio of 1/4 was within 1.2 dB of that for a taper ratio of 1. The spectrum for a taper ratio of 1/2 (not shown) was within 0.4 dB of that for a taper ratio of 1. In contrast, the spectrum calculated for zero taper ratio was about 3 dB higher at very low frequencies, 1.2 dB lower at maximum-amplitude frequency, and more than 8 dB higher at very high frequencies. Maximum amplitude occurred within the same one-third-octave band for all taper ratios. However, the calculated maximum amplitude decreased as taper ratio was decreased. This occurred because the frquency was far below the tip region's maximum-amplitude frequency. At large frequencies relative to the maximum-amplitude frequency, some portion of the tip region was at its local frequency for maximum amplitude and therefore radiated more noise than the large-chord inboard regions. Because few civil aircraft have taper ratios less than 1/4, the nondimensional spectrum calculated from Eq. (9) will be assumed to apply for all taper ratios.

Use of a calculated flat-plate boundary layer thickness corresponds to the assumption that the wing upper surface and lower surface boundary layers are unaffected by wing lift coefficient. To examine the effect of lift coefficient, boundary layer properties were calculated for a typical business-jet airfoil section, chord length, and approach speed. The airfoil pressure distribution had a leading edge suction peak on the upper surface at lift coefficients larger than 0.6 and on the lower surface at lift coefficients less than 0.2. Increasing the lift coefficient in the range between 0.2 and 0.6 caused a small increase of upper surface boundary layer thickness and a small decrease on the lower surface. Resulting calculated amplitudes and spectrum shapes were essentially independent of lift coefficient. A further increase of lift coefficient to 0.8 caused a relatively larger increase of upper surface boundary layer thickness. Calculated OASPL and low-frequency noise were increased about 2 dB, but the spectrum at higher frequencies varied less than 1 dB for the range of lift coefficients from 0.2 to 0.8. This range covers the low-speed flight conditions of practical interest for aircraft with leading-edge and trailing-edge high-lift devices retracted. Therefore the effect of lift coefficient was neglected in further calculations.

By trial and error, it was found that the measured spectra tabulated in Ref. 9 were matched by Eq. (9) if the peak frequency was taken as 0.1 times the ratio of velocity to boundary layer thickness. That is, peak Strouhal number was taken as 0.1 referenced to the thickness calculated from Eq. (5).

3.1.3 Directivity

Airframe noise directivity in the flyover plan has been measured at Douglas Aircraft Co. for the DC-10 aircraft (Ref. 15). Special acoustic treatment was used with the high bypass ratio turbofan engines to reduce engine noise below the airframe noise. Acoustic data were corrected for the variation of far-field radial distance with direction angle; distance and angle were evaluated at the retarded time. The resulting measured variation of distance-adjusted OASPL with angle for a clean DC-10 aircraft was compared in Figures 17 and 18 of Ref. 15 with two analytical models. These figures are reproduced in Figure 5 herein. A lift dipole without convection amplification, as used in the drag element method of Ref. 14, matches the data between about 60° and 110° angles from the approach horizontal direction. Adding the source motion effect, as is done in the NASA ANOPP version of that method, improves agreement at smaller angles but worsens the agreement at larger angles. The directivity function for trailing edge noise, without source motion, matches the data within ± 5 dB for all angles less than 140°. Convective amplification worsens the agreement. It was concluded in Ref. 15 that a combination of a lift dipole, a drag dipole which is correlated with the lift dipole, and an uncorrelated drag dipole (all with convective amplification) gave the best fit to measured directivity. No method was given for generalizing the relative strengths and phasings of these dipoles.

Adjusted OASPL directivity data for several flights of the clean DC-10 airframe had also been given in Figure 14 of Ref. 16. These data are compared in Figure 6 with the directivity predicted for trailing edge noise without convective amplification. This prediction closely matches the data for these three flights. The convective amplification effect on trailing edge noise directivity therefore was omitted from the method presented herein. However, the convective effect on frequency (Doppler shift) was included.

Airframe flyover noise for aircraft in the clean configuration should be a sum of trailing edge noise from the wing and horizontal tail. For typical ratios of tail area to wing area, the resulting total airframe noise should be 0.5 to 1 dB greater than OASPL from the wing. However, calculated peak frequency of horizontal tail noise is larger than that for wing noise. Thus the portion of the calculated spectrum which is heavily weighted in predicting annoyance-weighted noise was almost equally affected by noise from the wing and horizontal tail. It was found that measured spectra were best predicted

[15]Munson, A. G.: A Modeling Approach to Nonpropulsive Noise. AIAA Paper 76-525, July 1976.

[16]Pendley, R. E.: Recent Advances in the Technology of Aircraft Noise Control. Journal of Aircraft, Vol. 14, No. 7, July 1976, pp 613-619.

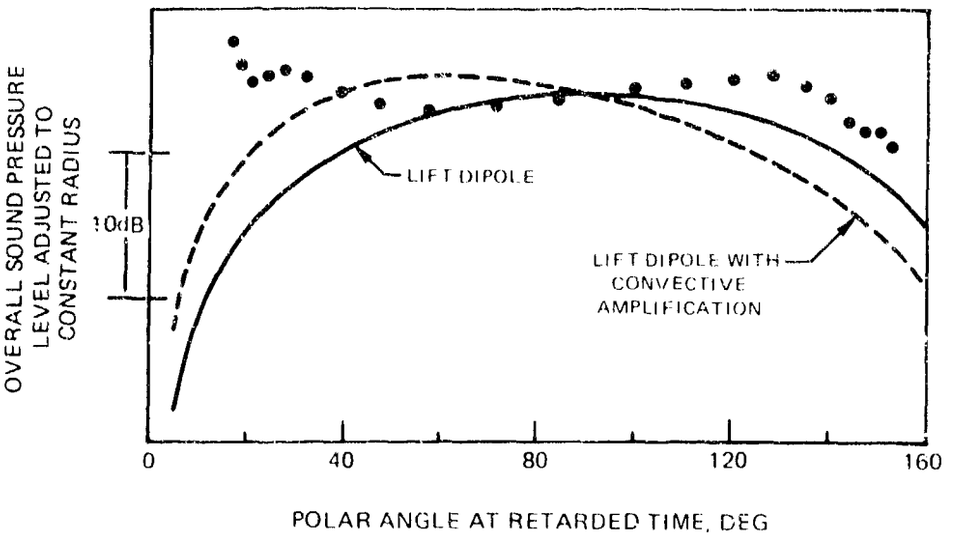

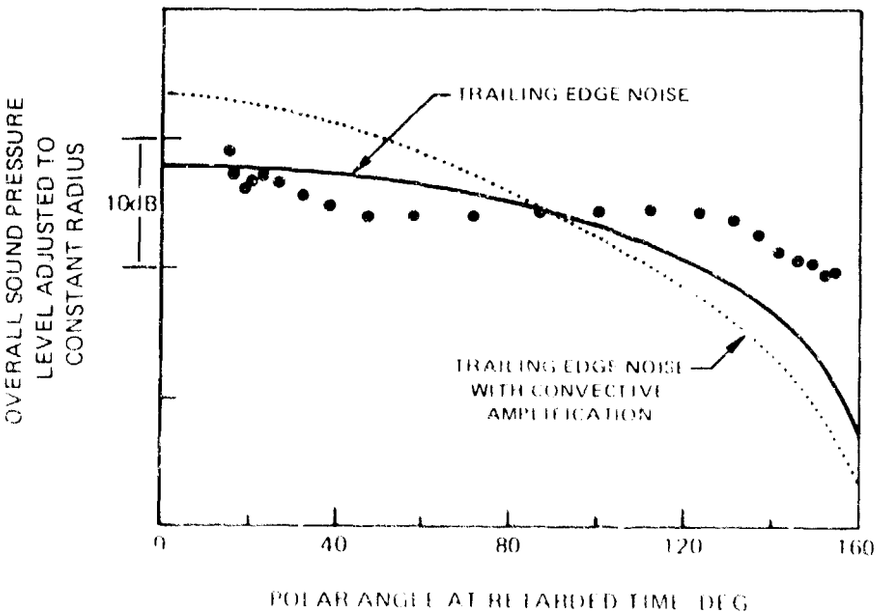

FIGURE [illegible] COMPARISON OF MEASURED DC-10 AIRFRAME NOISE DIRECTIVITY AT CONSTANT RADIUS WITH CALCULATED DIRECTIVITIES FOR LIFT DIPOLE SOURCE AND TRAILING EDGE NOISE

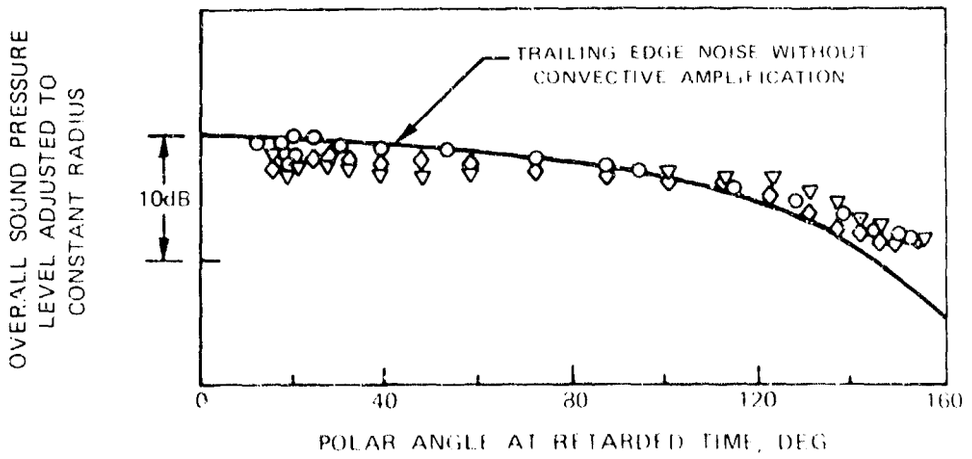

FIGURE [illegible] - COMPARISON OF SEVERAL MEASUREMENTS OF [illegible] AVERAGED OVER [illegible] DIRECTIVITY AT CONSTANT RADIUS WITH CALCULATED FAR-FIELD [illegible] OF TRAILING EDGE NOISE WITHOUT CONVECTIVE AMPLIFICATION

by assuming that wing OASPL was 2 dB lower than the values that would match the solid lines on Figure 2 for total airframe OASPL. Including the directivity effect, OASPL for the wing was therefore taken as

$$OASPL_w = 50\log(V/100\,kt) + 10\log(\delta_w b_w/h^2) + 8(ND) + 10\log(\cos\phi \sin\theta \cos\theta/2)^2 + 104.3\,dB \quad (10)$$

Here, ND is set equal to one for conventional-construction low subsonic speed aircraft and for aircraft which have extensive trailing edge flap track shields. It is set equal to zero for aerodynamically clean aircraft such as high-performance sailplanes and for jet aircraft that have relatively simple trailing edge flaps. Horizontal tail OASPL is obtained by replacing the wing span and boundary layer thickness by values for the horizontal tail.

This difference between noise from an aerodynamically clean sailplane and a conventional airplane with retracted slats, flaps, and landing gear also occurs in Revell's Drag Element Method (Ref. 14). In that method, OASPL usually is dominated by the calculated wing profile drag noise. Mean square acoustic pressure for such noise is predicted by that method to vary with wing profile drag coefficient cubed. This coefficient can be about half as large for a sailplane wing as for a conventional low-speed airplane wing. Thus the airframe noise calculated by the method of Ref. 14 can vary within about 9 dB, depending on an arbitrary estimate of aerodynamic cleanness. The method given herein uses an arbitrary choice of either the lower or upper extreme of this range.

Trailing edge noise from the vertical tail is radiated toward the sidelines and decreases to zero intensity in the flyover plane. Amplitude of this noise is obtained by replacing the wing properties in Eq. (10) by those of the vertical tail and replacing the directivity term $\cos\phi$ by $\sin\phi$. However, the peak frequency used in the last term of Eq. (9) for calculating an approximation to atmospheric attenuation is the peak frequency of wing trailing edge noise.

One poorly understood feature in some of the published spectra has been the presence of a moderate-frequency broadband peak which does not change frequency as flight speed is varied. This peak occurs in a frequency range of strong engine noise from the idling turbojet or turbofan engines. Engine noise should not vary with sideline angle while wing-generated noise should vary with cosine squared of the angle from the flyover plane. Calculated vertical tail noise is low enough to be neglected for this comparison. These variations may explain the sideline directivity result shown by NASA in

Figure 9 of Ref. 17 for the Lockheed JetStar and by RAE in Figure 24 of Ref. 12 for the Vickers VC 10. From both sets of OASPL data, it was concluded that sideline noise of a clean airframe varies only inversely with radius squared, without an additional dependence on sideline angle. Unpublished NASA sideline noise measurements for the Convair 990 in the clean configuration (run 3, 314 knots) were obtained for detailed examination. These data include spectra measured at intervals of 0.1 to 0.2 sec on a line perpendicular to the flight path, at sideline distances to 1476 ft, for a relatively low-altitude (230 ft) flight. For the following analysis, the time at which the airplane passed the instrumentation line was back-figured from direction angles measured at the nominal flyover position. Acoustic travel times to each microphone were added to this time, and measured spectra were examined for the retarded time at which the Doppler effect on frequency was closest to zero.

Resulting variations of overall sound pressure level, and one-third octave sound pressure levels at 200 and 1600 Hz center frequencies, with sideline distance are plotted in Figure 7. Also shown are variations that would be expected for acoustic radiation from a horizontal surface and for a variation inversely with radial distance but independent of sideline angle. Notice that for the lower frequency, where airframe noise should greatly exceed engine noise, the rapid decrease predicted for surface-radiated noise did occur. OASPL, and the higher-frequency noise attributed here to engine noise, matched the smaller predicted decay rate. Airframe noise given by the analysis developed under this contract therefore uses the theoretically-predicted variation with sideline angle rather than the slower decrease indicated by the data of Refs. 12 and 17.

4.4 Noise Component Method

As was indicated in previous sections, the method developed herein is an airframe noise component method. That is, noise radiation from individual portions of the airframe is calculated without regard for other noise sources. This viewpoint that the several noise sources do not interact had been used in both the drag element method (Ref. 14) and the component analysis method (Ref. 4). Each noise component is assumed herein to be given by whatever aeroacoustic mechanism, velocity dependence, directivity, and spectrum seems to be appropriate. This approach also was used in the component analysis method. In contrast, the drag element method had attributed all components of airframe noise to essentially the same mechanism so that all had the same functional dependence and normalized spectrum.

[17] Gaspar, E. J. and Putnam, F. W.: Preliminary Measurements of Aircraft Aerodynamic Noise. AIAA Paper 73-[illegible], June 1973.

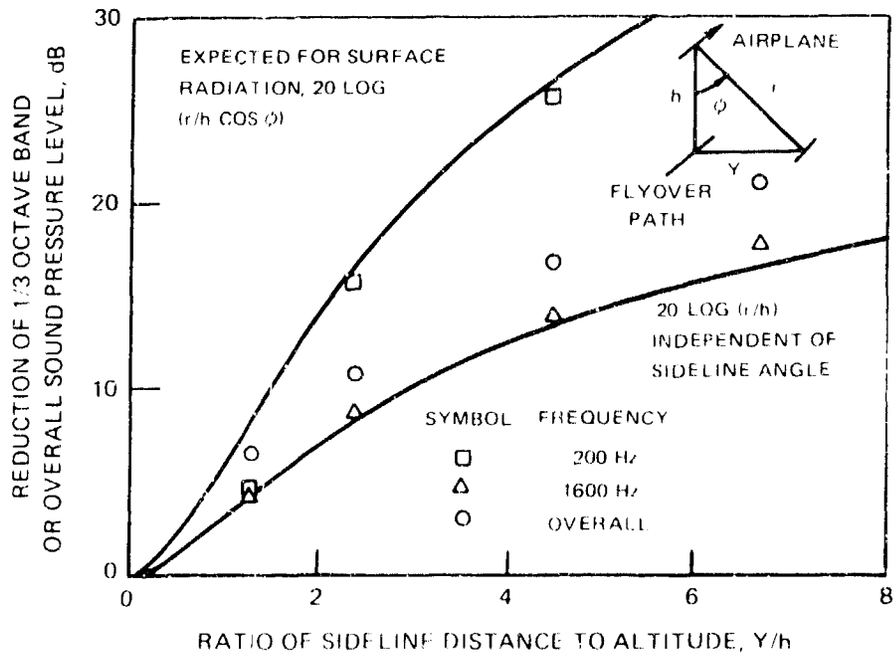

FIGURE 7 - VARIATION OF OVERALL AND 1/3 OCTAVE SOUND PRESSURE LEVELS WITH SIDELINE DISTANCE FOR CONVAIR 990 IN CLEAN CONFIGURATION, EVALUATED AT CONSTANT RETARDED TIME

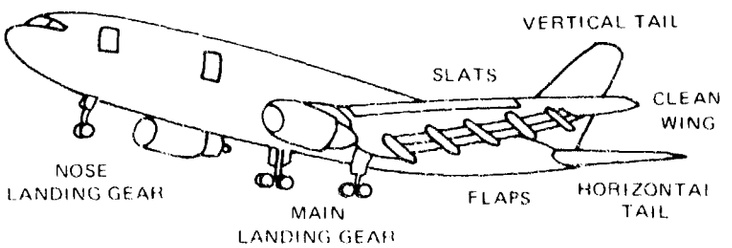

FIGURE 8 - INDIVIDUAL NOISE-RADIATING AIRFRAME COMPONENTS

The individual noise-radiating airframe components represented by the method developed herein are sketched in Figure 8. Noise from the clean wing, horizontal tail, and vertical tail were previously discussed. Noise contributions from the nose landing gear and main landing gear are calculated separately because generally each has a different size and therefore a different peak frequency. Noise from the trailing edge flaps is calculated independent of whether the landing gear are extended or retracted. As pointed out in Ref. 4, this would seem to be a questionable assumption. Extending the landing gear generates turbulence from the wheels, struts, and open cavities. This turbulence is convected past the trailing edge flaps and would be expected to generate incidence fluctuation noise. This type of interaction noise could be calculated if the intensity, scale length, and lateral extent of the landing gear turbulent wake was known. Noise from leading edge slats was found to be most easily represented as a sum of noise from the slat itself plus increased trailing edge noise from the wing. This was the one noise component for which an interaction had to be included in the calculations described herein.

The assumed absence of interactions between various noise components can be checked by comparing measured flyover noise spectra, at constant airspeed, for an airframe with components extended individually and in combination. Flights of this type had been conducted for the Vickers VC 10 jet transport at 600 ft altitude and approximately 160 knots airspeed (Ref. 12). Tabulated one-third octave spectra for these flyovers were obtained from the RAE. The spectrum measured for the clean airframe with idling engines was logarithmically subtracted from those for the airframe with only the leading edge slats extended, only the landing gear extended and wheel-well doors closed, and only the trailing edge flaps at 45° deflection. Resulting noise increments from each of these components are plotted in Figure 9. Also plotted as a solid line is the logarithmic sum of measured noise for the clean airframe and those three noise increments. This experimental prediction of total airframe noise in the approach configuration is seen to be in excellent agreement with the measured spectrum for the approach configuration, up to 4000 Hz center frequency. The comparison shown in Figure 9 therefore validates the use of a noise component method in which no interaction occurs between noise from landing gear, trailing edge high-lift devices, and leading edge high-lift devices.

3.3 Landing Gear Noise

Noise from extended landing gear has been investigated experimentally at DFVLR (Ref. 18). From a comparison of relative dimensions for nose gear and main gear of several jet transports, they found that the ratios of strut

[18]Heller, H. H. and Dobrzynski, W. M.: Sound Radiation From Aircraft Wheel-Well/Landing Gear Configurations. AIAA Paper 76-52, July 1976.

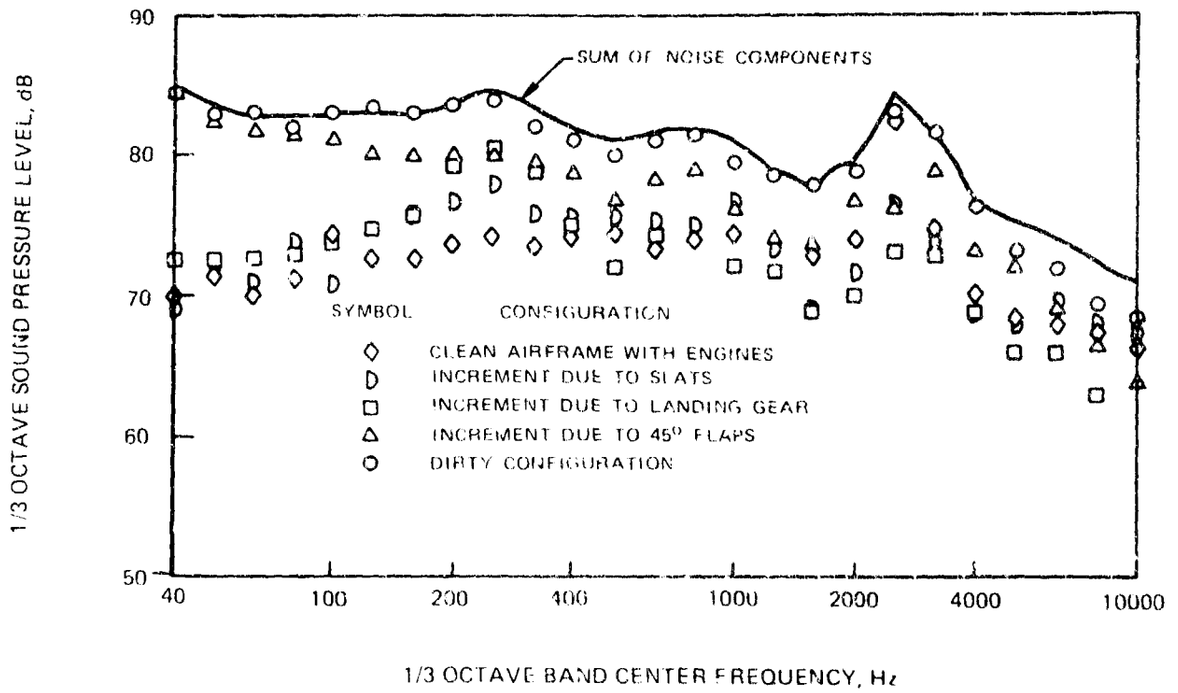

FIGURE 9 - COMPARISON OF SUM OF MEASURED NOISE COMPONENTS WITH MEASURED TOTAL NOISE FOR VICKERS VC 10 AIRCRAFT IN APPROACH CONFIGURATION

diameter, exposed strut length, wheel lateral spacing, and wheel width to wheel diameter were fairly constant. Test models therefore consisted of a two-wheel configuration typical of nose gear for large airplanes and main gear for moderate-size airplanes, and a four-wheel configuration typical of the main gear for large airplanes. By testing several components separately, it was found that the strong tones and higher-frequency broadband noise radiated by an isolated landing-gear cavity were greatly suppressed by the presence of bluff-body landing gear. Also, most of the noise was found to be associated with the struts, drag braces, and actuators rather than the wheels themselves. Use of these measured spectra scaled as expected for dipole noise was found to predict the measured landing gear noise spectra for the JetStar, Hawker Siddley HS 125, and Vickers VC 10 airplanes and to over-predict that for the British Aircraft Corp. BAC 1-11.

Free-field spectra were given only for different azimuthal angles in a plane perpendicular to the flight direction. Spectra for the two-wheel landing gear models in the flyover and sideline positions, and 45° between them, were given in Figure 7 of Ref. 18. These spectra are plotted in the upper left portion of Figure 10. They appear to be the sum of one noise process that is independent of azimuth angle and another that varies with sine squared of the angle from the flyover plane. Fluctuations of side force on the cylindrical strut are likely to be the cause of the second noise process. These curves were approximated by the arbitrary empirical equation

$$SPL = 60 \log(V/194\ \text{kt}) + 20 \log(D/r) + 10 \log(10^{G1} + 10^{G2}) \tag{11}$$

where

$$G_1 = 13 + \log 4.5 (fD/V)^2 \left[12.5 + (fD/V)^2\right]^{-2.25} \tag{12}$$

$$G_2 = 13 + \log 2 (fD/V)^2 \left[30 + (fD/V)^8\right]^{-1} (0.34 H/D) \sin^2 \phi \tag{13}$$

and the normalizing velocity 194 kt is equal to 100 m/sec. Spectra calculated by this equation are shown in the remainder of Figure 10 to match the data within about 1 dB. The ratio of exposed strut length H to wheel diameter D is included in the sideline noise term to allow prediction of noise from long-strut nose landing gear and short-strut tail wheels. By numerical integration of Eq. (11)

$$OASPL = 60 \log(V/194\ \text{kt}) + 20 \log(D/r) + 10 \log(10^{12.52} + 10^{G3}) \tag{14}$$

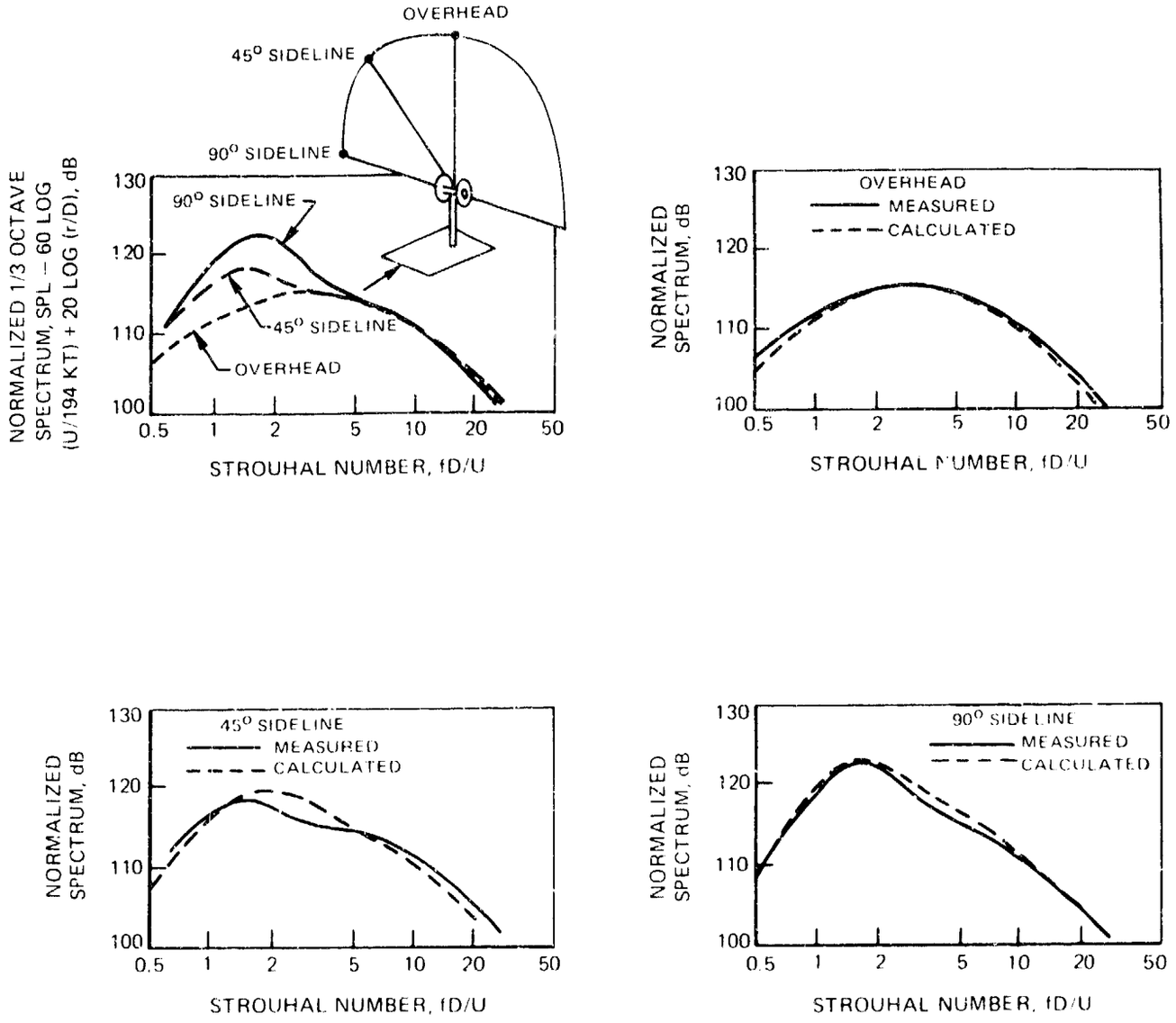

FIGURE 10 - PRESENTATION OF FREE FIELD ACOUSTIC SPECTRA, AND COMPARISONS WITH EMPIRICAL APPROXIMATION, FOR NOISE OF TWO-WHEEL LANDING GEAR

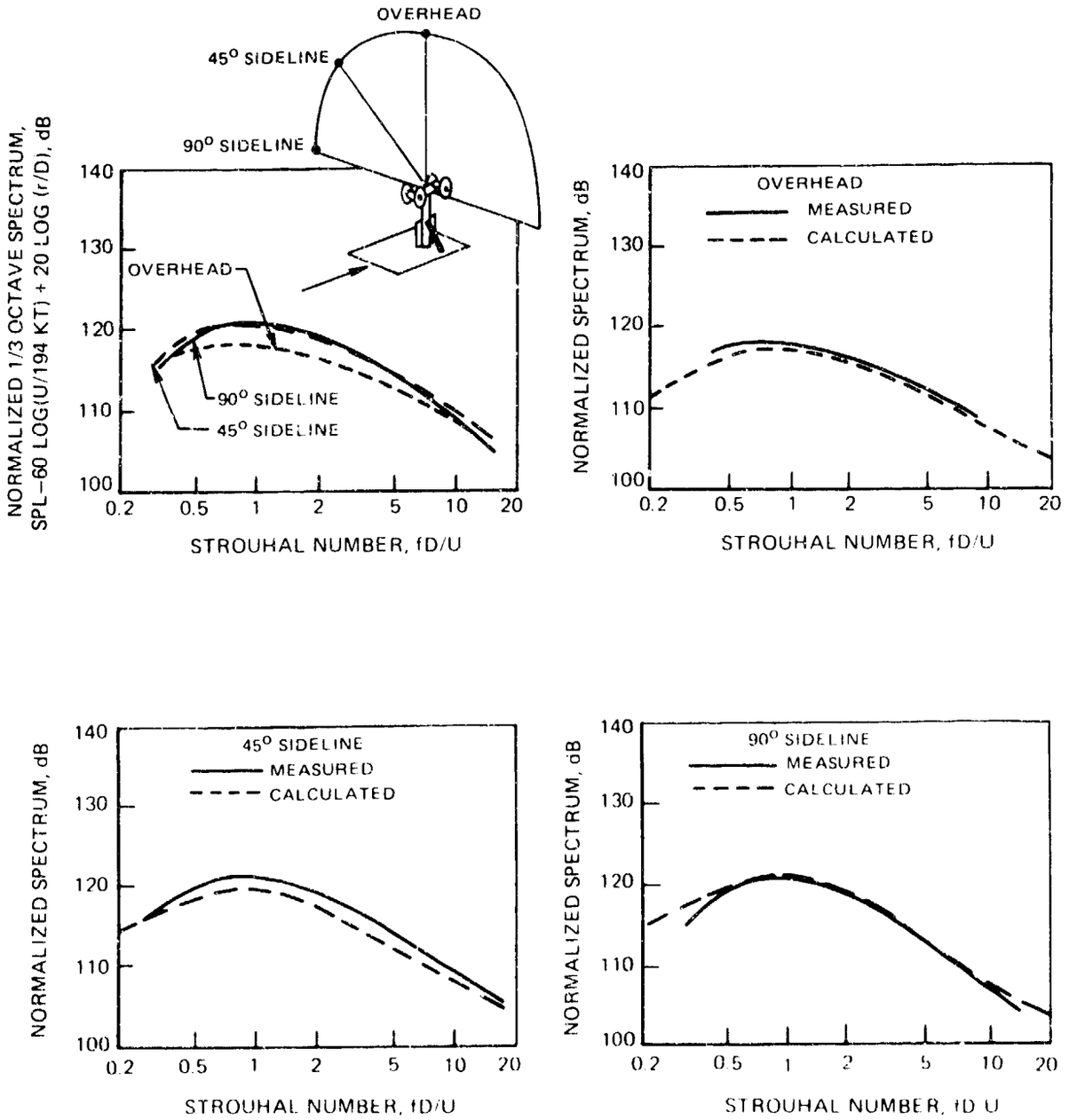

FIGURE 11 - PRESENTATION OF FREE FIELD ACOUSTIC SPECTRA, AND COMPARISON WITH EMPIRICAL APPROXIMATION, FOR NOISE OF MODEL FOUR-WHEEL LANDING GEAR

76 09 153 1

where $$G_3 = 12.79 + \log(0.34\,H/D)\,\sin^2\phi \qquad (15)$$

These equations can be generalized for landing gear having either one or two wheels by arbitrarily taking the nonsideline intensity for a one-wheel landing gear as half of that for a two-wheel landing gear. That is, 0.3 is subtracted from G_1, and from the exponent 12.52 in Eq. (12), if a landing gear has one rather than two wheels.

Spectra for the four-wheel main landing gear models, taken from Figure 10 of Ref. 18, are plotted in the upper left portion of Figure 11. These spectra were arbitrarily fitted by the sum of one term which was independent of azimuth angle and another which corresponds to a fluctuating side force. The spectrum for this sideline-directed noise was flatter and weaker than that for sideline noise from two-wheel landing gear. Spectra calculated from the empirical equations

$$SPL = 60\log(V/194\,kt) + 20\log(D/r) + 10\log(10^{G4} + 10^{G5}) \qquad (16)$$

$$G_4 = 12 + \log(fD/V)^2\left[0.4 + (fD/V)^2\right]^{-16} \qquad (17)$$

$$G_5 = \left\{12 + \log\,7(fD/V)^3\left[1.06 + (fD/V)^2\right]^{-3}\right\}\,\sin^2\phi \qquad (18)$$

are compared with the measured spectra in the remainder of Figure 11. Overall sound pressure level is given by

$$OASPL = 60\log(V/194\,kt) + 20\log(D/r) + 10\log(10^{12.79} + 10^{G3}) \qquad (19)$$

Calculated spectra for noise radiated from four-wheel landing gear are compared in Figures 12 and 13 with the noise increment caused by extended landing gear on the Vickers VC 10 and with noise of the Boeing 747 with gear extended. Spectra calculated from Eqs. (16) and (17) are plotted as solid lines. Noise amplitude is overpredicted at low frequencies and markedly underpredicted at

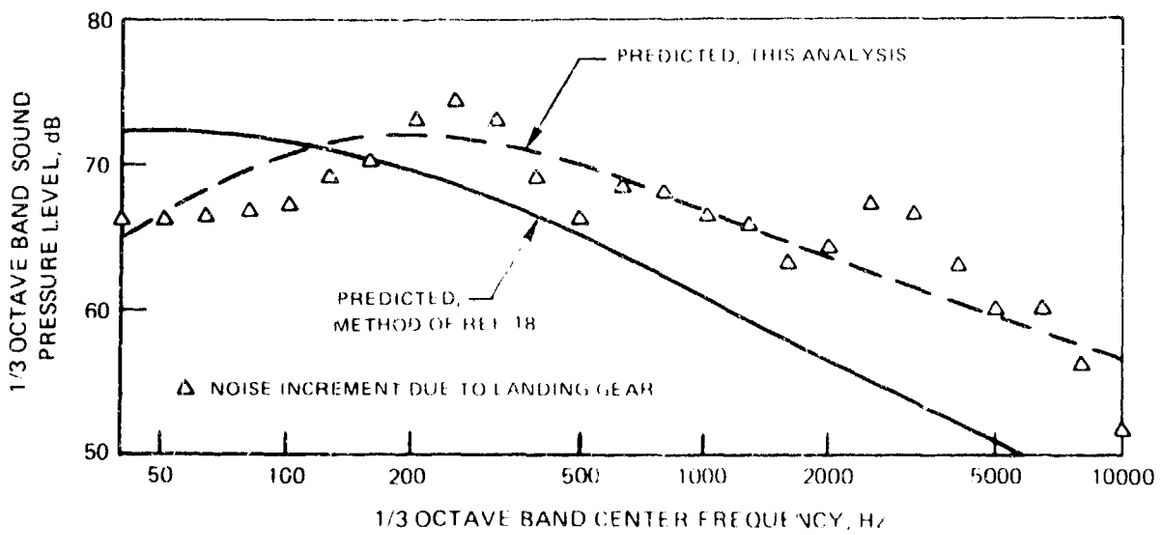

FIGURE 12 - COMPARISON OF MEASURED AND PREDICTED NOISE INCREMENT CAUSED BY EXTENDED LANDING GEAR ON VICKERS VC 10 AIRCRAFT

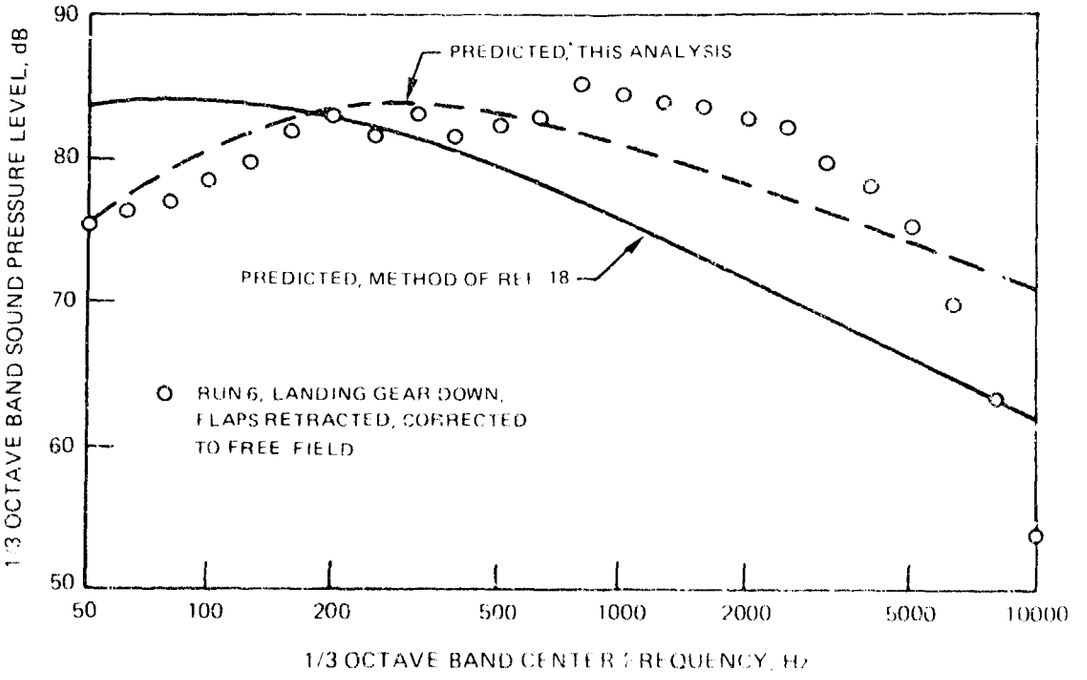

FIGURE 1[illegible] - COMPARISON OF MEASURED AND PREDICTED NOISE FOR BOEING 727 AIRCRAFT WITH EXTENDED LANDING GEAR

high frequencies. It was observed that the low-frequency portion of the data was closely predicted by use of Eqs. (11) and (12) for two-wheel landing gear, but the measured high-frequency decay was much smaller. The function G_4 given by Eq. (17) therefore was replaced by

$$G_4 = 12 + \log 0.6(fD/V)^2\left[1 + 0.25(fD/V)^2\right]^{-1.5} \qquad (20)$$

which has essentially no effect on Eq. (19) for OASPL. The resulting calculated spectra, shown in Figures 12 and 13 as dash lines, generally match the oscillatory spectra. The high-frequency decay term calculated from Eq. (8), which approximates atmospheric attenuation, should be added to these calculated spectra to obtain a closer match to data such as that of Figure 13 at high frequency.

3.4 Trailing Edge Flap Noise

Noise radiation from trailing edge flaps had been represented by the NASA ANOPP noise component analysis (Ref. 4, p. 47) as the separately calculated trailing edge noise from each flap segment. The drag element method (Ref. 14) represents this noise as a sum of two components. One is proportional to flap profile drag coefficient squared and is associated with wake turbulence. The other component, associated with the wing and flap trailing vortex system, is proportional to induced drag coefficient cubed. The prediction method developed herein regards the flap panels as being immersed in the turbulent wake of the wing and upstream flap segments. Flap noise thus is assumed to be lift fluctuation noise caused by incident turbulence. Such noise could be predicted explicitly if the turbulence spectrum, scale length, and intensity were known. Because this information is not known, an empirical approach was used.

Noise spectra generated by incident turbulence at low and moderate subsonic flight speeds should coalesce if the amplitude and frequency scales are properly adjusted. For convenience, flap noise was arbitrarily assumed to be independent of the number of chordwise flap segments. Amplitude should vary directly with flap area, inversely with far-field distance squared, and directly with flight speed to the sixth power. Frequency should be scaled as a Strouhal number relative to flap total chord. Here, flap chord was taken as the ratio of total trailing edge flap area (usually known for each airplane) to flap span as scaled from a three-view sketch of the airplane. Noise spectra due to flap deflection were obtained from the data of Ref. 12 for the Vickers VC 10 at 20°, 35°, and 45° flap deflection, and the data of Ref. 11 for the Boeing 747 at 25° flap deflection, the Convair 990 at 30° flap deflection, and the Lockheed JetStar at 50° flap deflection. The VC 10 and

747 have triple-slotted flaps; the other two airplanes have double-slotted flaps. For the VC 10 and CV 990, the measured spectra for the clean airframe with engines at flight idle were subtracted from spectra measured with flaps deflected. This procedure neglects the fact that clean-airframe noise from the undeflected portion of the wing will be somewhat smaller than noise radiated by the entire clean wing. The portion of the VC 10 spectra near 1600 Hz center frequency was not included because of large contributions from engine noise at fan blade passing frequency. The CV 990 spectra were not analyzed beyond 4000 Hz because the difference between spectra with flaps extended and retracted then decreased below 1 dB. Spectra were not available for the JetStar in these two configurations and nearly the same flight speed. A spectrum for the clean airframe was scaled to the flaps-extended flight speed, assuming an amplitude dependence on velocity to the fifth power and either Strouhal scaling of frequency directly with velocity or (Ref. 11) no variation of frequency with velocity. The resulting levels never were closer than 6 dB below the flaps-deflected spectrum and generally were at least 10 dB below it. Therefore the JetStar spectrum with flaps deflected was completely attributed to trailing edge flap noise.

Spectra also were available from Ref. 17 for the Aero Commander Shrike with landing gear extended and the trailing edge flaps either deflected or retracted, at constant airspeed and altitude. Below 250 Hz center frequency, deflecting the flaps decreased the apparent landing-gear cavity tone and therefore reduced the noise. At larger frequencies the measured noise increase caused by flap deflection was only about 2 dB. The resulting noise due to flap deflection is inherently much less accurate than the other flap noise spectra.

Amplitudes of the resulting adjusted spectra were found to increase with increasing flap deflection. This increase seemed to be much less rapid than that given by the drag element method (Ref. 14). In that method, trailing edge flap noise at constant airspeed and lift coefficient is predicted to vary with flap profile drag coefficient squared. Flap drag coefficient varies approximately with flap deflection to the second or third power. Therefore, the drag element method predicts that flap noise intensity varies with flap deflection to about the fifth power. The comparison of measured spectra seemed to vary roughly with sine squared of the flap deflection angle.

The resulting amplitude-adjusted and frequency-adjusted spectra for maximum flyover noise caused by trailing edge flaps are plotted in Figure 15. The spectra generally agreed at low Strouhal numbers. However, the high-frequency break point occurred at larger Strouhal numbers for triple-slotted flaps than for simpler flaps. This spectrum shape, having a gradual decay at moderate Strouhal numbers and an abrupt change to approximately inverse frequency cubed at high Strouhal numbers, is typical (Ref. 8) of noise radiated from airfoils in turbulent flow. Acoustic noncompactness (acoustic wavelength becoming smaller than the airfoil chord) causes the rapid decay of

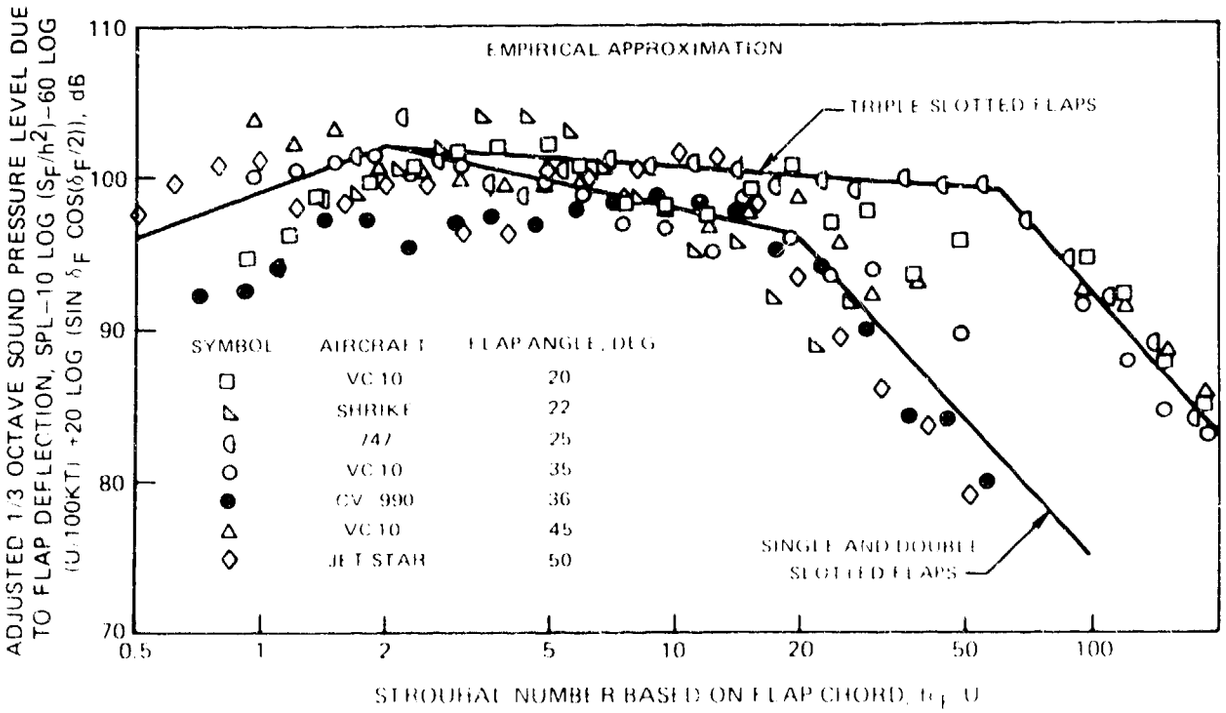

FIGURE 15 - NORMALIZED SPECTRA OF MEASURED TRAILING EDGE FLAP NOISE

noise radiation at high frequencies. The observed spectra would be expected if double-slotted flaps have two flap segments of roughly equal chord, and triple-slotted flaps have a small-chord vane followed by two larger flap segments.

Directivity was arbitrarily assumed to be that for a lift dipole normal to the deflected flap. For steady level flight, the combination of inverse-square dependence on far-field distance and the deflected lift-dipole directivity causes the flyover noise to vary with $\sin^2 \theta \sin^2 (\theta+\delta_F)$, where δ_F is the flap deflection angle. It can be shown that this quantity is largest for a retarded-time angle θ equal to $90^o-\delta_F/2$. That is, the noise which will be measured as maximum flyover noise leaves the trailing-edge flaps before they pass over the observer. The resulting one-third octave spectrum due to deflection of trailing edge flaps, decreased 3 dB for comparison with data from post-mounted rather than ground-board microphones, were arbitrarily approximated by straight lines in Figure 14. The result becomes

$$OASPL = 112.0 + 10\log(S_F \sin^2\delta_F/h^2) + 60\log(V/100kt) + 20\log\left[\sin\theta\cos^2\phi\sin(\theta+\delta_F)\right] \quad (21)$$

for single- and double-slotted flaps, and 1.0 dB more for triple-slotted flaps.

$$SPL_F = G_{6,7} + 10\log(S_F \sin^2\delta_F/h^2) + 60\log(V/100kt) + 20\log\left[\sin\theta\cos^2\phi\sin(\theta+\delta_F)\right] \quad (22)$$

where

$$G_6 = 99.0 + 10\log(fc_F/V),\ fc_F/V < 2 \quad (23)$$

$$G_6 = 103.82 - 6\log(fc_F/V),\ 2 \le fc_F/V < 20 \quad (24)$$

$$G_6 = 135.04 - 30\log(fc_F/V),\ 20 \le fc_F/V \quad (25)$$

for single- and double-slotted flaps, and

$$G_7 = 99.0 + 10\log(fc_F/V),\ fc_F/V < 2 \tag{26}$$

$$G_7 = 102.61 - 2\log(fc_F/V),\ 2 \le fc_F/V < 75 \tag{27}$$

$$G_7 = 155.11 - 30\log(fc_F/V),\ 75 \le fc_F/V \tag{28}$$

for triple-slotted flaps.

The assumed simple variation of trailing edge flap noise amplitude on sine squared of the deflection angle can be illustrated by use of the measured spectra for the Vickers VC 10 aircraft (Ref. 12). Spectra are plotted in Figure 15a for the clean airframe with flaps retracted and for 20°, 35°, and 45° flap deflection angles. These spectra include 6 dB increase above free field. Noise increments caused by flap deflection were determined by logarithmic subtraction of the flaps-retracted spectrum. These increments are plotted in Figure 15b for the three flap angles. Next, the quantity 20 log $\sin\delta_F$ was subtracted from each spectrum to account for the effect of flap deflection on noise amplitude. The small quantity 20 log $\cos(\delta_F/2)$ also was subtracted to account for the forward rotation of flap noise directivity. The resulting three deflection-adjusted spectra are plotted in Figure 15c. Data symbols for all three flap angles are intermixed and generally are coalesced by this adjustment. Also shown is the empirical curve from Figure 14 for triple-slotted flaps. The spectra are generally in good agreement with this curve. Worst agreement occurred at frequencies near 2500 Hz, the fan blade passing frequency. This comparison validates the assumption that trailing edge flap noise varies with sine squared of the flap deflection angle.

3.5 Leading Edge Slat and Flap Noise

Leading edge slats would be expected to cause noise by three processes. Trailing edge noise would be caused by the slat boundary layer as it flows past the slat trailing edge. Bluff-body noise would be generated by high-speed airflow past exposed actuators and tracks protruding through the slat gap. In addition, the wing upper-surface boundary layer thickness and turbulence intensity would be changed by the slat wake. Only two sets of data were available for examining slat noise. Flyover noise had been measured with the Vickers VC 10 aircraft (Ref. 12) with and without leading edge slats deployed. Slats increased OASPL by about 5 dB at constant altitude, airspeed, and engine setting. Noise data for a wind tunnel model of the Boeing 747 were reported

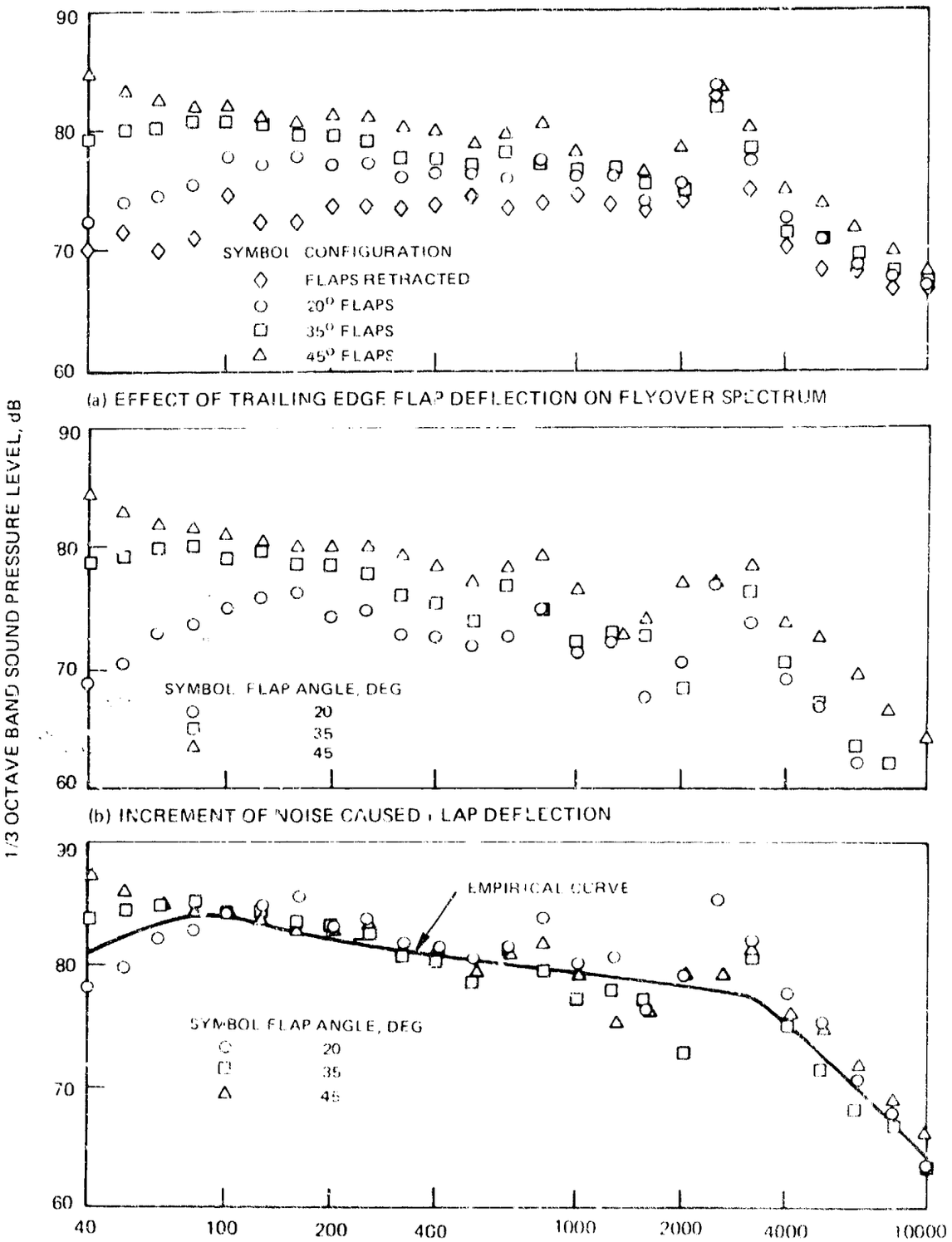

FIGURE 15 - EVALUATION OF PREDICTED DEPENDENCE OF TRAILING EDGE FLAP NOISE ON SINE SQUARED OF DEFLECTION ANGLE FOR VICKERS VC 10 AIRCRAFT

76 12 131

in Ref. 19. Airframe noise for the clean configuration could not be detected above the tunnel background noise. Extending the leading edge flaps raised the airframe noise to detectable levels. When a gap existed between the leading edge flaps and the wing, the configuration resembled a leading edge slat. This slat configuration was about 3 dB louder at all frequencies than the model with gap sealed. A general comparison with noise data for the full-scale aircraft was shown, but absolute levels were not given. Comparing the spectra shown in Figures 12 and 13 of Ref. 19, it is apparent that noise from leading edge high-lift devices does not extend to frequencies as high as those for trailing edge flap noise.

Because of the absence of detailed data and low levels of leading edge slat and flap noise relative to trailing edge flap noise, a simple approximation was used. Leading edge flaps deflected to an angle appropriate for the aircraft lift coefficient have been assumed to raise the wing noise to that from Eq. (10) with ND equal to one, and to generate no additional noise. Of course, use of highly deflected leading edge flaps at low lift coefficients in an early part of descent can increase the noise. At that flight condition the airspeed is high, lift coefficient is low, and separated flow can occur on the lower surface of a leading edge flap.

The one-third octave spectrum of the measured noise increase caused by VC 10 slat deployment (Ref. 12) is plotted in Figure 16. Also shown are the measured engine noise spectrum, the increment between that and the clean-aircraft flyover noise, and a prediction of that noise by the method developed herein. Measured levels shown are 3 dB lower than the original data taken with flush microphones. For most of the frequency range, engine noise and clean-aircraft noise increment were less than 3 dB apart. Clean-airframe noise was predicted to have peak amplitude within the one-third octave band centered at 125 Hz. It is possible that the higher-frequency noise increment attributed to the clean aircraft was actually produced by the engine. If so, then the peak frequency for slat noise was higher than that for noise of the clean airframe. The calculated amplitudes shown in this figure are for conventional low-speed aircraft with an OASPL 8 dB above that given by Eq. (6).

Slat noise was approximated as the sum of two spectra, each having the normalized spectrum shape appropriate for trailing edge noise. Leading edge slats typically have a chord about 15% of the wing chord. Peak frequency of slat trailing edge noise should then be $0.15^{-0.8}$ or about 4.56 times that for the wing noise. Measured slat noise for the VC 10 was approximately matched between 315 and 1600 Hz if amplitude of this peak of slat noise was taken to

[19]Shearin, J. G., Fratello, D. J., Bohn, A. J., and Burggraf, W. D.: Model and Full-Scale Large Transport Airframe Noise. AIAA Paper 76-550, July 1976.

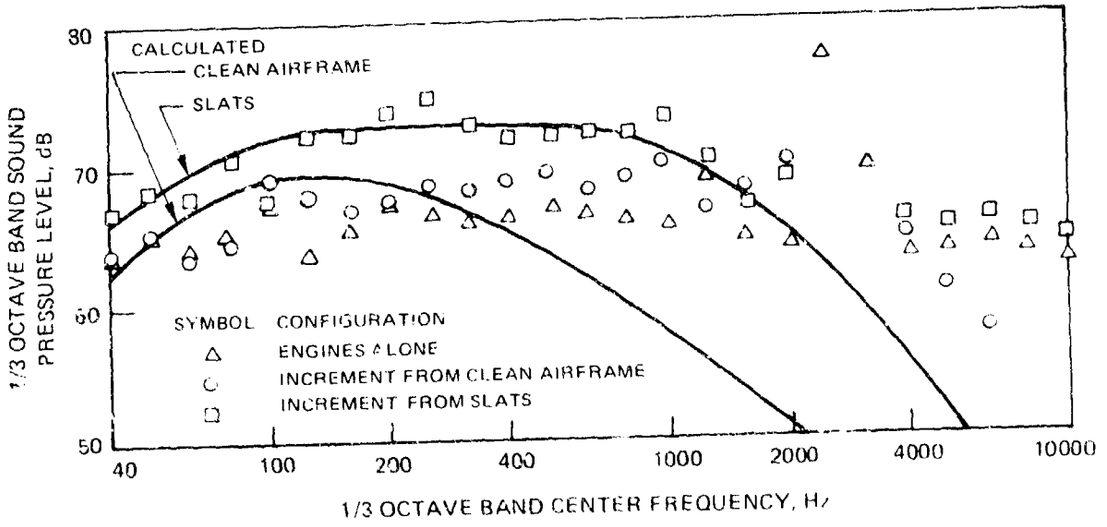

FIGURE 16 - MEASURED AND CALCULATED NOISE INCREMENTS DUE TO VICKERS VC-10 CLEAN AIRFRAME AND LEADING EDGE SLAT

be 3 dB above that for the clean wing. The low-frequency portion of the slat noise spectrum was then matched by assuming that the slat also produced an increment of wing trailing edge noise 3 dB above the clean-wing noise. The resulting presentation of the slat noise spectrum, plotted in Figure 16, gives a general approximation to those data on which it was based. Rather than represent the high-frequency portion of this spectrum as having an intensity proportional to slat area, all slats are assumed to have roughly the same ratios of slat area to wing area and slat chord to wing chord. Thus the only geometric parameters used in calculating slat noise were those for the wing.

3.6 Graphical Method

A graphical method was developed for predicting airframe noise. Predicted levels are 3 dB above free field, as with measurements conducted for noise certification purposes as described in FAR 36. This method neglects all source motion effects (convective amplification and Doppler shifts) on noise measured by a fixed observer. Figures are presented for determining OASPL and normalized spectrum for various noise components of airframes flying at 500 ft altitude in a sea-level standard atmosphere. The change of noise amplitude caused by flight at other altitudes is given by an inverse dependence on altitude squared. The resulting correction in decibels is plotted in Figure 17 for the range from 100 ft to 2000 ft altitude.

3.6.1 Clean Airframe

Maximum overall sound pressure level for clean configurations was approximated by neglecting the effect of wing aspect ratio and assuming an arbitrary ratio of horizontal tail area to wing area. The maximum flyover OASPL for a very clean airframe (sailplane, supersonic transport, subsonic jet transport without external flap track fairings) can be determined from Figure 18 as a function of wing area and flight velocity. For conventional subsonic propeller-driven airframes and for jet transports with numerous large trailing edge flap track fairings, add 8 dB to these levels.

Spectrum of clean-airframe noise is a function of the flat-plate turbulent boundary layer thickness at the wing trailing edge. This quantity can be obtained from Figure 19 as a function of flight velocity and wing mean geometric chord. The wing mean geometric chord is the ratio of gross wing area to total wing span (equivalent to the square root of the ratio of gross wing area to wing aspect ratio). For each one-third octave center frequency, the nondimensional Strouhal number must be calculated. This is the product of center frequency (Hz) and boundary layer thickness (ft) obtained from Figure 19, divided by flight velocity in ft/sec (1.69 times flight velocity,

knots). The amount by which the one-third octave sound pressure level of that center frequency is less than OASPL is given by the normalized spectrum labeled Clean Wing in Figure 20.

3.6.2 Leading Edge Devices

Leading edge flaps are assumed to raise OASPL to that for a conventional low-subsonic-speed clean wing, 8 dB above that given by Figure 18. Normalized spectrum is given by the Clean Wing spectrum of Figure 20.

Leading edge slats are assumed to raise the wing OASPL to that for a conventional low-subsonic-speed clean wing. Also, they are assumed to generate a noise increment 6 dB larger than that for the low-subsonic clean wing. The normalized spectrum of this noise increment relative to OASPL of the low-subsonic clean wing is given by the curve in Figure 20 labeled Leading Edge Slat.

3.6.3 Trailing Edge Flaps

Maximum flyover OASPL for the noise increment caused by trailing edge flaps is obtained from two figures. OASPL amplitude due to flight velocity and trailing edge flap area is obtained from Figure 21. This quantity must be decreased by the adjustment for flap deflection angle given in Figure 22. Deflection angle affects both the flap noise amplitude and directivity, so maximum flyover noise is predicted to occur near 70° rather than at 90° flap deflection. These values of flap OASPL are independent of the type of flap. However, the normalized spectrum shape for trailing edge flap noise (Figure 23) is different for triple-slotted flaps. Note that Strouhal number for trailing edge flaps is referenced to the total flap chord (ratio of flap planform area to flap span as scaled from a top or bottom view of the wing planform).

3.6.4 Landing Gear

Maximum OASPL for flyover of a pair of two-wheel or four-wheel main landing gear assemblies can be obtained from Figure 24 in terms of the tire diameter and flight velocity. These values should be decreased 3 dB for aircraft which have a one-wheel main landing gear. They should then be increased in proportion to the total number of main landing gear on an aircraft (3 dB for four main gear as on some wide-body jet transports). Noise from the nose landing gear can be neglected relative to that from the main gear. Normalized one-third octave spectrum, which is different for four-wheel gear than for one- or two-wheel gear, can be obtained from Figure 25.

3.6.5 Annoyance-Weighted Noise Levels

Variations of calculated A-weighted noise level (dB(A)) and perceived noise level (PNL) with overall sound pressure level, as determined by the noise component method for a range of test cases, are plotted in Figure 26. As a rule of thumb, it seems reasonable to approximate airframe noise dB(A) as 4.6 dB less than OASPL with a standard deviation of 1.3 dB and PNL as 7.1 dB more than OASPL with a standard deviation of 2.1 dB. A more accurate prediction would be obtained by (1) use of the preceding method to calculate the spectrum for each noise component, (2) adding these spectra logarithmically to obtain the aircraft noise spectrum for the particular configuration, and (3) calculating dB(A) and PNL by standard methods.

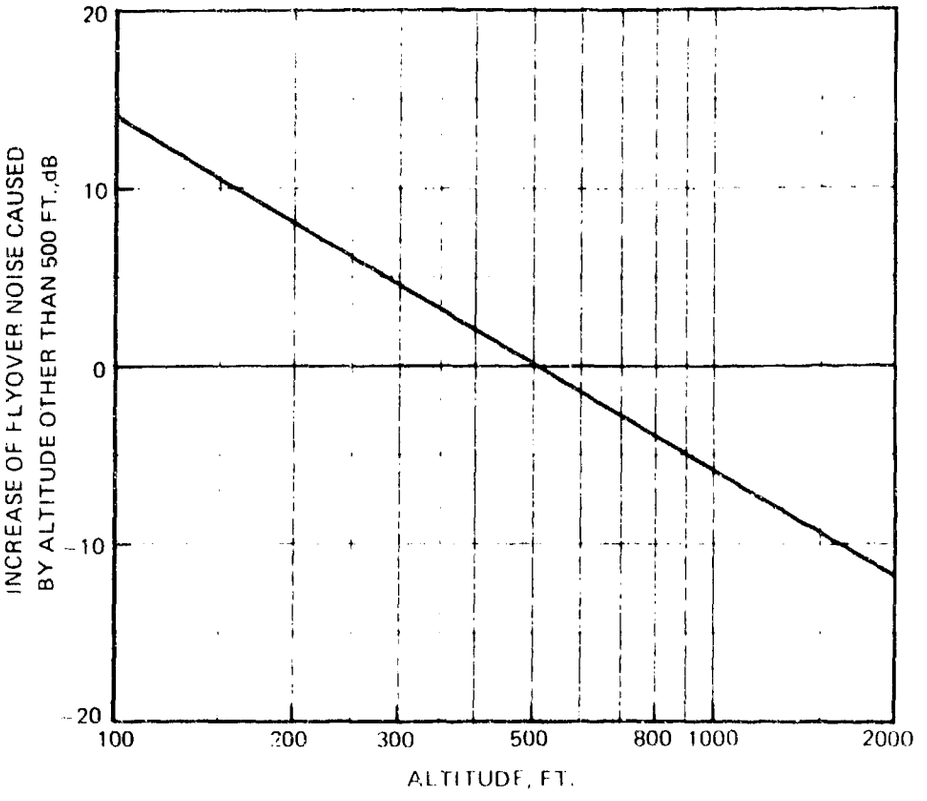

FIGURE 17 - EFFECT OF FLIGHT ALTITUDE ON OVERALL AND 1/3 OCTAVE SOUND PRESSURE LEVELS DETERMINED FOR 500 FT ALTITUDE

76 12 95 9

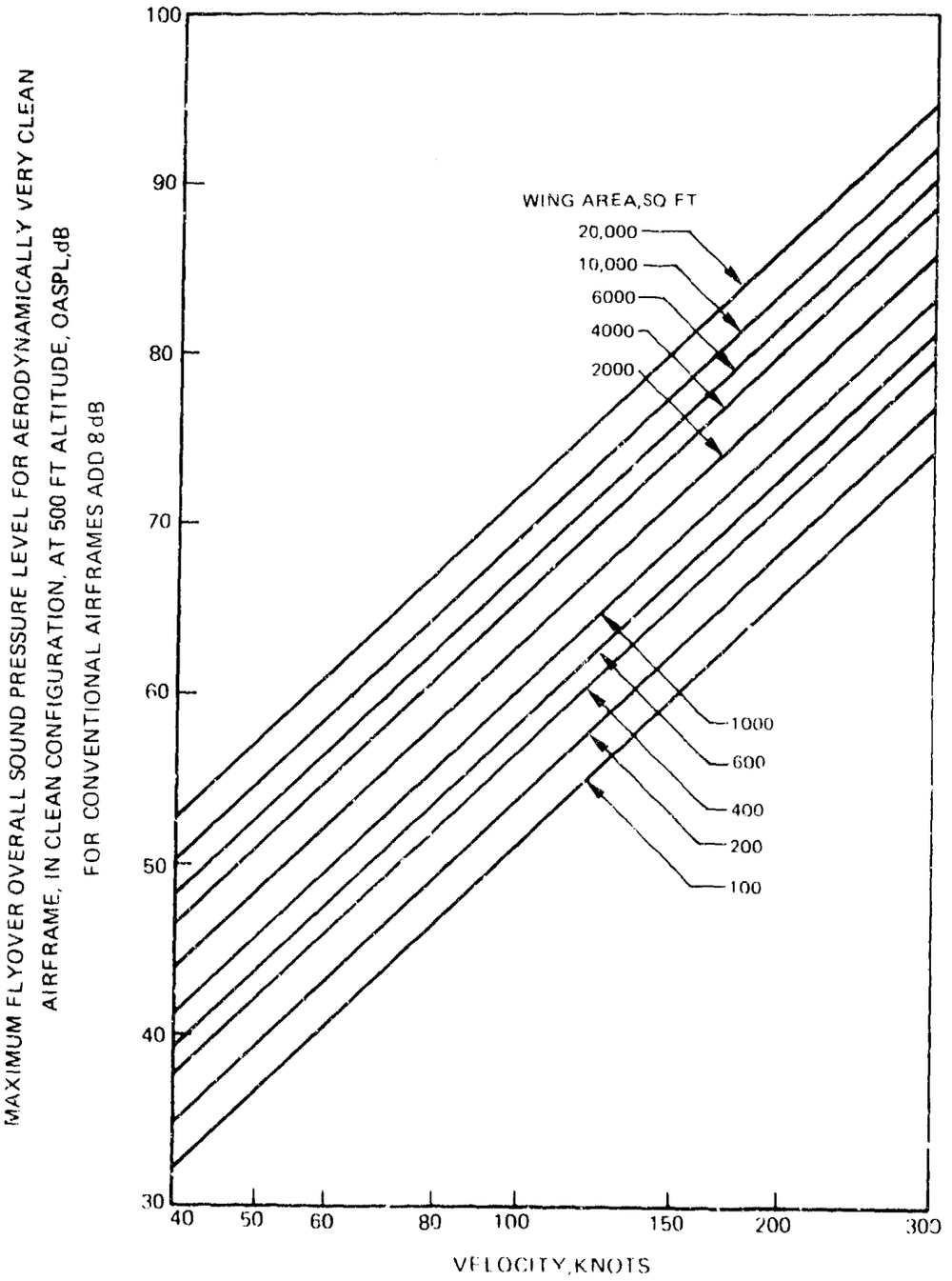

FIGURE 18 - GRAPH FOR DETERMINING MAXIMUM OVERALL SOUND PRESSURE LEVEL OF CLEAN AIRFRAMES

76 12 05 3

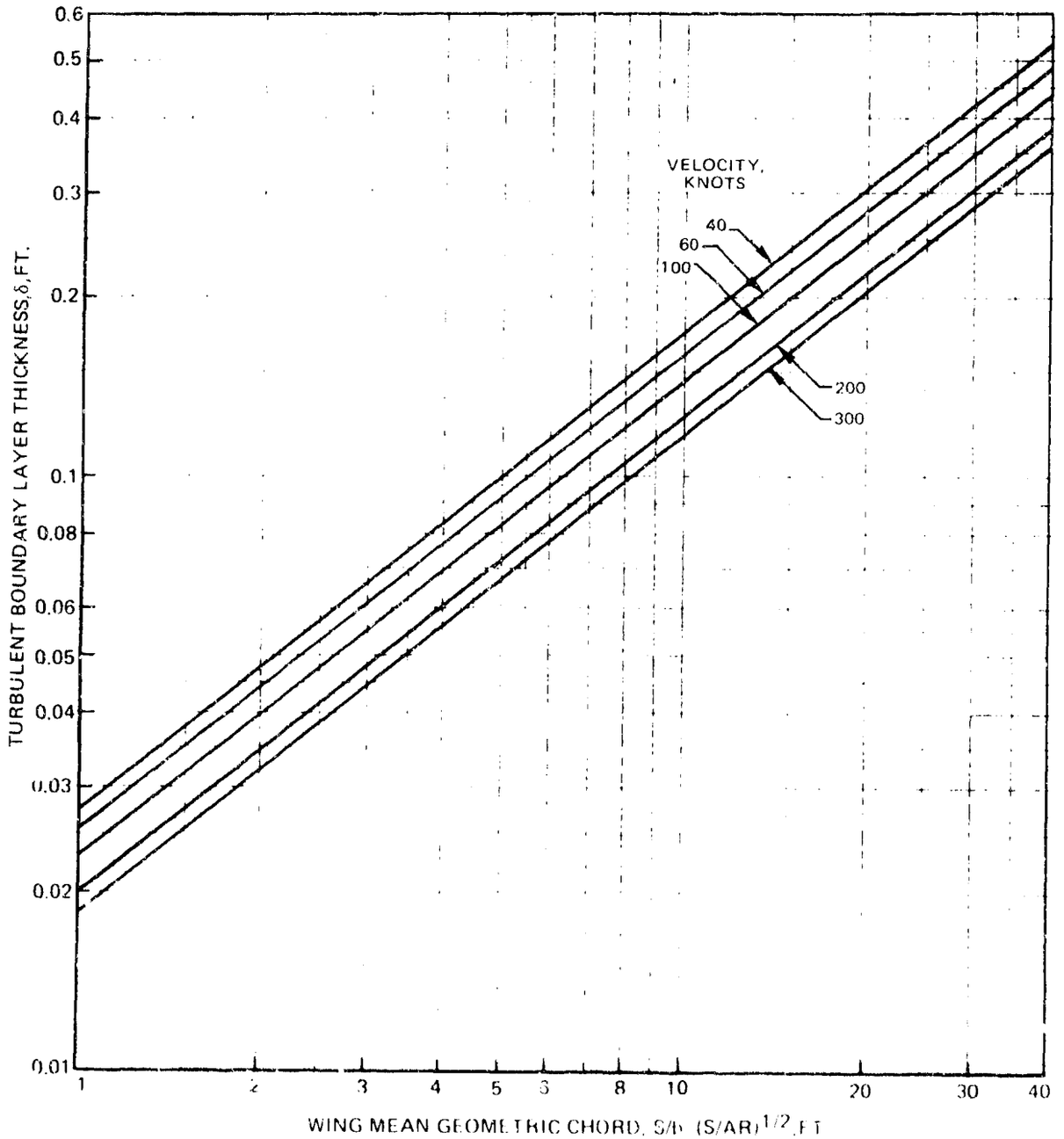

FIGURE 19 - GRAPH FOR DETERMINING WING TRAILING EDGE BOUNDARY LAYER THICKNESS, FOR USE IN OBTAINING SPECTRA FOR CLEAN AIRFRAMES

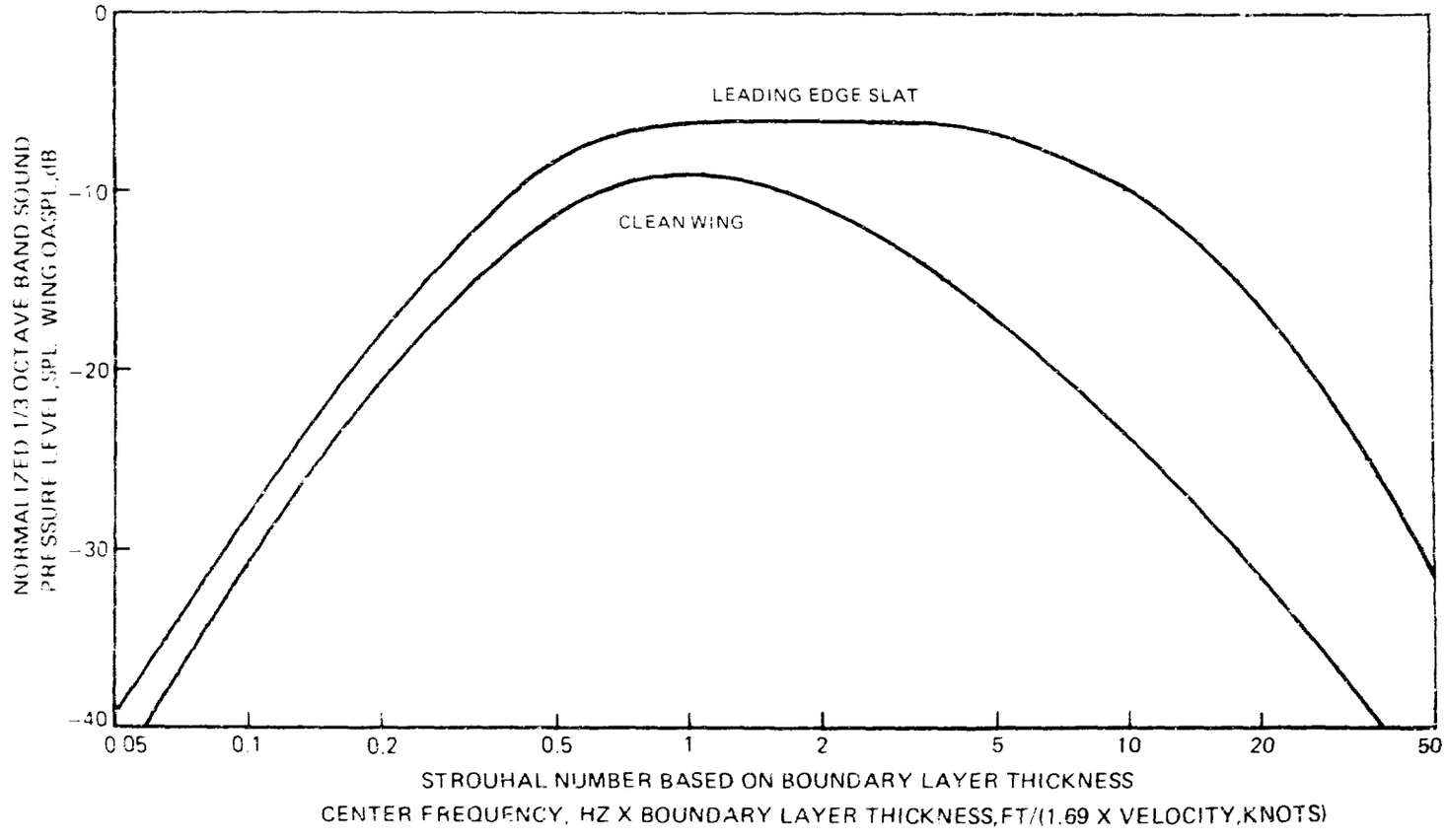

FIGURE 20 - NORMALIZED 1/3 OCTAVE SPECTRA FOR CLEAN AIRFRAMES AND LEADING EDGE SLATS

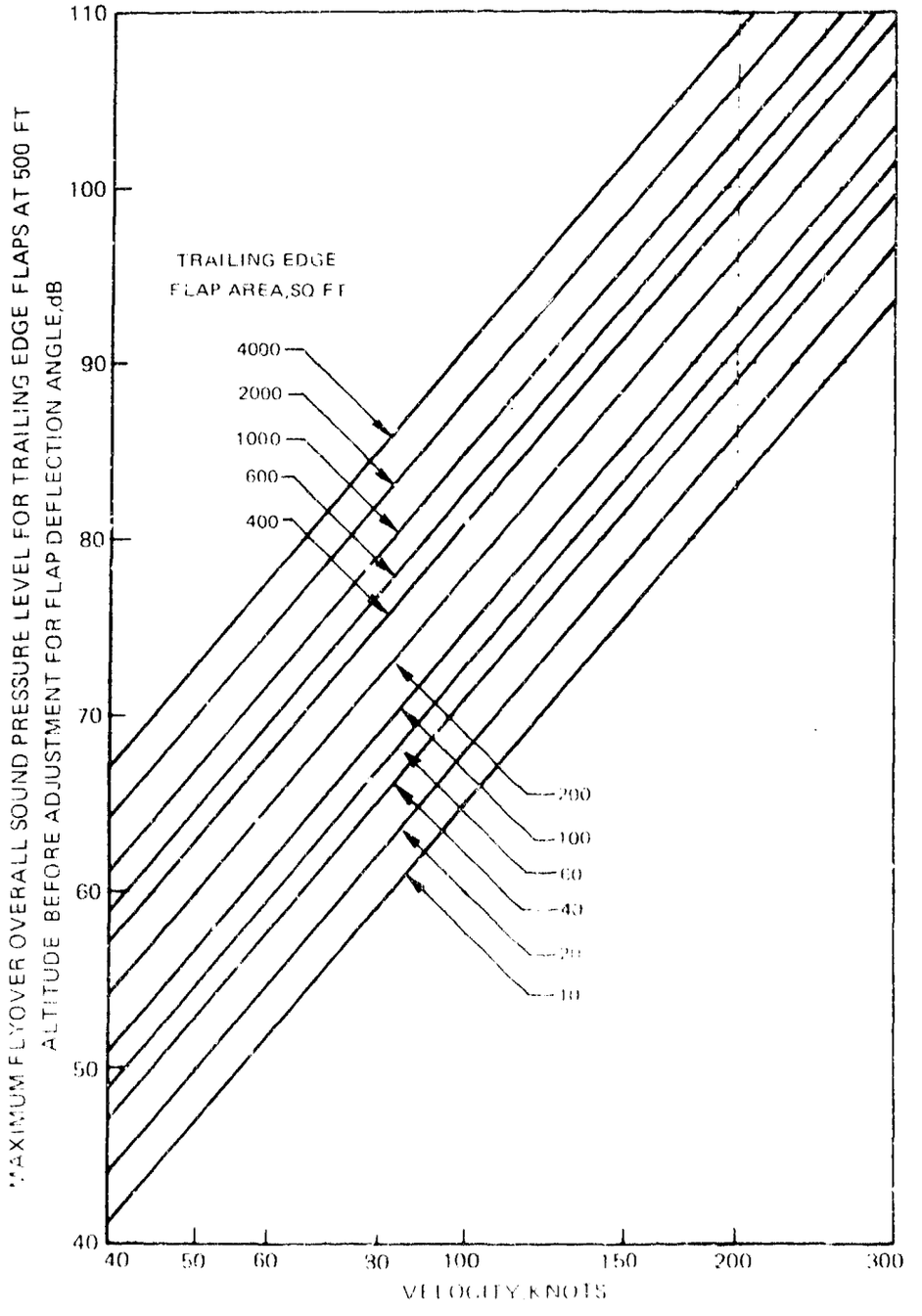

FIGURE 3.1 - GRAPH FOR DETERMINING THE PORTION OF TRAILING EDGE FLAP MAXIMUM OVERALL SOUND PRESSURE LEVEL THAT IS NOT AFFECTED BY FLAP DEFLECTION ANGLE

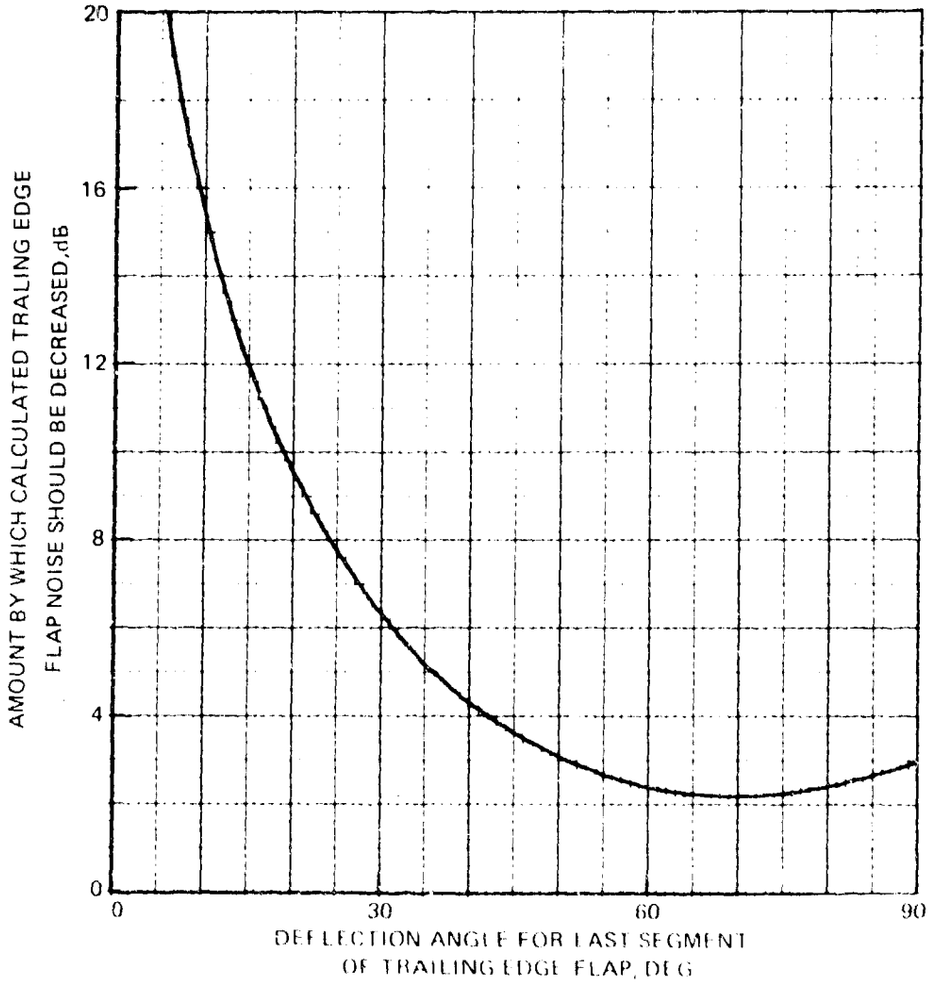

FIGURE 22 - GRAPH FOR DETERMINING THE ADJUSTMENT TO TRAILING EDGE FLAP MAXIMUM OVERALL SOUND PRESSURE LEVEL DUE TO FLAP DEFLECTION ANGLE

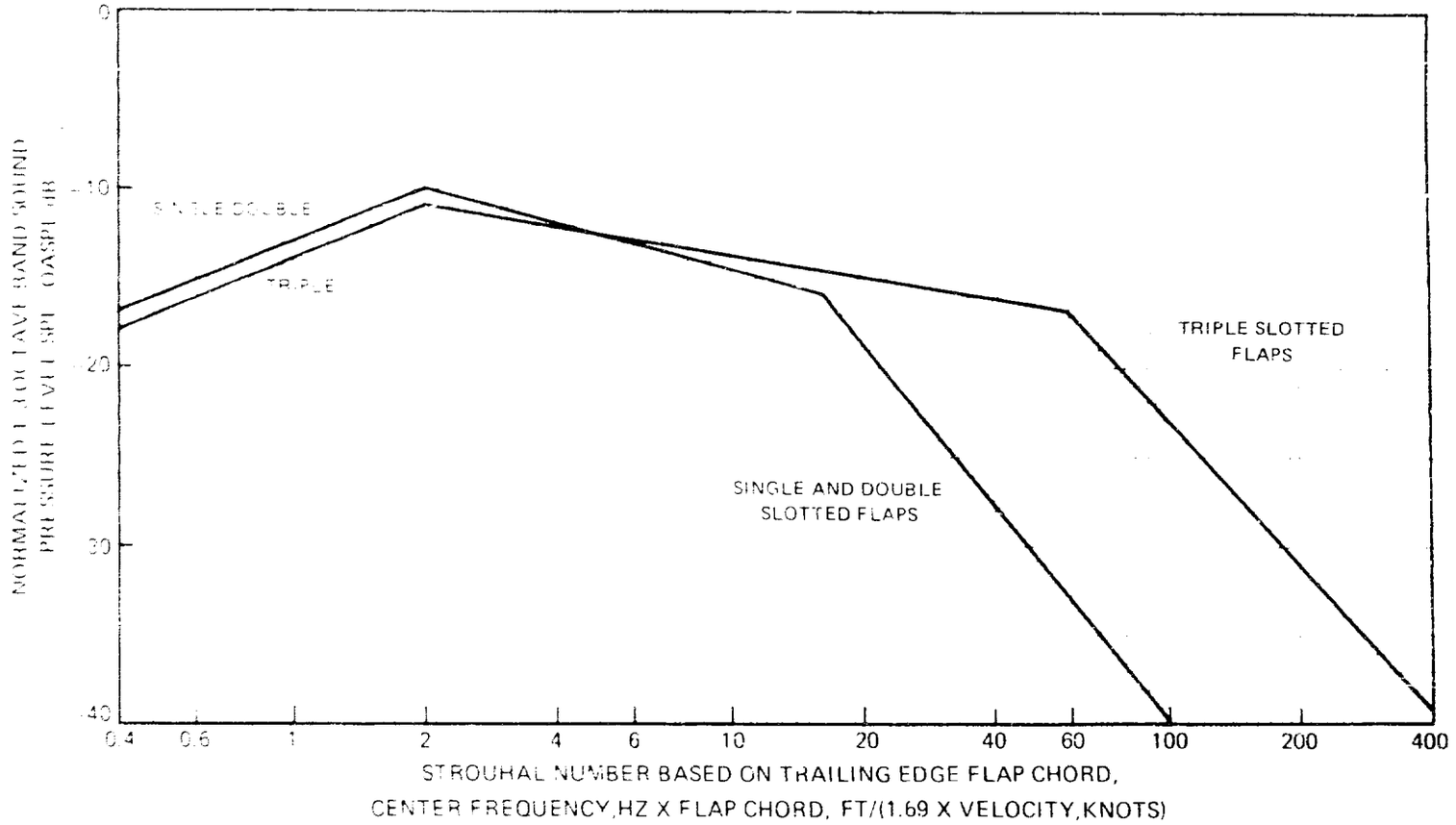

FIGURE [illegible] NORMALIZED 1/3 OCTAVE BAND SOUND PRESSURE LEVEL FOR TRAILING EDGE FLAPS

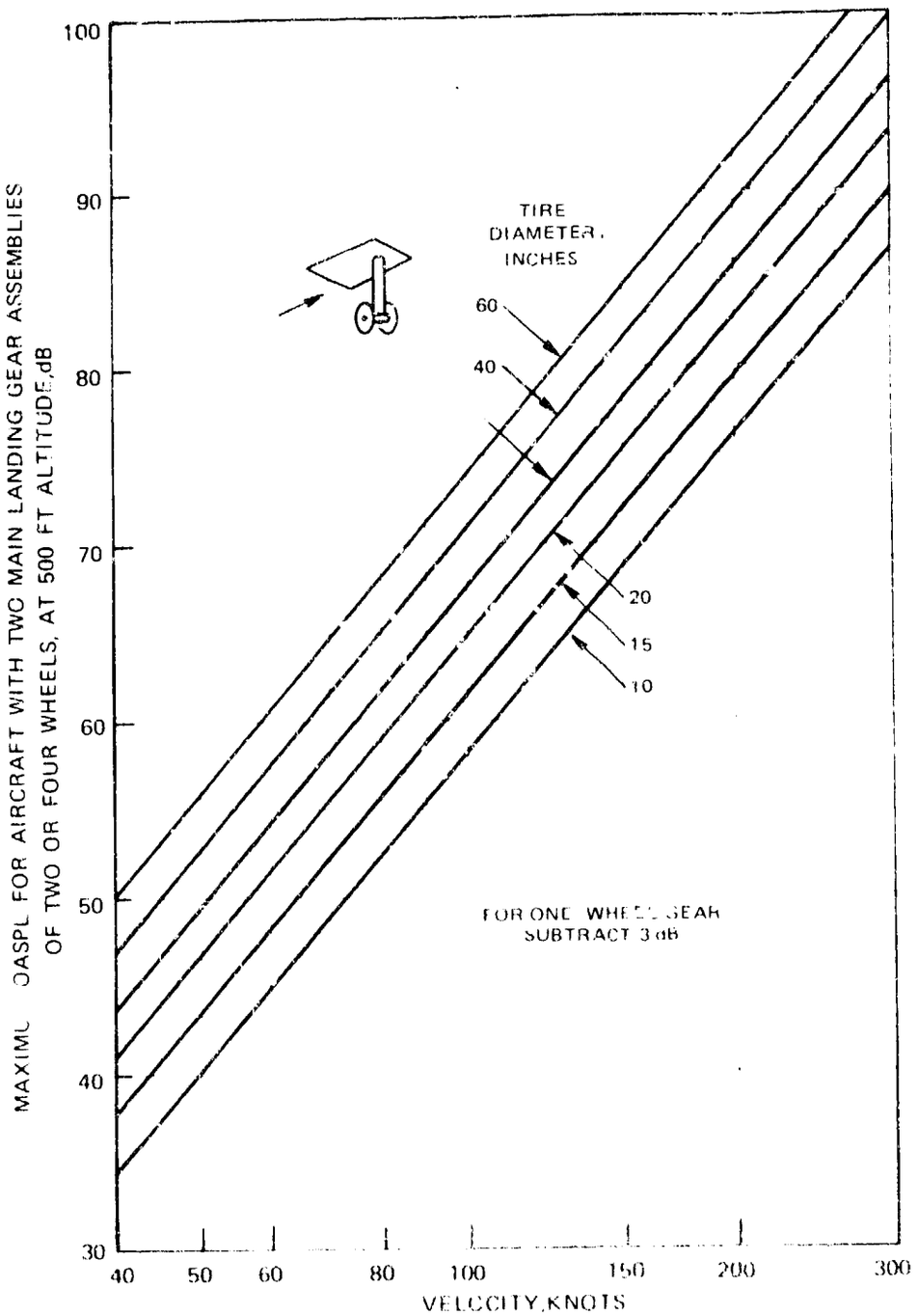

FIGURE 24 - GRAPH FOR DETERMINING MAXIMUM OVERALL SOUND PRESSURE LEVELS OF LANDING GEAR

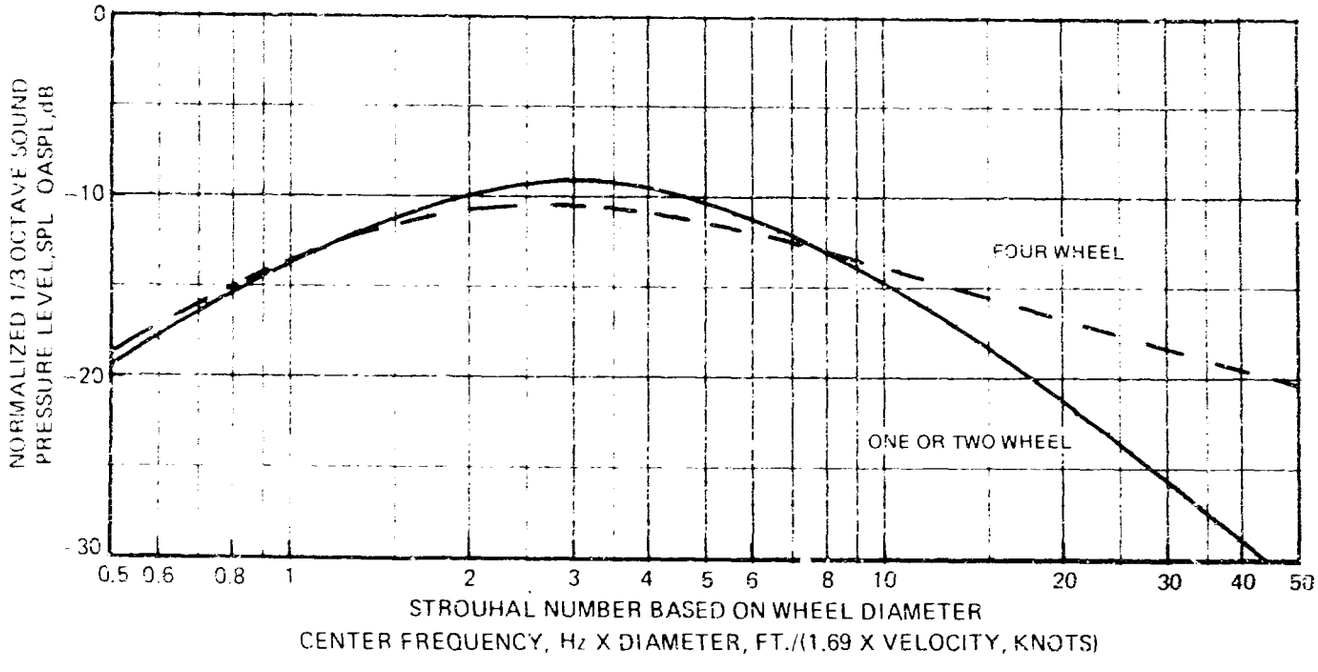

FIGURE 25 - NORMALIZED 1/3 OCTAVE SOUND PRESSURE LEVEL FOR LANDING GEAR

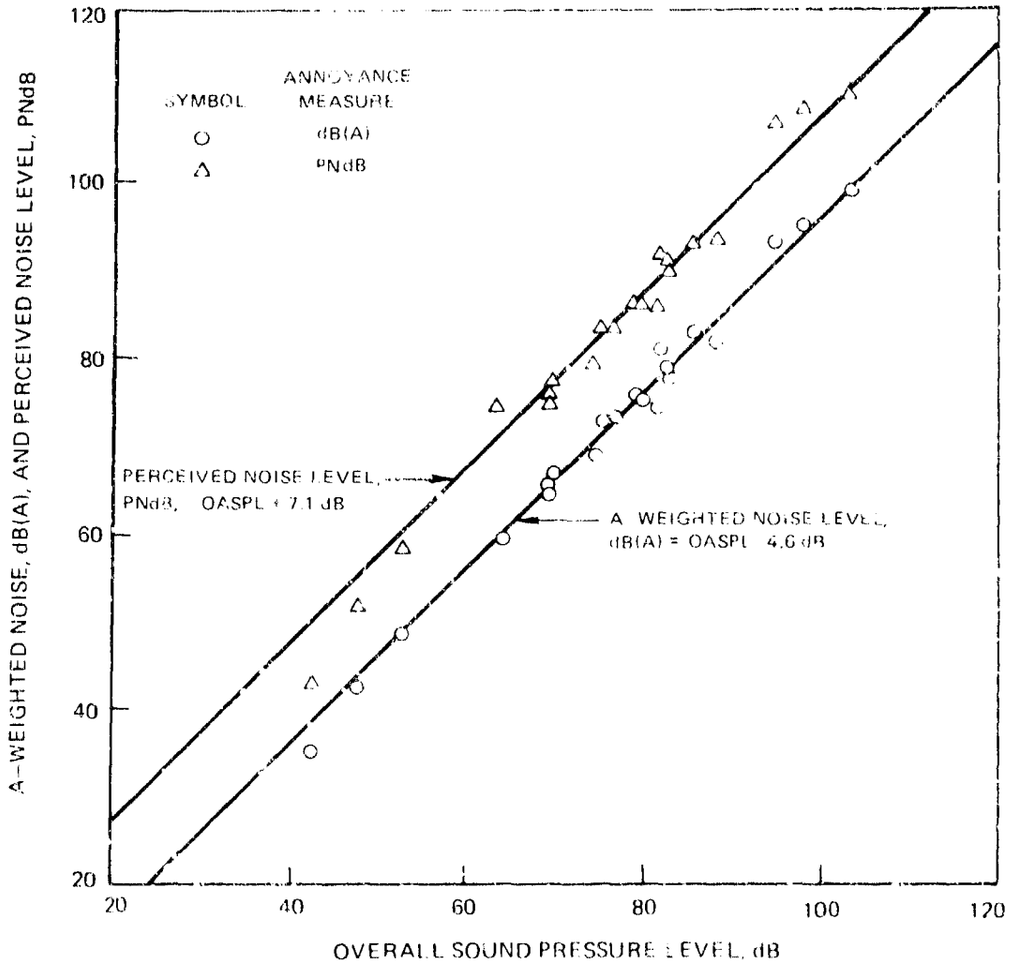

FIGURE 26 - VARIATIONS OF A-WEIGHTED NOISE LEVEL AND PERCEIVED NOISE LEVEL WITH OVERALL SOUND PRESSURE LEVEL

4.0 NASA ANOPP METHODS

Two NASA Aircraft Noise Prediction Program (ANOPP) methods for calculating airframe noise were obtained from NASA within one computer program. Option 1 of that computer program is the total aircraft noise method developed by Hardin (Ref. 4) for clean airframes. It was derived from a regression analysis of measured peek OASPL for selected aircraft flyovers. Mean square acoustic pressure was assumed to vary inversely with distance squared. Exponents for velocity, wing area, wing aspect ratio, and gross weight were determined which minimize the rms error. The data base did not include any jet aircraft other than the C-5A. This method was shown in Ref. 5 to underestimate OASPL of business jets by about 8 dB and low aspect ratio delta-wing aircraft by about 20 dB. Comparisons between measured and calculated spectra for this method had not been published.

Options 2 through 8 of the NASA-supplied computer program calculate airframe noise from seven components as given by Revell's drag element method (Ref. 14). These components are the noise caused by wing profile drag (including trailing edge flaps), wing induced drag, and profile drag of the fuselage, nacelles, horizontal tail, landing gear, and leading edge slat. Input data for these calculations include flight speed, altitude, airframe geometry, lift coefficient, and the drag coefficient for each component. Flow velocity at the wing upper surface trailing edge, as calculated from the magnitude and chordwise location of wing maximum velocity by use of Eq. (43) of Ref. 14, also is needed. For prediction of airframe flyover noise, spectra calculated for the selected options must be logarithmically summed by the user and adjusted for the variation of far-field distance with airframe direction angle.

The computer program developed by NASA for the drag element method contains Mach number convection terms which were not included in Ref. 14. Use of the low Mach number approximation was discussed on pp 5-6 of Ref. 14. However, the resulting equations were applied in Ref. 14 to flyover noise prediction for the Lockheed JetStar aircraft at Mach numbers from 0.38 to 0.55 where these effects are not small. Convection effects on directivity pattern are included in the ANOPP method, causing calculated maximum OASPL to occur at a retarded-time position upstream of the overhead position. However, the Doppler shift of calculated spectra was omitted for all direction angles. Thus the spectra calculated by the corrected NASA ANOPP drag element method and presented in this report would match those given by direct application of equations in Ref. 14 for the limit of very low subsonic Mach numbers (less than 0.1) but would not necessarily match any other version of that method.

Considerable aerodynamic information is required as input for calculation of airframe noise by the drag element method. Profile drag coefficients for airframe wing, tail, fuselage, and nacelle surfaces were estimated by use of the table on p 95 of Ref. 20. The increment of profile drag caused by trailing edge flap deflection was obtained from Figure 2-68 of that reference. Lift coefficient for each flight-test case was calculated from the known gross weight, wing area, flight speed, and standard-atmosphere air density. Induced drag coefficient was calculated from the lift coefficient and wing geometry by use of Eq. (2-86) of Ref. 20. Resulting calculated variations of total drag coefficient with lift coefficient, at lift coefficients corresponding to flight conditions, generally were within 10% of available unpublished flight test data for one of these aircraft with landing gear retracted and flaps both retracted and extended. As had been recommended in Ref. 14, drag coefficient of the landing gear (referenced to wing planform area) was taken equal to the ratio of total landing-gear frontal area to wing planform area. Airfoil velocity distributions, and therefore the trailing edge velocity, were calculated for each airfoil shape and lift coefficient by use of tables in Ref. 21.

[20]Perkins, C. D. and Hage, R. E.: Aircraft Performance, Stability, and Control. John Wiley & Sons, Inc., New York, 1949.

[21]Abbott, I. H. and von Doenhoff, A. E.: Theory of Wing Sections, Including a Summary of Airfoil Data. Dover Publications, Inc., New York, 1959.

5.0 COMPARISON OF MEASURED AND PREDICTED FLYOVER NOISE

5.1 Limitations of Available Data

Airframe noise data utilized for these comparisons were measured by three different organizations. The measurements and data reduction processes used in each test program are discussed here. Most of these data were obtained by NASA Dryden Flight Research Center; overall sound pressure level (OASPL) and some spectra were reported in Refs. 11, 17, and 22. Tabulated flyover spectra were supplied by NASA for the 0.1 second time increment which yielded maximum OASPL. These spectra were adjusted by NASA for the difference between atmospheric attenuation at the measured temperature and humidity and that for a standard atmosphere, over a path length equal to flight altitude h. They were further adjusted by NASA to a 500 ft altitude by adding the increment 20 log (h/500) at all frequencies, plus the change in standard-atmosphere attenuation over the distance (h-500) at each center frequency. Values of OASPL and perceived noise level (PNL) were calculated by NASA for the resulting spectra. Such spectra have been described by NASA as maximum OASPL condition, corrected to standard atmosphere and 500 ft altitude. The aircraft geometric position at this measurement time was not specified. These data had been measured with microphones flush-mounted in large flat plates laid over the ground. To obtain sound levels that could be compared with predictions for tripod or post-mounted microphones as for FAA noise certification measurements, the tabulated values of OASPL, PNL, and one-third octave SPL were decreased 3 dB. The assumption that a 3 dB decrease in all one-third octave SPL's produces a 3 dB decrease of PNL is not rigorous but introduces less than 1 PNdB error at the maximum amplitude for these data. Values of A-weighted sound pressure level, dB(A), were calculated for these decreased-amplitude spectra as part of this contract.

Spectra measured by Lockheed-California Co. and tabulated in Ref. 9 were obtained as the maximum measured values in each one-third octave band during each flight. The resulting composite spectra therefore consists of individual one-third octave maxima which did not all occur at the same instant of time. However, OASPL of these composite spectra only slightly exceeded the largest measured value of OASPL. Measured spectra and OASPL were presented in two forms. The actual composite spectra and their OASPL's were tabulated. Also, smoothed spectra were plotted. These smooth curves eliminated strong ground reflections at low frequencies, narrowband-random peaks caused by feathered propellers, and discrete peaks caused by airframe protrusions such

[9] Hersh, A. S., Putnam, T. W., Lasagna, P. L., and Burcham, F. W., Jr.: Semi-Empirical Airframe Noise Prediction Model. AIAA Paper 76-527, July 1976.

as radio antennas. OASPL's for the smoothed, idealized spectra also were tabulated. The smoothed data were regarded in Ref. 9 as representing fundamental airframe noise excluding the peculiarities of each specific airframe and measurement installation. These data were taken with tripod-mounted microphones and correspond to 500-ft flight altitude, unspecified atmospheric properties, and no corrections for atmospheric attenuation. Values of PNL and dB(A) for the selected spectra were calculated from both tabulated and smoothed spectra as part of this contract.

Spectra measured by NASA Lewis Research Center (Refs. 23 and 24) were presented as functions of the retarded-time direction angle. These one-third octave spectra exceed the engine noise for only a limited frequency range. NASA had fitted the normalized spectrum curve of Ref. 9 to these data. The resulting smoothed extrapolated spectra were utilized by NASA to calculate airframe-noise maximum OASPL and the variation of PNL with direction angle. The spectra were measured with tripod-mounted microphones and were not corrected for ground reflection.

Calculated spectra and integrated amplitudes utilized for comparison with these data were evaluated for the retarded-time angle, in 10 deg increments, that gave maximum OASPL. Calculated maximum PNL always occurred at the same angle as maximum OASPL. Individual calculated one-third octave sound pressure levels could exceed these levels because of Doppler shifts between the airframe-fixed and ground-fixed coordinate system and different directivity shapes for various noise mechanisms. Composite spectra comprising the largest calculated one-third octave SPL's during a flyover would be within 1 dB of the spectra presented.

5.2 Aircraft for Noise Comparisons

The aircraft for which measured and calculated noise spectra were compared had been chosen to provide a large range of type and shape. Within each type, the specific aircraft chosen was one for which data existed over a range of flight configurations. Another constraint was the need to choose aircraft for which propulsion-system noise did not overwhelm the airframe noise.

[23]Burley, R. R.: Preliminary Measurement of the Airframe Noise From an F-106B Delta Wing Aircraft at Low Flyover Speeds. NASA TM X-71527, March 1974.

[24]Burley, R. R.: Suppressor Nozzle and Airframe Noise Measurements During Flyover of a Modified F-106B Aircraft With Underwing Nacelles. ASME Paper 74-WA/Aero-1, Nov. 1974.

Data are available for the Boeing 747 (Ref. 11) and Lockheed C-5A (Ref. 25) large wide-body jet transports and the Convair 990 (Ref. 11) and Vickers VC 10 (Ref. 12) four-engine and BAC 1-11 (Ref. 12) two-engine narrow-body jet transports. Spectra for the C-5A have the disadvantage that engine noise at and above fan blade passing frequency was dominant at frequencies that strongly affect annoyance-weighted noise levels. Also, flyover altitude was roughly equal to the wing span so the data may not have been far-field. The BAC 1-11 and Convair 990 were only tested at three of the four combinations of flap and gear position (clean airframe, landing gear extended, trailing edge flaps extended, and both gear and flaps extended). Spectra were available for the Vickers VC 10 over the largest range of configurations (three flap deflections). However, calculated flyover spectra are available for the Boeing 747 as given by the highly detailed airframe noise component prediction of Ref. 4. That method had not been evaluated by any published comparisons with data. Therefore, use of the Boeing 747 as a test airframe would allow evaluation of an additional airframe noise prediction method. Data from the Vickers VC 10 and Convair 990 were used, however, in developing the airframe noise component method given herein.

Data are available for two business jets, the Lockheed JetStar (Refs. 11 and 17) and Hawker Siddley 125 (Ref. 12). The same range of configurations (clean, gear extended, flaps extended, flaps and gear extended) were available for both aircraft. However, spectra for the Hawker Siddley 125 were clearly dominated by engine noise at and above 1600 Hz center frequency even with the flaps and landing gear extended. Also, spectra calculated by the drag element method had been published (Ref. 14) for the JetStar. Proper use of the NASA ANOPP computer program for this method could be checked by seeing whether an independent estimate of aerodynamic inputs for this aircraft would yield the same predicted spectrum.

Another important class of general-aviation airframe is the light twin-engine propeller-driven aircraft. The only aircraft for which spectra were available both in the clean configuration (Ref. 9) and with landing gear and flaps extended (Ref. 17) was the Aero Commander Shrike. Data were supplied by NASA for gear extended and both gear and flaps extended at on airspeed, and gear extended at a higher airspeed. Clean-airframe data existed at both those airspeeds.

Sailplane noise data were of interest because there is no question of contamination from propulsive-system noise. As noted in Ref. 4, much of the sailplane noise data are relatively old and had been measured at low flight

[25] Gibson, J. S.: Nonengine Aerodynamic Noise Investigation of a Large Aircraft. NASA CR-2378, Oct. 1974.

altitudes. The data of Ref. 9 for the Prue-2 sailplane avoided these difficulties. Comparisons were made at three airspeeds to evaluate the unexpected poor agreement found between data and predictions which used one of the specified methods.

Finally, the Convair F-106B delta-wing supersonic aircraft (Refs. 23 and 24) was picked as a small-scale representative supersonic transport configuration. Aircraft with low aspect ratio wings, such as this and the Handley Page 115 (Ref. 12), tend to have their airframe noise levels greatly overestimated by simple prediction methods. Directivity had been measured for the F-106B.

The resulting aircraft configuration test cases and run numbers are listed in Table 1. They comprise a total of thirteen configurations and five airframes. Because comparisons were made for some configurations at more than one airspeed, a total of seventeen cases were examined. The airspeeds for these cases, along with measured and predicted OASPL, dB(A), and PNL, are given in Table 2. Measured and predicted spectra are plotted in Figures 27 through 41. Other comparisons are given in Figures 42 through 45. Tabulated spectra and airframe geometric properties are given in Tables 3-8 of Appendix III.

5.3 Prue-2 Sailplane

Spectra measured with this aircraft in two runs at each of three nominal airspeeds are plotted in Figures 27 through 29. The lower run number for each set of data denotes a gross weight 81% of that for the higher run number. Predicted spectra are shown for the NASA ANOPP total aircraft method and drag element method, and for the FAA noise component method developed under this contract. The difference in gross weights was calculated to cause a 0.6 dB change in spectrum levels for the total aircraft method and less than 0.1 dB for the other methods. Only one calculated curve is shown for each method.

At the lower two velocities, the strongest individual one-third octave bands were below 200 Hz center frequency and had amplitudes approximately independent of velocity. Measured OASPL's were dominated by the low-frequency background noise, which had been faired out of the smoothed spectra. Spectra calculated by the NASA ANOPP total aircraft noise method generally matched these measured high values of OASPL. However, they were about 8 dB above the measured spectra for center frequencies greater than 1000 Hz. PNL and dB(A) were overpredicted by about the same increment. This method had previously been evaluated in Refs. 3 and 4 by comparing only the measured and calculated OASPL. Good agreement had been obtained, as shown in Table 2.

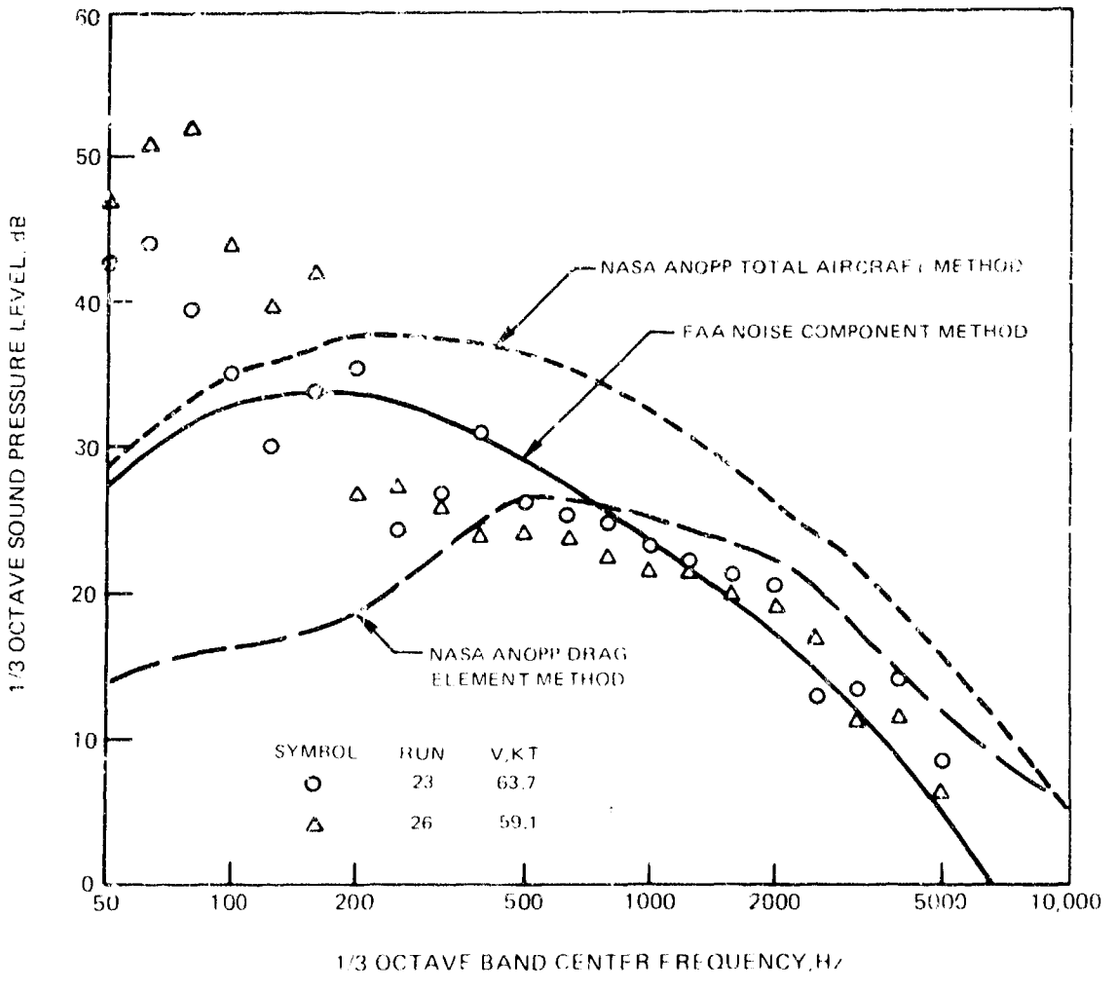

FIGURE 27 - COMPARISON OF MEASURED AND CALCULATED FLYOVER NOISE SPECTRA FOR PRUE-2 SAILPLANE AT 61 KNOTS AIRSPEED

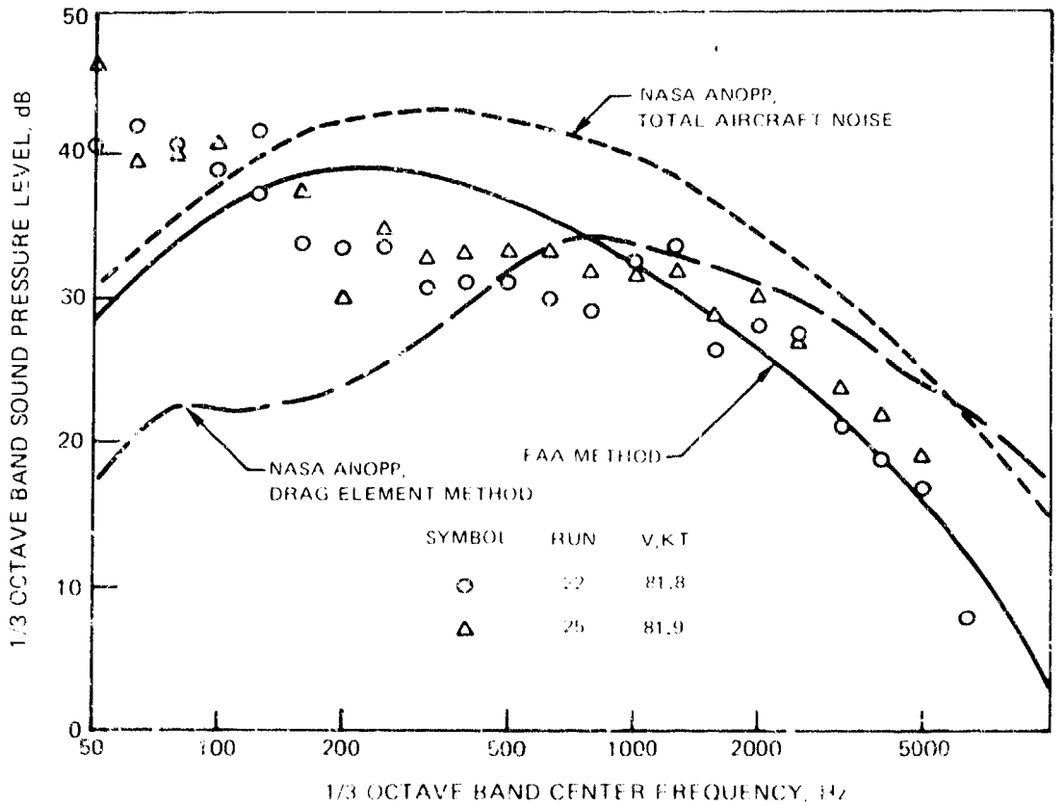

FIGURE 28 - COMPARISON OF MEASURED AND CALCULATED FLYOVER NOISE SPECTRA FOR PRUE-2 GATE PLANE AT 80 KNOTS AIRSPEED

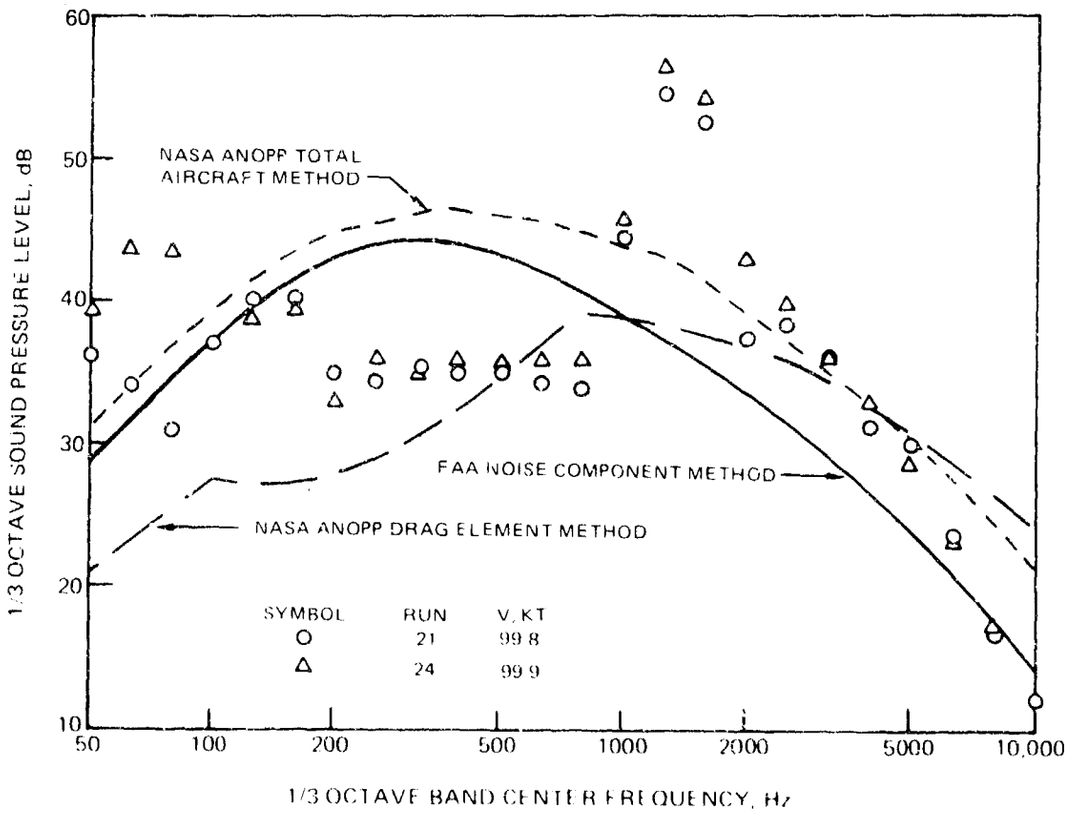

FIGURE 29 - COMPARISON OF MEASURED AND CALCULATED FLYOVER NOISE SPECTRA FOR PROP-2 AIRPLANE AT 100 KNOTS AIRSPEED

The NASA ANOPP drag element method underpredicts the data at low frequencies and overpredicts at high frequencies. It gives good predictions of annoyance-weighted noise levels even though the spectrum shape is not closely matched. The FAA noise component method comes closer to the general trend of the data. The calculated curve tends to be parallel to the data at highly weighted frequencies (1000 to 4000 Hz). This method also gives good predictions of annoyance-weighted noise levels.

Data for the highest airspeed of 100 knots (Figure 29) are dominated by a laminar instability tone that protrudes 20 dB above the lower-frequency base. This combination of roughly 1400 Hz frequency and 100 knots airspeed was calculated by the method of Ref. 10 to be associated with Tollmein-Schlichting laminar instability at the trailing edge of a 17 in. chord surface. That dimension corresponds to the Prue-2 horizontal tailplane mean geometric chord, rather than the larger (28.5 in.) wing tip chord. Such tones are usually associated with low Reynolds number and therefore low flight speed, if radiated by the wing. Evidently this tone can occur only for the proper range of horizontal tail deflection, which is a function of airspeed. OASPL given by the NASA ANOPP total airframe method approximately matches that of this narrowband-random peak. Both the total airframe method and drag element method generally match the measured one-third octave levels at frequencies above this peak, between 2000 and 5000 Hz center frequency. These measured levels may be dominated by harmonics of the laminar instability peak. The FAA noise component method underpredicts those levels but is close to the data below 200 Hz and above 6300 Hz center frequencies.

Laminar instability tones can be eliminated by tripping the boundary layer upstream of the trailing edge. Inability of the noise component method to predict such noise is unimportant. Tone noise can be identified by the frequency prediction of Ref. 10 and eliminated at negligible cost in weight and friction drag.

5.4 Aero Commander Shrike

Measured spectra (Ref. 9) for the Aero Commander Shrike at 154 knots in the clean configuration and two gross weights are plotted in Figure 30. Both piston engines were off and the propellers were feathered. The lighter weight was 78% of the heavier weight. No systematic effect of gross weight occurred in the data. Peak amplitudes in the spectra occurred as a possible ground reflection near 100 Hz and noise from the feathered propellers in the 315 and 400 Hz one-third octave bands. The spectrum calculated by the NASA ANOPP total aircraft method has an OASPL which matches that of the actual data including these peaks. This method progressively overestimates the measured one-third octave SPL's as frequency is increased above 400 Hz. Closer agreement would have been obtained by that method if OASPL had been decreased

several dB and peak frequency had been reduced by about two one-third octave bands. Spectra calculated by both the drag element method and the noise component method are in good agreement with each other and with the data between 500 and 4000 Hz frequencies. Both methods therefore closely predict annoyance-weighted noise levels.

An Aero Commander Shrike had been tested by NASA Dryden Flight Research Center (Ref. 17) at this airspeed and the smaller gross weight with landing gear extended. Both the nose and main gear have single wheels. Acoustic data were measured with flush-mounted microphones. Reported levels were decreased 3 dB for comparison with these predictions. Resulting adjusted levels are plotted in Figure 31. This spectrum is considerably higher than that for the clean airframe (Figure 30) below 125 Hz because of landing gear cavity noise. It matches the propeller-noise peak of the clean airframe at 315 and 400 Hz, is about 6 dB higher near 1000 Hz, and decays to the clean-aircraft levels above 5000 Hz. Landing gear noise is calculated by the drag element method to peak at a relatively low frequency. Thus the cavity noise is qualitatively predicted near 50 Hz, but the calculated spectrum matches that calculated for the clean airframe above 400 Hz. The drag element method therefore underpredicts annoyance-weighted noise levels for this configuration. In contrast, the noise component method underpredicts the low-frequency cavity noise but closely predicts the landing gear noise spectrum at high-annoyance frequencies. Both methods overpredicted the measured noise above 5000 Hz frequency.

Spectra for the clean configuration (Ref. 9) at 113 knots are plotted in Figure 32. Amplitudes of the low-frequency peaks at 100 and 315 Hz center frequencies match those shown in Figure 30 for this aircraft at 153 knots airspeed. The spectrum predicted by the total aircraft method ranges from about 6 to 10 dB above the data above 500 Hz center frequency. As with the comparison at the higher airspeed, this predicted spectrum appears to be displaced about two one-third octave bands too high in frequency in addition to being about 5 dB high in amplitude. The drag element and noise component methods closely match the data at frequencies above the feathered-propeller noise peak.

NASA spectra for this airspeed and two flights, one with the landing gear extended and one with landing gear and single-slotted trailing edge flaps extended, are shown in Figure 33. Extending the flaps decreased the low-frequency noise from the landing gear cavity but increased the noise several dB at greater than 200 Hz center frequency. Thus OASPL was decreased but PNL was increased by flap extension with the landing gear down. As at the higher airspeed (Figure 31), noise radiated by the airplane with landing gear down was underpredicted by the drag element method and was closely predicted by the noise component method. Noise measured with both the gear and flaps down, at frequencies above 500 Hz, was closely predicted by both methods. Data for the configuration did not extend high enough in frequency to check the

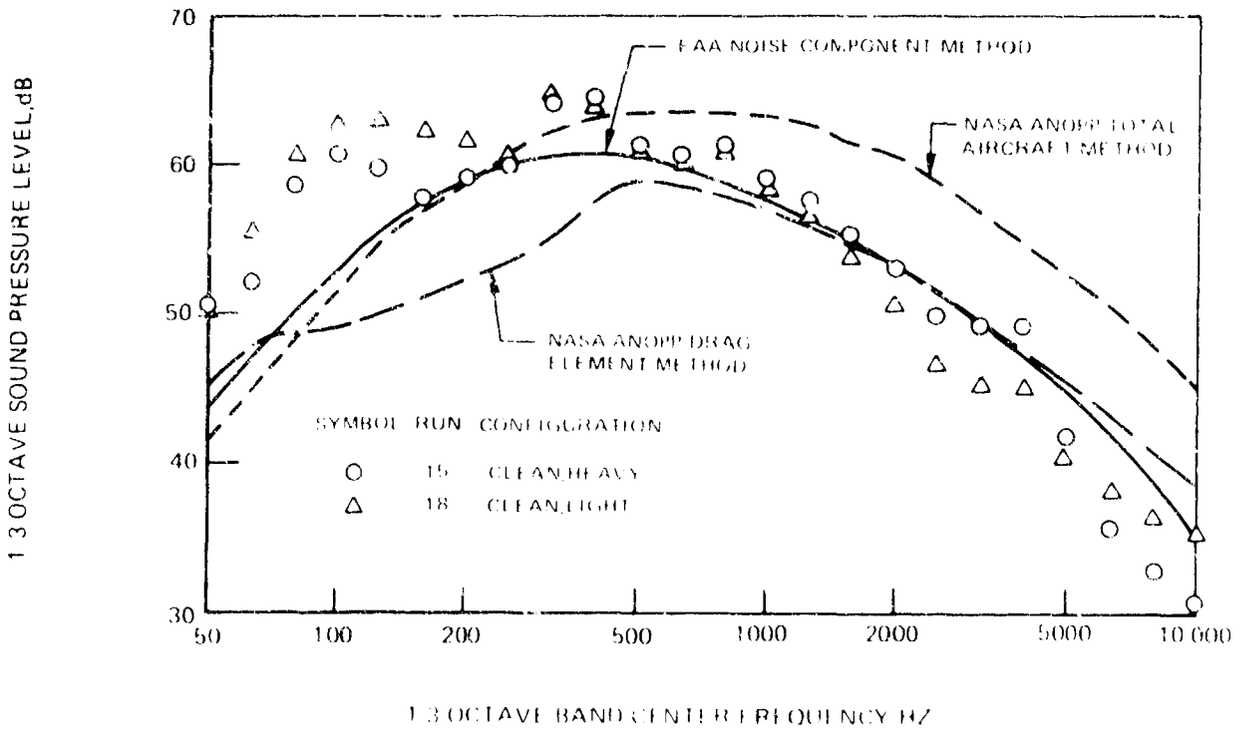

FIGURE [illegible] - COMPARISON OF MEASURED AND CALCULATED FLYOVER NOISE SPECTRA FOR AERO COMMANDER SHRIKE IN CLEAN CONFIGURATION AT [illegible] FT (305 METERS)

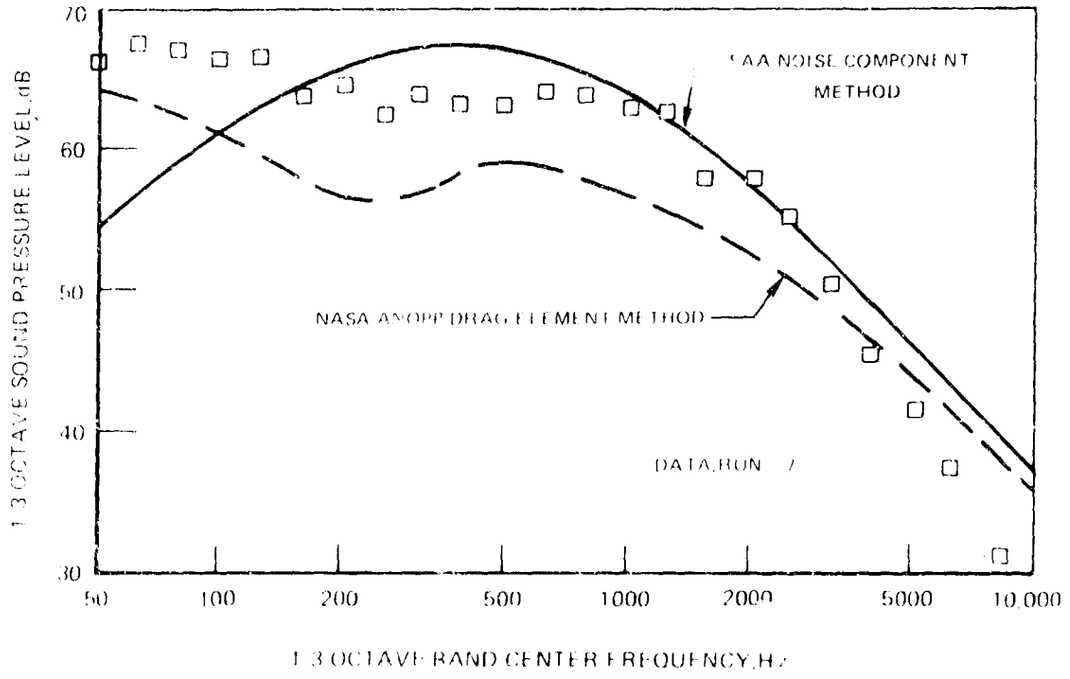

FIGURE 41 - COMPARISON OF MEASURED AND CALCULATED FLYOVER NOISE SPECTRA FOR AERO COMMANDER SHRIKE WITH LANDING GEAR EXTENDED AT 153 KNOTS AIRSPEED

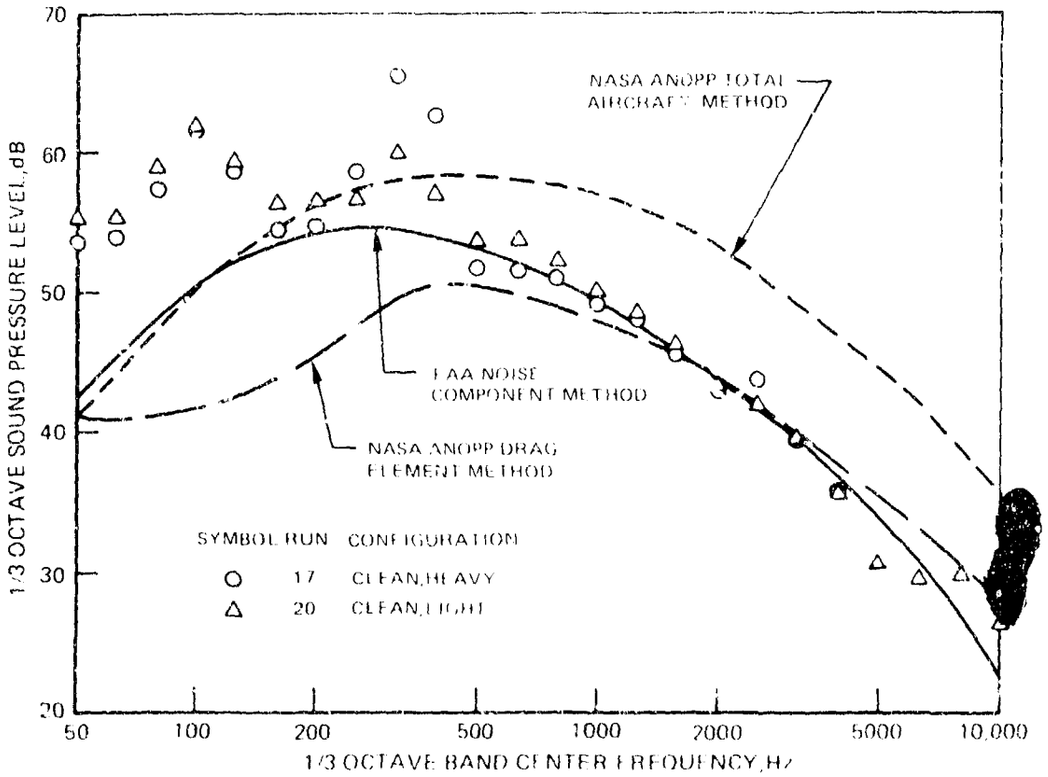

FIGURE 32 - COMPARISON OF MEASURED AND CALCULATED FLYOVER NOISE SPECTRA FOR AERO COMMANDER SHRIKE IN CLEAN CONFIGURATION AT 113 KNOTS AIRSPEED

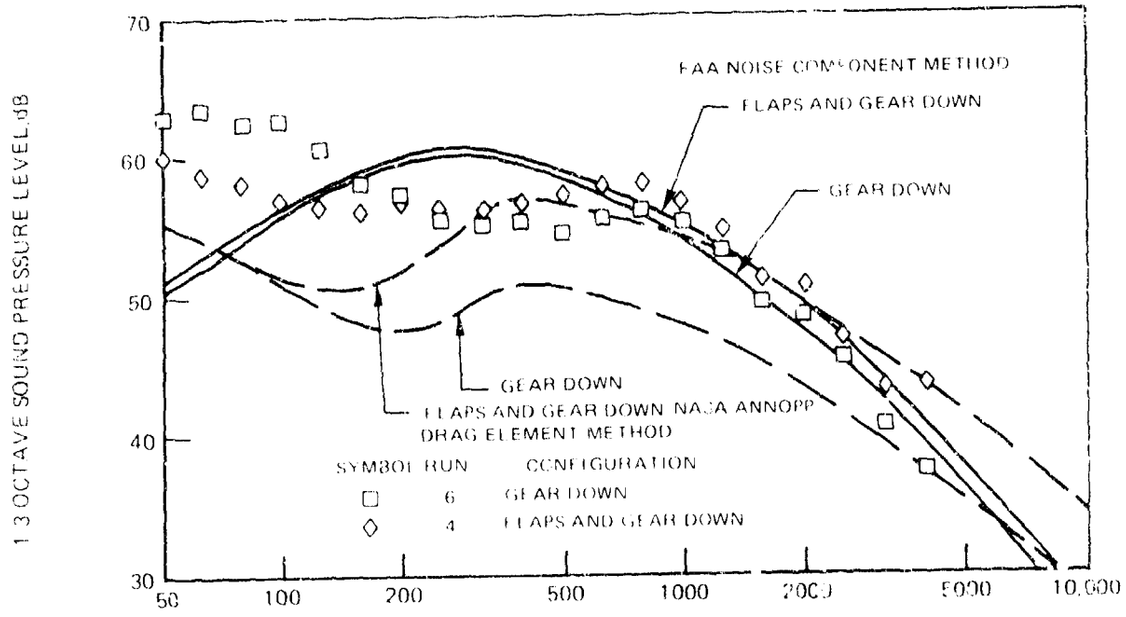

FIGURE 33 - COMPARISON OF MEASURED AND CALCULATED FLYOVER NOISE SPECTRA FOR AERO COMMANDER SHRIKE WITH LANDING GEAR EXTENDED, AND WITH LANDING GEAR AND TRAILING EDGE FLAPS EXTENDED, AT 113 KNOTS AIRSPEED

difference between predictions above 5000 Hz. Note that for the frequency range of good agreement, noise from the trailing edge flaps as predicted by the drag element method is in coincidental good agreement with the sum of measured flap and landing gear noise.

5.5 Lockheed JetStar

Noise measurements for the Lockheed JetStar business jet were obtained by NASA Dryden Flight Research Center and were reported in Refs. 11 and 17. A flyover noise spectrum for the clean configuration at 247 knots airspeed is plotted in Figure 34. This aircraft and airspeed were of interest because good agreement had been shown in Figure 10 of Ref. 14 between these data and predictions by the drag element method. The spectrum calculated by the NASA ANOPP computer program for that method, shown in Figure 34, generally matches that calculated spectrum. The total airframe method generally predicts one-third octave SPL's 15 dB above the data, and the noise component method generally is 5 to 10 dB low.

One peculiarity of spectra presented in Refs. 11 and 17 for clean jet aircraft was a peak located near 1600 Hz for a range of aircraft size (Lockheed JetStar, Convair 990, and Boeing 747) at all flight speeds. Calculations therefore were repeated for the JetStar in clean configuration and 358 knots, the highest speed for which data were available. The comparison of calculations and data for this condition is given in Figure 35. Here, spectra determined from the drag element method and the noise component method are about 10 dB apart. The measured spectrum is consistently lower than that from the drag element method. It is above the noise component method except for good agreement near 500 Hz and above 5000 Hz frequencies.

These data were obtained by NASA with the engines set at whatever thrust level provided steady level flight. Thrust and therefore engine noise had been increased to achieve the higher airspeed. The JetStar uses turbojet engines which generate considerable low-frequency exhaust noise and high-frequency compressor noise. It is likely that the broad peak near 1600 Hz shown in Figures 34 and 35, which dominates both OASPL and PNL, was engine compressor noise rather than airframe noise.

A further indication exists of the importance of engine noise in measurements for the clean configuration. The variation of OASPL with sideline distance for this aircraft had been plotted in Figure 9 of Ref. 17. It was noted that OASPL varied inversely with measurement distance squared, without an angular directivity dependence as would be expected for airframe noise. These spectra had been requested from NASA Dryden Flight Research Center for analysis in this study. They were not supplied because they were stated to be contaminated by engine noise at most measurement directions.

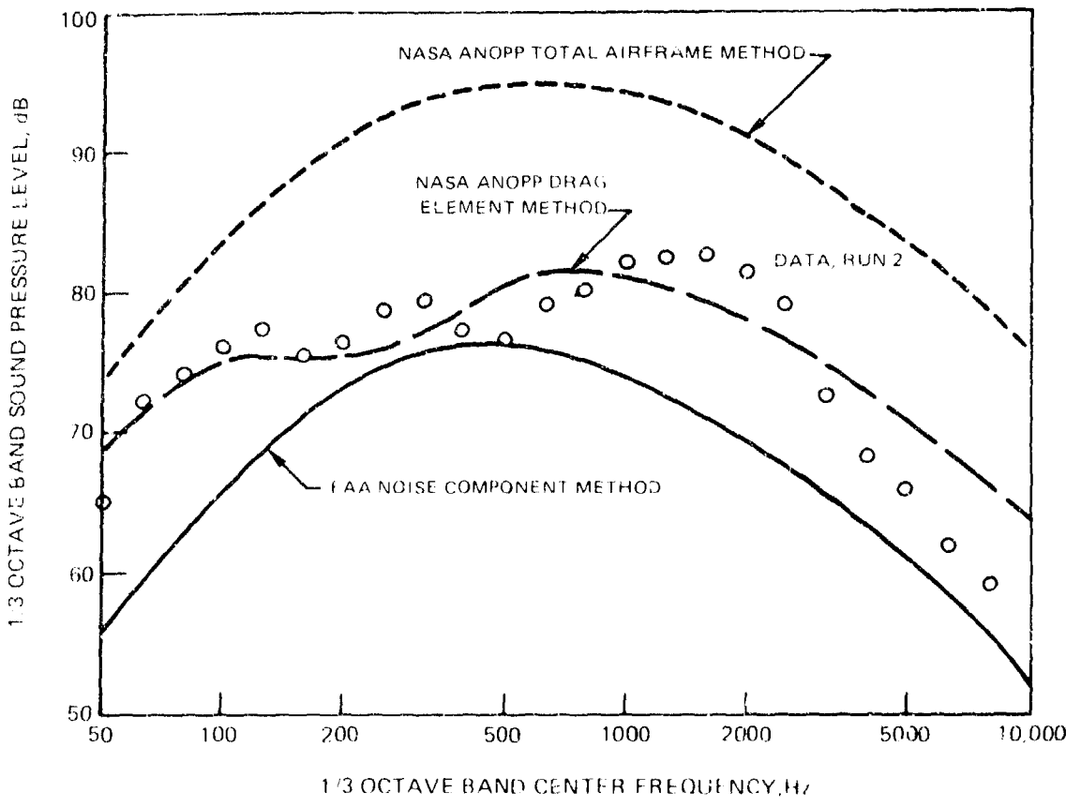

FIGURE 4b - COMPARISON OF MEASURED AND PREDICTED FLYOVER NOISE SPECTRA FOR LOCKHEED JETSTAR IN CLEAN CONFIGURATION AT 250 KNOTS AIRSPEED

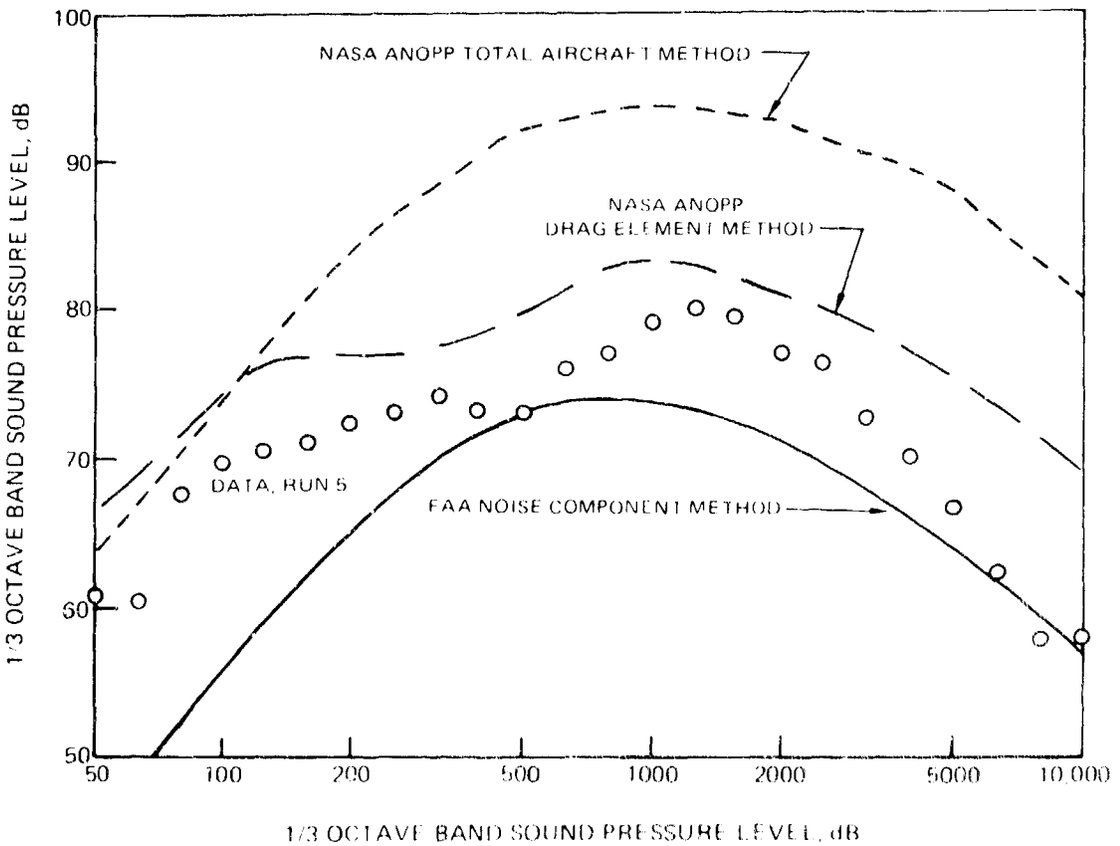

FIGURE 35 -COMPARISON OF MEASURED AND PREDICTED FLYOVER NOISE SPECTRA FOR LOCKHEED JETSTAR IN CLEAN CONFIGURATION AT 365 KNOTS AIRSPEED

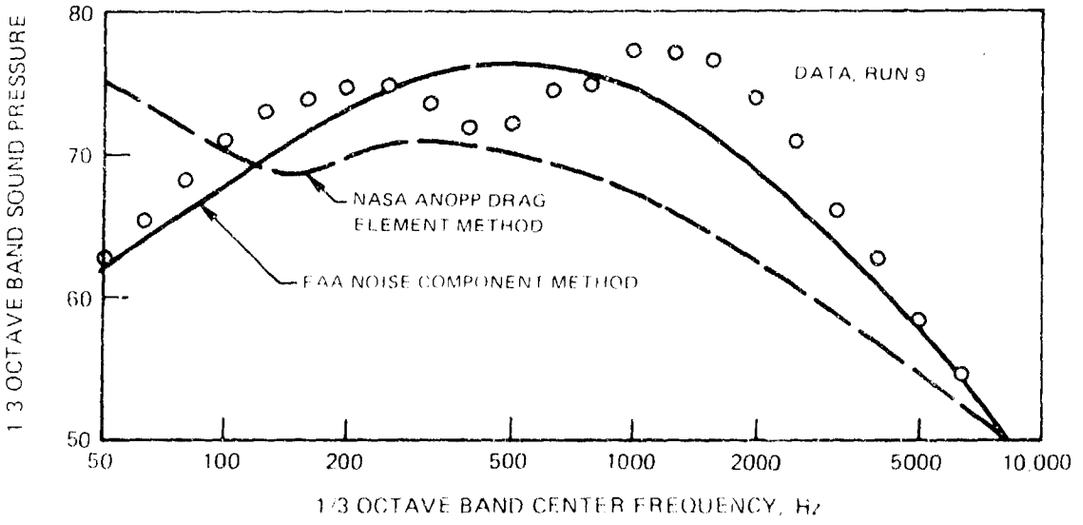

FIGURE 20 - COMPARISON OF MEASURED AND CALCULATED FLYOVER NOISE SPECTRA FOR LOCKHEED JETSTAR WITH LANDING GEAR EXTENDED AT 150 KNOTS AIRSPEED

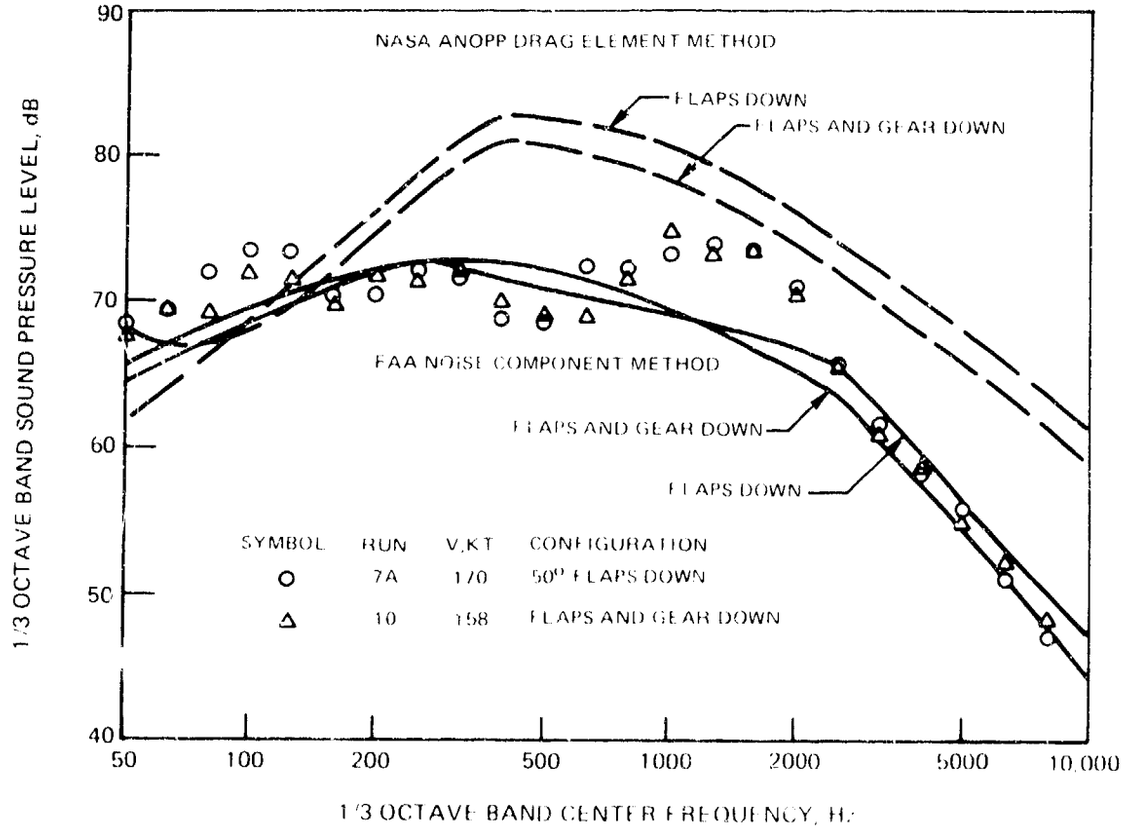

FIGURE 37 - COMPARISON OF MEASURED AND CALCULATED FLYOVER NOISE SPECTRA FOR LOCKHEED JETSTAR WITH TRAILING EDGE FLAPS EXTENDED AT 170 KNOTS AND WITH FLAPS AND LANDING GEAR EXTENDED AT 158 KNOTS

A spectrum for this aircraft at 182 knots with landing gear down is plotted in Figure 36. As with the comparison for the Aero Commander Shrike, landing gear noise as calculated by the drag element method was predicted to occur only at low frequencies. This method underestimated the measured noise by about 10 dB between 1000 and 2500 Hz and about 5 dB over most other frequencies. The noise component method gave the general level of the data, which oscillated roughly ±5 dB relative to this prediction. Worst agreement occurred near the peak which was attributed to engine noise.

Measured spectra are shown in Figure 37 for the JetStar at 170 knots with trailing edge flaps down and at 158 knots with landing gear and flaps down. There was no systematic difference between the two spectra; the decrease of flap noise caused by reduced velocity was approximately matched by the added landing gear noise. These spectra, as with all others for different configurations of this aircraft, contain a peak from 1000 to 2000 Hz frequency. The drag element method predicts a large amount of trailing edge flap noise caused by high profile drag at 50° flap deflection. Airframe noise is generally overestimated about 10 dB for this configuration. Decreasing the airspeed and lowering the landing gear is predicted to cause about 2 dB noise reduction, contrary to the lack of change in measured levels. In contrast, the noise component method closely predicts these spectra except for the peak of apparent engine noise. This peak occurs at frequencies which are highly weighted in predicting annoyance-weighted noise levels, so the drag element method more closely predicts dB(A) and PNL. Spectra calculated by the noise component method for the two configurations and airspeeds intersect each other, in agreement with the data.

5.6 Boeing 747

A flyover peak noise spectrum for the clean configuration at 233 knots is compared with predictions in Figure 38. Both the drag element method and the noise component method predict the general level of data up to 500 Hz center frequency. Above 630 Hz the data have higher levels as would be expected for engine noise. This portion of the spectrum agrees with the noise levels predicted by the total aircraft method. The aircraft used in these tests was an early Boeing 747-100 with thin-lip inlets equipped with blow-in doors. Turbulence generated by this type of inlet and convected into the fan is known to cause engine installation noise. Current Boeing 747's use a thick-lip inlet without blow-in doors, and have less propulsive-system noise.

A test program to measure airframe noise of the McDonnell-Douglas DC-10 was described in Ref. 15. That aircraft uses a large high-bypass-ratio turbofan engine similar in general size to that in the Boeing 747. It was found necessary as part of the DC-10 tests to install additional sound-absorbing

material in the inlet, fan exit duct, and core exit duct to suppress flight-idle engine noise. Only after those changes was it possible to measure the clean-airframe noise. Thus it is likely that spectra from the unmodified larger, louder Boeing 747 were dominated by installed-engine noise at frequencies where such noise is important.

A spectrum measured for the Boeing 747 at 233 knots with landing gear extended is plotted in Figure 39. This aircraft has four four-wheel main landing gear and a two-wheel nose landing gear. As with other aircraft, the spectrum predicted by the drag element method matches that predicted for the clean airframe except at low frequencies. Measured one-third octave SPL's are underestimated by about 10 dB between 100 and 500 Hz frequencies and more than 15 dB in the apparent engine-noise peak. The noise component method is 2 to 3 dB high below 500 Hz, about 8 dB low for most of the higher-frequency peak, and in general agreement above 4000 Hz. Another predicted curve, obtained from the component prediction method described within the NASA ANOPP airframe noise document (Ref. 4), is plotted as a dot-dash curve. This curve was obtained from the predicted spectra plotted in Figures 55 and 57a of Ref. 4 for this aircraft with landing gear extended and flaps down to obtain landing-gear noise and clean-aircraft noise at 177 knots. Amplitude was scaled with velocity to the sixth power and inversely with altitude squared; frequency was scaled directly with velocity. The resulting predicted spectrum closely matches that shown for the noise component method. However, the noise component prediction is dominated by calculated landing gear noise. Landing gear noise had been calculated by the component prediction method of Ref. 4 to be about 15 dB below the clean wing and horizontal tail noise at the frequencies shown. Landing gear noise as given by that method appears only as cavity noise at very low frequencies. Thus the spectrum shown for the component prediction method really applies to clean airframes. Comparing with the clean-airframe spectrum shown in Figure 38, it would match the general level of the engine-attributed noise above 800 Hz but would be more than 10 dB higher than most of the lower-frequency data. The agreement shown in Figure 39 between data and the component prediction method for the aircraft with gear down therefore is fortuitous.

Spectra measured with the Boeing 747 at approximately 198 knots with trailing edge flaps extended, and with flaps and landing gear extended, are plotted in Figure 40. Extending the landing gear added 3 to 4 dB at frequencies from about 250 to 5000 Hz. Spectra predicted by the drag element method for the configuration with deflected flaps are about 5 dB too high between 200 and 500 Hz and about 8 dB too low between 2000 and 6300 Hz center frequencies. The increased noise caused by landing gear extension at frequencies of interest is not predicted. The NASA-sponsored component prediction taken from Figure 56b of Ref. 4 combines spectra separately calculated for the wing, the horizontal tail, and each of the three chordwise flap segments. This prediction is only 2 to 3 dB low for most of the frequency range below the region of

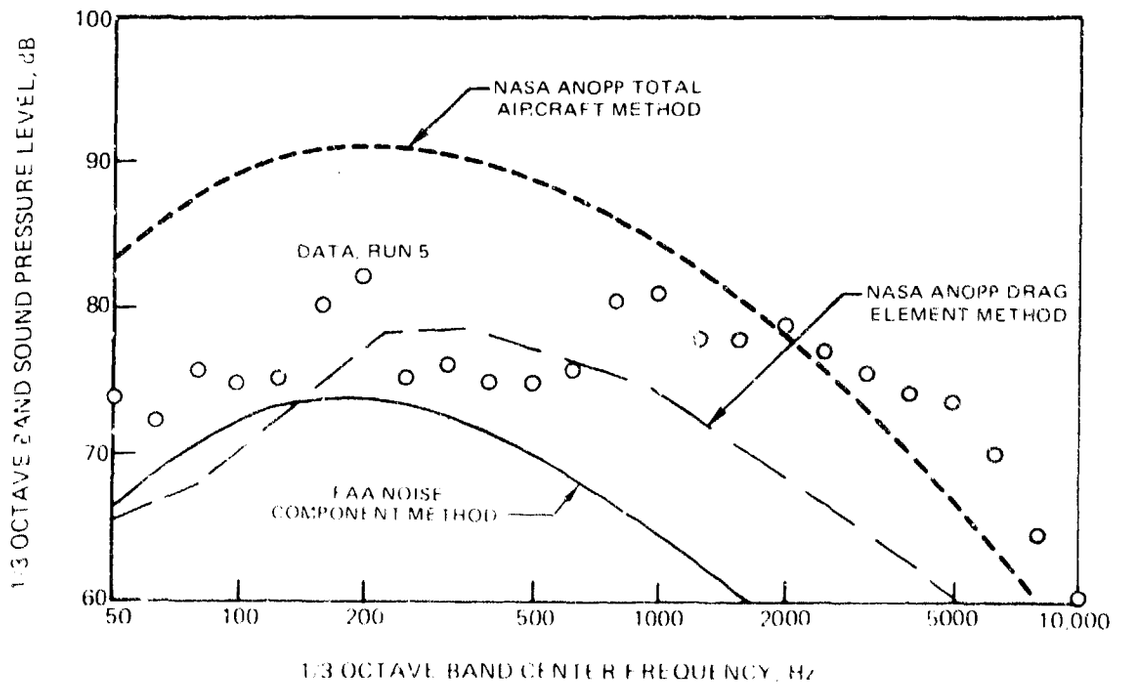

FIGURE 38 - COMPARISON OF MEASURED AND CALCULATED FLYOVER NOISE SPECTRA FOR BOEING 747 IN CLEAN CONFIGURATION AT 244 KNOTS AIRSPEED

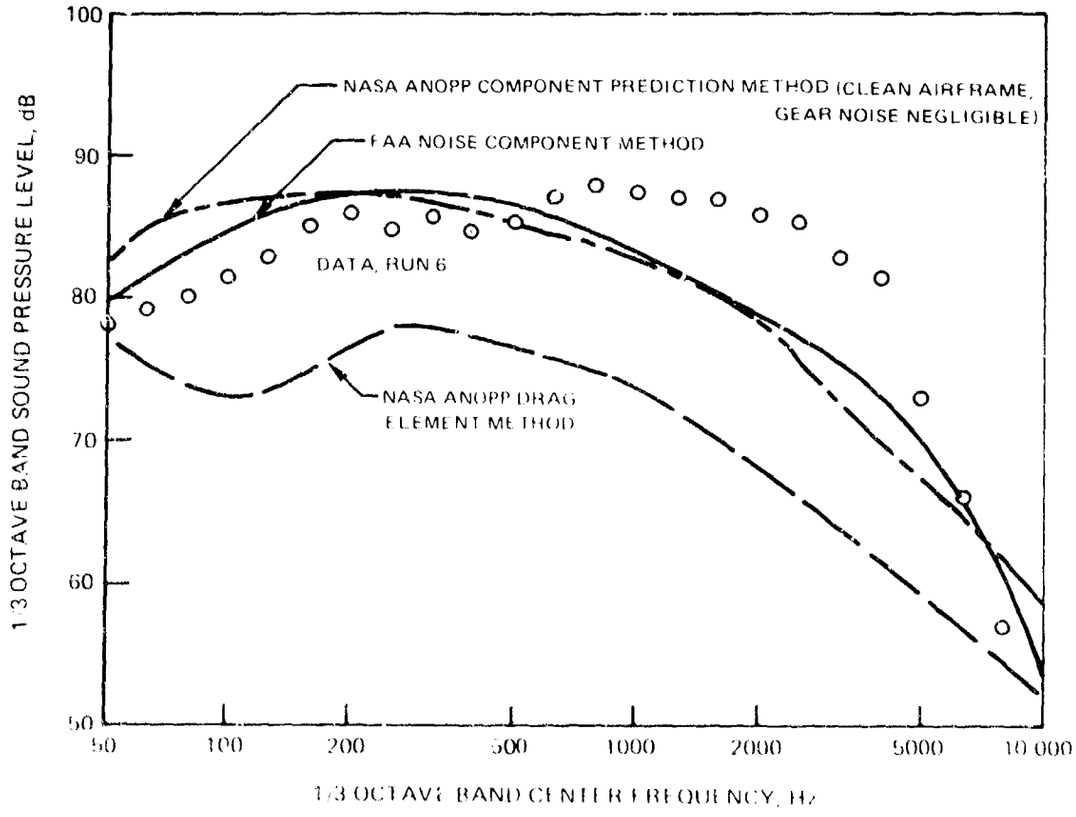

FIGURE 39 - COMPARISON OF MEASURED AND CALCULATED FLYOVER NOISE SPECTRA FOR BOEING 747 WITH LANDING GEAR EXTENDED AT 287 KNOTS AIRSPEED

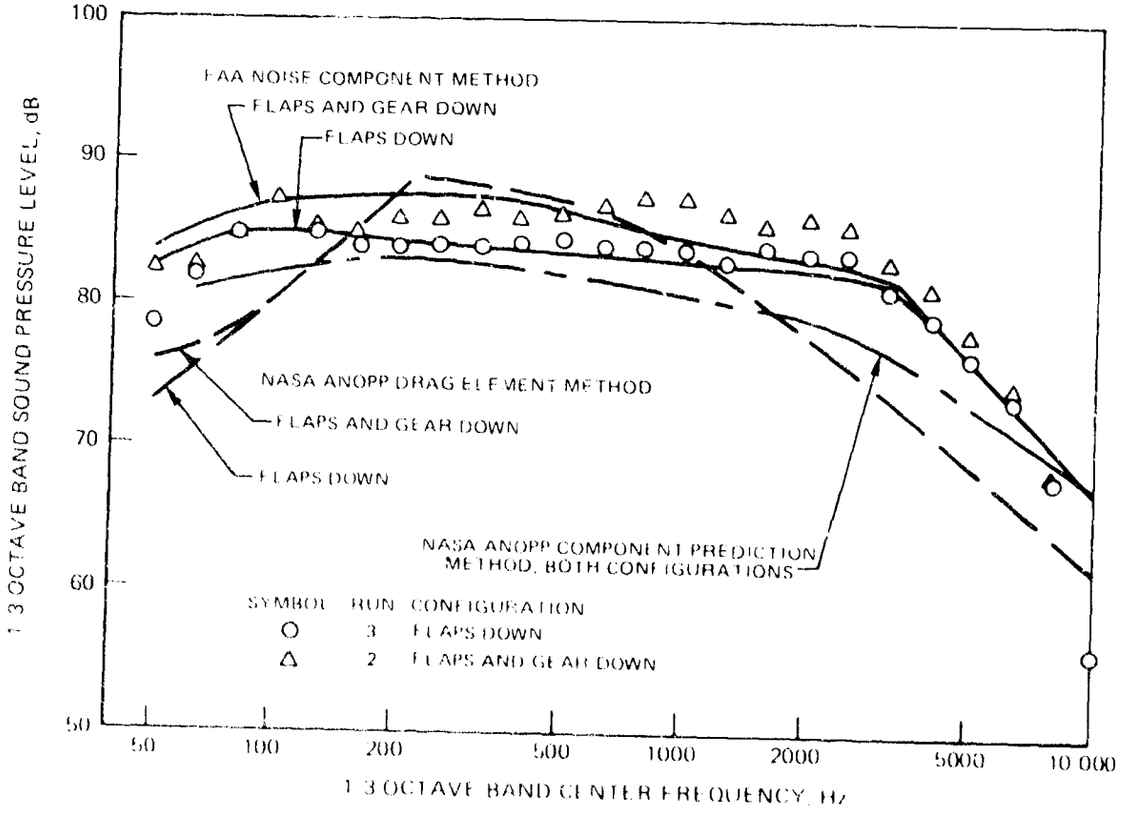

FIGURE 6c. - COMPARISON OF MEASURED AND CALCULATED FLYOVER NOISE SPECTRA FOR BOEING 727 WITH TRAILING EDGE FLAPS EXTENDED, AND WITH FLAPS AND LANDING GEAR EXTENDED, AT 200 KNOTS AIRSPEED

possible engine noise. However, this method incorrectly predicts too low a level of landing gear noise. The noise component method developed under this study closely predicts the flaps-down spectrum and generally predicts the spectrum measured with both flaps and gear down. It is about 3 dB below the data for the highly weighted range between 800 and 2500 Hz, but the closest other prediction (component prediction method) is about 7 dB too low. Both the noise component method and component prediction method gave a close approximation to the general spectrum shape. For aircraft with deflected trailing edge flaps, the drag element method gives a more sharply peaked spectrum which has the normalized shape associated with clean-airframe noise and an amplitude set by deflected-flap profile drag.

5.7 Convair F-106B

Airframe noise spectrum and directivity measurements are available from a study (Refs. 23 and 24) of in-flight jet noise suppression. In those tests, conducted by NASA Lewis Research Center, an F106B turbojet-powered supersonic delta-wing interceptor was used as a test airframe. Two small afterburning turbojets were attached beneath the aircraft. Various noise suppression devices were mounted on these turbojets, and changes in noise amplitude and spectrum were determined at supersonic transport climb-out conditions. Because jet noise has considerable variation with direction angle, the flyover noise instrumentation and data reduction was chosen to permit accurate measurement over a considerable range of aircraft position. Airframe noise was determined as background noise that would have to be subtracted from the total noise spectrum at each direction angle. The spectrum of measured maximum airframe noise without the small engines, at center frequencies from 200 to 1250 Hz, is shown in Figure 41 along with several predictions. The portion of the spectrum below 200 Hz was dominated by jet noise from the main turbojet at flight-idle thrust; the high-frequency portion was dominated by compressor noise from that engine. Spectra are given in Figures 7 and 11 of Ref. 23 and Figure 13 of Ref. 24 for retarded-time direction angles from 60° to 80°. Also, the normalized spectrum shape given in Figure 4 of Ref. 5 had been fitted to this airframe noise portion of the spectrum to allow calculation of maximum OASPL.

The total aircraft noise method overpredicts the measured spectrum by 20 to 30 dB. As noted on p 31 of Ref. 4, this measurement was specifically excluded from the least-squares data correlation utilized in developing that method. This 20 to 30 dB overestimate also occurs (not shown here) if the total aircraft noise method is applied to predicting airframe noise from the Handley Page HP-115 low aspect ratio delta-wing aircraft (Ref. 5).

The drag element method predicts a spectrum that generally agrees with the data. A comparison between these data and a calculation by this method had been shown in Figure 11 of Ref. 14, the major presentation of the drag element method. The calculated curve shown in that figure is less wavy, somewhat larger in amplitude, and in closer agreement with the data. Differences between these two spectra calculated by the same method reflect differences in aerodynamic coefficients and wing trailing edge velocity ratio estimated for the same aircraft in these two studies and small differences in the Lockheed-California and NASA ANOPP computer programs.

Two curves are shown for the noise component method. The method as programmed uses a relatively simple analytical expression for wing trailing edge noise spectrum. This prediction matches the general level of the data for low frequencies but gives too small a peak frequency and too rapid a decay. However, that result had found (Figure 4) to underestimate the high-frequency noise at wing taper ratios less than 1/4. The spectrum therefore was recomputed for zero taper ratio. The resulting curve would be about 1 dB lower near peak frequency and, as shown in Figure 41, does not give as bad an underestimate (6 dB rather than 9 dB) at 1250 Hz frequency. The noise component method clearly gives a worse prediction than the drag element method for this supersonic-transport type of highly tapered low aspect ratio wing.

By use of a normalized spectrum fitted to these data for different direction angles, the variation of OASPL with direction angle had been obtained and was given in Figure 10a of Ref. 23. This variation is reproduced in Figure 42. Maximum OASPL and PNL occurred near 70° from the approach direction. Also shown are directivities calculated by the three prediction methods. Both the total aircraft method and drag element method as programmed by NASA have the directivity of a lift dipole with convective amplification. For this flight Mach number of 0.4, the calculated directivity is relatively constant between 60° and 4° from upstream. The noise component method, which uses the directivity of trailing edge noise without convective amplification, also gives relatively constant levels in this angle range. The data agree with this predicted trend. At larger angles the calculated amplitude for a convected lift dipole decays more rapidly than that for trailing edge noise. The data follow the less rapid decay used in the noise component method. The original calculation of directivity for the drag element method, Eq. (7) of Ref. 14, was that for a lift dipole without convective amplification. That directivity would be maximum at 90° angle and symmetrical about that angle, in poor agreement with data.

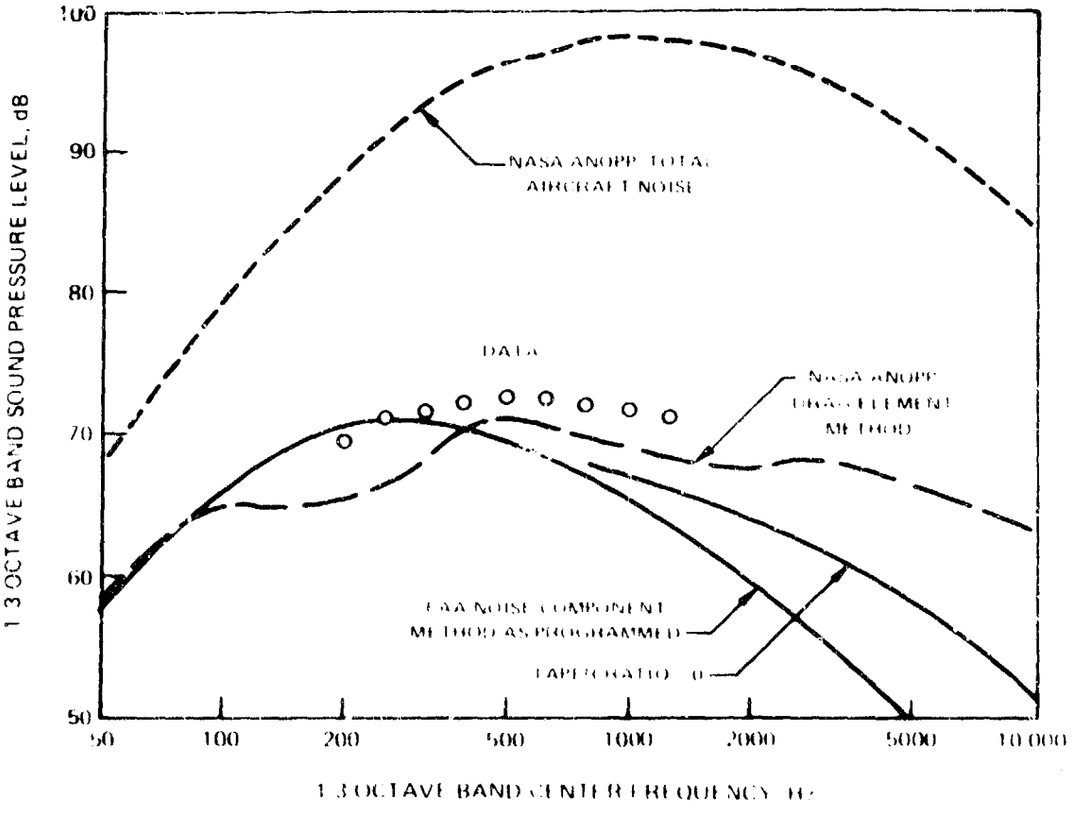

FIGURE 61 - COMPARISON OF MEASURED AND PREDICTED FLYOVER NOISE SPECTRA FOR CONVAIR F-106B TA CLEAN CONFIGURATION AT MACH 0.9 AND [illegible]

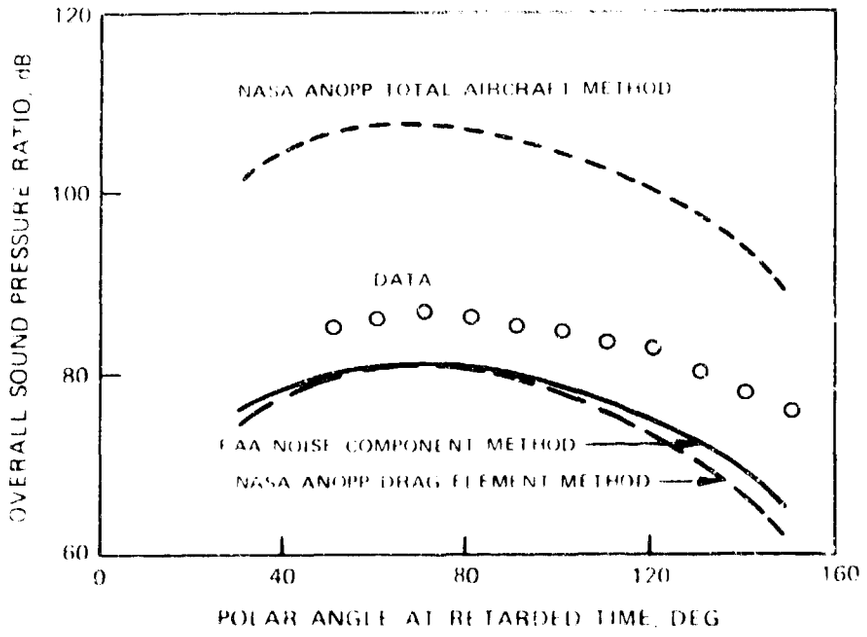
120
100
80
60
0
40
80
120
160
OVERALL SOUND PRESSURE RATIO, dB
NASA ANOPP TOTAL AIRCRAFT METHOD
DATA
FAA NOISE COMPONENT METHOD
NASA ANOPP DRAG ELEMENT METHOD
POLAR ANGLE AT RETARDED TIME, DEG

[illegible]

5.8 Additional Aircraft

To further evaluate this noise component method, flyover spectra were also calculated for several other airframes for which tabulated data were available. Measured spectra had been given in Ref. 9 for the Douglas DC-3 and Convair 240 twin-engine propeller-driven transports in the clean configuration with engines off and propellers feathered. Calculations were conducted by the noise component method and the NASA ANOPP total aircraft method for these two aircraft at their highest airspeeds tested, for 500 ft altitude. Spectra measured with the Convair 990 jet transport with 30° trailing edge flap deflection, and the landing gear retracted or extended, also were compared with predictions by the noise component method.

Spectra for the Douglas DC-3 at 148 knots and the Convair 240 at 190 knots are compared with predictions in Figures 43 and 44. Both aircraft had local spectrum peaks centered at 125 Hz which caused OASPL of the actual spectra to be about 2 dB larger than that for smoothed spectra. Spectra calculated from the total aircraft method generally were about 3 dB larger than those from the noise component method. They matched the actual OASPL but overpredicted the measured spectra, particularly above 1000 Hz where large contributions to noise annoyance occur. The noise component method underpredicted the data below 200 Hz frequency but generally agreed with the data for higher frequencies.

Note that the two spectra shown in Figure 44 for the Convair 240 have essentially the same levels below 1000 Hz center frequencies but differ at higher frequencies. Spectra for test runs 5, 6, and 7 of Ref. 9 for this airplane, flown on the same day, have a more rapid high-frequency decay than those for test runs 1-4 for the same airplane and same range of airspeeds but 13% higher gross weight. This difference has proven to be important because the method for prediction of peak frequency developed in Ref. 9, and utilized in the NASA ANOPP total aircraft method of Refs. 3 and 4, was strongly influenced by these data. Peak frequency was determined from spectra measured with the Aero Commander Shrike, Douglas DC-3, and Convair 240. The first two airplanes have wing thickness ratios of 12.0% and 12.8%; their peak frequencies could have been scaled by use of either wing chord or wing maximum thickness as a length parameter for Strouhal number. The Convair 240 has 15.3% thickness ratio, so scaling the peak frequency inversely with maximum thickness reduces that frequency by about one-third octave. Spectra measured for test runs 1-4 of the Convair 240 can be shown to match those for the other two airplanes when scaled with a Strouhal number based on wing chord. However, the other three test runs for the Convair 240 would then appear to be displaced at too low a Strouhal number. Use of Strouhal number based on wing maximum thickness causes the two sets of scaled spectra for this airplane to bracket the spectra for the other two airplanes. The low measured amplitudes at high frequencies for one day's flights of the Convair 240 may have been

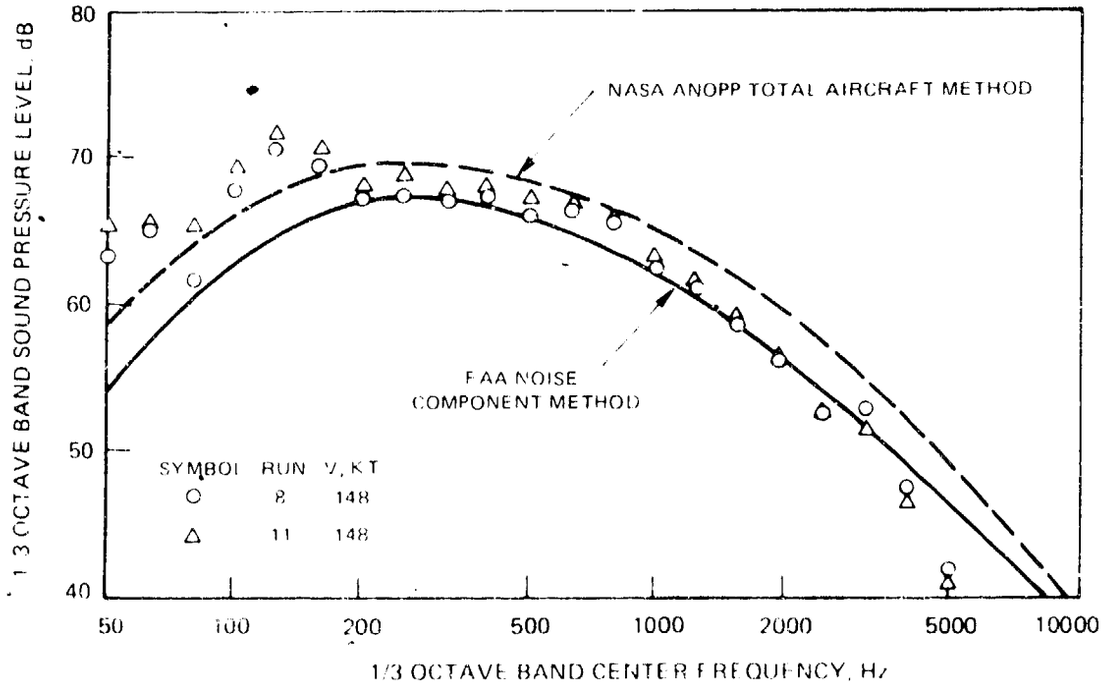

FIGURE 5-2 COMPARISON OF MEASURED AND PREDICTED FLYOVER NOISE SPECTRA FOR [illegible] IN CLEAN CONFIGURATION AT 148 KNOTS AIRSPEED

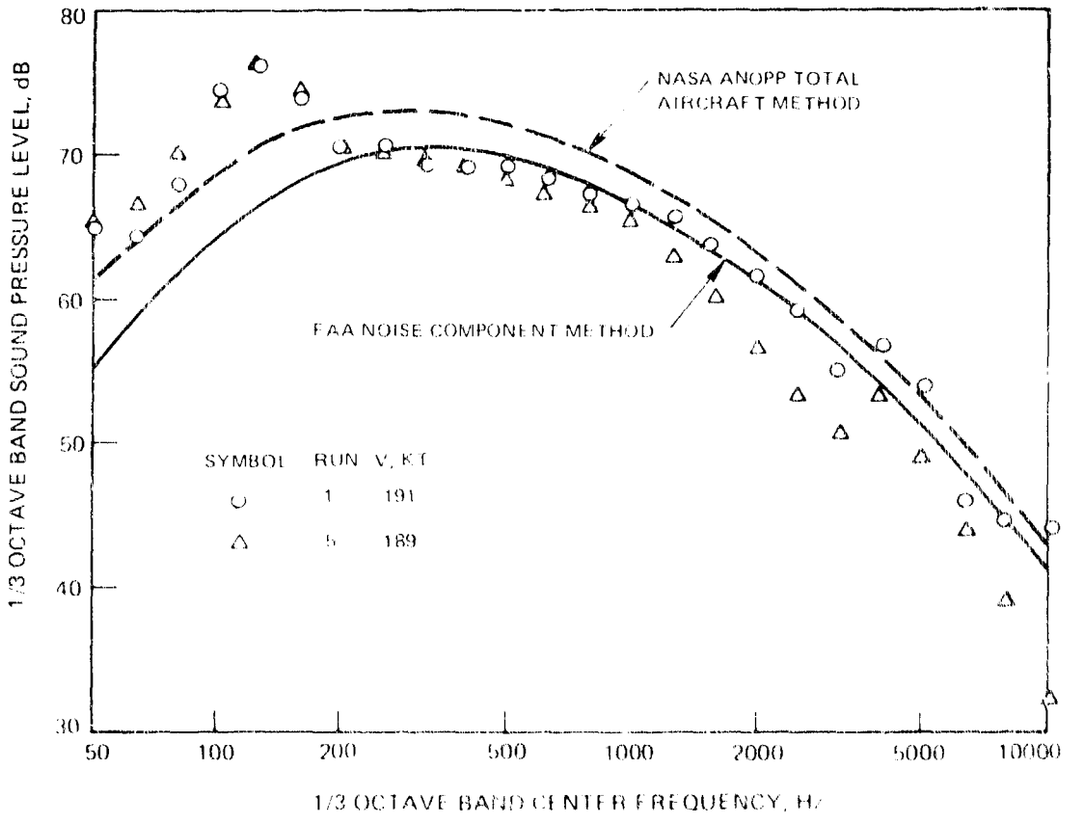

FIGURE 46. - COMPARISON OF MEASURED AND PREDICTED FLYOVER NOISE SPECTRA FOR CONVAIR 990 IN CLEAN CONFIGURATION AT 190 KNOTS AT 6 DEGREES

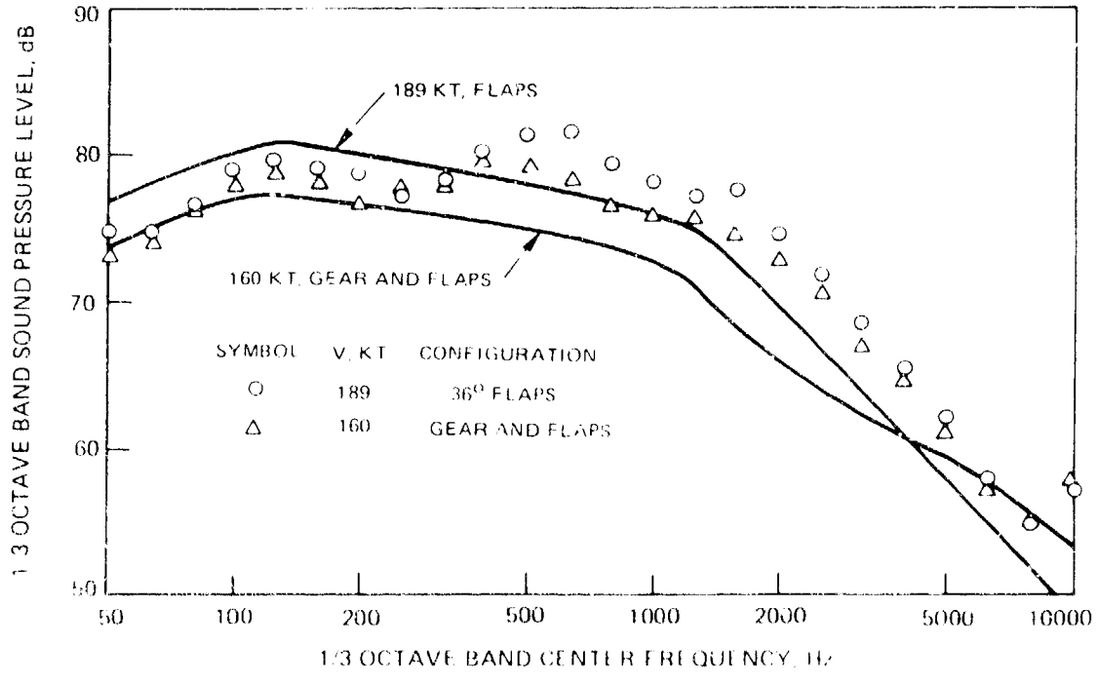

FIGURE 5. – COMPARISON OF MEASURED AND PREDICTED FLYOVER NOISE SPECTRA FOR CONVAIR 990 WITH TRAILING EDGE FLAPS DEFLECTED AT 189 KNOTS AIRSPEED AND WITH FLAPS AND LANDING GEAR DEFLECTED AT 160 KNOTS AIRSPEED

caused by a change of atmospheric humidity and therefore atmospheric attenuation that day. This difference has resulted in use of wing maximum thickness as the Strouhal number reference length for predicting clean-airframe spectra by some current methods.

A comparison of measured spectra for the Convair 990 with predictions by the noise component method is given in Figure 45. The peaks near 500 and 1250 Hz correspond to peak frequencies in the noise spectrum for the engines at idle power (Figure 4 of Ref. 26). The data for the flight with trailing edge flaps extended oscillated ± 3 dB about the prediction below 1250 Hz frequency. However, rapid decay of spectrum amplitude at high frequencies was predicted to occur about one or two one-third octave bands too low in frequency. The measured spectrum above 500 Hz frequency was underpredicted about 5 dB by the noise component method. Decreasing the airspeed, and extending the landing gear in addition to the flaps, caused about 3 dB noise reduction at midfrequencies and no reduction at low or high frequencies. The noise component method correctly predicted the size of noise reduction and its variation above 500 Hz frequency. As with the flaps-extended configuration, noise at important frequencies was underestimated by about 5 dB. Any modification to the trailing edge flap noise prediction method that would improve agreement for this aircraft would worsen agreement for the Lockheed JetStar. Additional data are needed on trailing edge flap noise, including dependence of the spectrum shape on chord of each flap segment rather than overall flap chord.

[26] White, E. C., Lasagna, P. L., and Putnam, T. C.: Preliminary Measurements of Aircraft Airframe Noise With the NASA CV-990 Aircraft. NASA TM X-73110, Jan. 1976.

TABLE 1 - FLYOVER NOISE TEST CASES

Type	Aircraft	Clean	Gear	Flaps	Both
Sailplane	Prue-2	Runs 21-26 Ref. 9			
Light Twin	Shrike	Runs 14-20 Ref. 9	Runs 6,7 Ref. 17		Run 4 Ref. 17
Business Jet	JetStar	Runs 2,5 Ref. 11	Run 9 Ref. 11	Run 7A Ref. 11	Run 10 Ref. 11
Jumbo Jet	Boeing 747	Run 5 Ref. 11	Run 3 Ref. 11	Run 6 Ref. 11	Run 2 Ref. 11
Delta	F-106B	Ref. 23			

TABLE 2 - COMPARISON OF MEASURED AND PREDICTED MAXIMUM NOISE

Configuration, Method	OASPL	dB(A)	PNdB
Prue-2 Sailplane			
61 kt Actual Spectra	52.1	35.7	43.7
Smoothed Spectra	35.4	33.3	40.5
Total Aircraft	47.8	42.4	51.8
Drag Element	35.5	34.0	42.8
Noise Component	42.8	35.3	43.1
82 kt Actual Spectra	49.5	40.8	51.0
Smoothed Spectra	43.5	40.8	51.0
Total Aircraft	53.1	48.9	58.3
Drag Element	42.9	42.1	52.7
Noise Component	48.2	42.7	52.1
100 kt Actual Spectra	58.5	58.6	67.5
Smoothed Spectra	47.5	45.3	57.6
Total Aircraft	56.2	52.9	63.1
Drag Element	47.8	47.4	58.5
Noise Component	52.9	48.6	58.5
Aero Commander Shrike			
Clean 118 kt			
Actual Spectra	69.6	62.5	72.9
Smoothed Spectra	63.1	60.1	70.7
Total Aircraft	69.3	66.7	77.7
Drag Element	59.5	56.9	67.0
Noise Component	64.0	59.5	74.8
Gear Down, 112 kt			
Actual Spectra	71.2	62.6	73.4
Drag Element	67.1	57.1	68.0
Noise Component	69.3	64.3	74.7
Gear and Flaps Down, 113 kt			
Actual Spectra	69.3	64.1	75.4
Drag Element	69.0	63.2	73.7
Noise Component	69.6	64.9	76.0
Clean, 156 kt			
Actual Spectra	72.7	68.4	78.7
Smoothed Spectra	70.8	67.5	77.9
Total Aircraft	74.3	72.5	84.0
Drag Element	67.5	65.8	77.0
Noise Component	70.1	67.6	77.5

Configuration, Method	OASPL	dB(A)	PNdB
Gear Down, 153 kt			
Actual Spectra	76.5	68.7	81.7
Drag Element	75.3	66.1	78.0
Noise Component	76.7	73.1	83.5
Lockheed JetStar			
Clean, 247 kt			
Actual Spectra	81.5	80.5	92.0
Total Aircraft	94.5	92.3	103.9
Drag Element	81.0	79.5	91.3
Noise Component	75.5	72.8	83.4
Clean, 358 kt			
Actual Spectra	88.0	87.6	98.8
Total Aircraft	102.5	101.6	113.1
Drag Element	92.6	91.7	104.0
Noise Component	82.2	80.9	91.9
Gear Down, 182 kt			
Actual Spectra	86.6	85.0	97.0
Drag Element	88.0	76.8	88.4
Noise Component	85.8	83.1	93.2
Flaps Down, 170 kt			
Actual Spectra	84.3	81.6	93.3
Drag Element	91.3	89.3	99.9
Noise Component	82.8	78.8	90.9
Gear and Flaps Down, 198 kt			
Actual Spectra	83.8	81.5	93.8
Drag Element	89.9	87.2	97.9
Noise Component	82.9	78.7	90.0
Boeing 747			
Clean, 233 kt			
Actual Spectra	90.7	88.8	101.5
Total Aircraft	101.1	94.2	105.5
Drag Element	87.6	83.7	94.6
Noise Component	82.1	74.6	86.0
Gear Down, 215 kt			
Actual Spectra	98.3	99.3	108.9
Drag Element	93.3	83.0	94.3
Noise Component	103.0	98.9	110.5

Configuration, Method	OASPL	dB(A)	PNdB
Flaps Down, 198 kt			
Actual Spectra	97.0	94.0	107.4
Drag Element	97.4	93.4	104.4
Noise Component	95.1	93.3	107.1
Gear and Flaps Down, 197 kt			
Actual Spectra	98.8	96.4	109.4
Drag Element	99.9	93.4	104.4
Noise Component	98.2	94.9	108.3
F-106B, Mach Number 0.4			
Actual Spectra	83	-	99
Total Aircraft	107.5	106.2	117.5
Drag Element	81.4	79.8	93.0
Noise Component	80.2	75.3	86.3

6.0 POTENTIAL CONCEPTS FOR AIRFRAME NOISE REDUCTION

6.1 Basic Geometry

Changes of the airframe basic geometry have relatively negligible effects on calculated airframe noise. Variations of wing taper ratio between 0.25 and 1.0 at constant wing area cause less than 1 dB change in one-third octave sound pressure levels. Reduction of wing aspect ratio at constant wing area would, in concept, lower the peak frequency of broadband noise from the clean wing, leading edge slats, and trailing edge flaps. This change would tend to reduce annoyance-weighted noise levels. However, reduced aspect ratio is accompanied by reduced lift coefficient and therefore higher airspeed during climb-out and approach. The increased noise amplitude and increased peak frequency associated with higher airspeed generally dominates the calculated change in annoyance. Increased trailing edge sweepback will reduce noise intensities by cosine squared of the sweep angle. Increased sweep also causes increased wing structural weight, decreased maximum lift coefficient, and increased minimum flight speed. Neglecting those adverse effects, the maximum noise reduction attainable by increasing the trailing edge sweepback from 20° to 35° would be only 1.2 dB.

As an extreme change of basic geometry, the wing area could be greatly increased to allow reduction of airspeed during takeoff and approach. Consider the effect of doubling the wing area at constant wing planform and wing flap technology. Wing weight of commercial transports is about 8% of gross weight. Flight speed is proportional to the square root of weight divided by the product of lift coefficient and wing area. At constant lift coefficient, doubling the wing area then would allow reducing airspeed to $(1.08/2)^{\frac{1}{2}}$ or 0.735 times that of the basic aircraft. (The additional fuel weight needed to maintain the same range and payload with the larger wing's profile drag is neglected.) This smaller airspeed, combined with the effect of a doubled wing area and flap area, would decrease the clean-wing noise, trailing edge flap noise, and landing gear noise by 3.7, 6.0, and 8.0 dB, respectively. Although these potential noise reductions are not negligibly small, they would be accompanied by a major increase of aircraft first cost and operating cost. The doubling of gust response, and resulting impairment of ride quality, probably would also be unacceptable. Therefore, airframe noise reduction should be achieved by attempts to modify each noise source at constant flight conditions.

6.2 Trailing Edge Flaps

The strongest single airframe noise component of commercial transports during landing approach is the trailing edge flap system. Noise from trailing edge flaps seems to be lift fluctuation noise caused by the wing turbulent wake convected past the flaps. One method for achieving small reductions of perceived noise is the avoidance of small-chord vanes within a multiple-slotted flap. Rapid decay of the flap noise spectrum then begins at a lower frequency. Use of the smallest flap deflection consistent with flight safety will also cause small noise reductions. For example, OASPL of the Vickers VC 10 airframe (clean except for deflected flaps) was reported in Ref. 12 to decrease 2.2 dB when flap deflection was decreased from 45° to 35°. The method developed herein predicts 1.8 dB noise reduction for this decreased deflection. Clearly, changes of flap geometry alone are inadequate to cause much noise reduction.

Experimental studies have been conducted (e.g., Refs. 27 through 33) of shape and surface modifications to reduce noise of airfoils with incident turbulence and of externally blown flaps. As described by Hayden in Ref. 28, these modifications usually can be classed as (1) changes of edge impedance, (2) changes of surface impedance, and (3) changes of flow mean and fluctuating properties. The first category includes serrated and slotted leading and

[27]Potter, R. C.: An Experiment to Examine the Effect of Porous Trailing Edges on the Sound Generated by Blades in an Airflow. NASA CR-66565, March 1968.

[28]Hayden, R. E., Kadman, Y., and Chanaud, R. C.: A Study of the Variable Impedance Surface Concept as a Means for Reducing Noise from Jet Interaction with Deployed Lift-Augmenting Flaps. NASA CR-112166, July 1972.

[29]Hayden, R. E., et al.: A Preliminary Evaluation of Noise Reduction Potential for the Upper Surface Blown Flap. NASA CR-112246, 1972.

[30]McKinzie, D. J. and Burns, R. J.: Externally Blown Flap Trailing Edge Noise Reduction by Slot Blowing - Preliminary Study. AIAA Paper 73-249, Jan. 1973.

[31]Scharton, T. D., et al.: A Study of Trailing Edge Blowing as a Means of Reducing Noise Generated by the Interaction of Flow With a Surface. NASA CR-132270, Sept. 1973.

[32]Pennock, A. P., Swift, G., and Marbert, J. A.: Static and Wind Tunnel Tests for the Development of Externally Blown Flap Noise Reduction Techniques. NASA CR-134675, Feb. 1975.

[33]Hersh, A. S., Hayden, R. E., and Soderman, P.: Investigation of Acoustic Effects of Leading-Edge Serrations on Airfoils. J. Aircraft, Vol. 11, No. 4, April 1974, pp 197-202.

trailing edges (Refs. 27 and 32) to provide spanwise variation of edge location, perforated or porous surfaces near the edges (Refs. 27, 28, 29, 32, and 34) to provide a gradual change of impedance with distance, and compliant flexible surfaces near the edges (Ref. 32) for the same purpose. Serrated leading edges tested at low Reynolds numbers and low turbulence (Ref. 33) have caused transition of an airfoil laminar boundary layer and therefore eliminated airfoil laminar tone noise (Ref. 10). Except for that one case at a low Reynolds number, serrations and slots at leading and trailing edges have not reduced noise and sometimes (Ref. 27) increased noise. Porous material with a relatively large (40%) open volume, and perforated thin sheet surfaces with or without acoustic bulk-absorbing backing, sometimes (Refs. 28, 29, and 34) were reported to give 6 to 10 dB noise reduction. In contrast, other studies (Refs. 27 and 32) achieved a maximum of 2 to 3 dB reduction with similar materials and geometry. Flexible surfaces (Ref. 32) had no effect on noise radiation, as might be expected from the relatively high frequencies at which acoustic radiation is important and the relatively large inertia of practical surface materials. Distributed surface impedance by use of compliant surfaces (Ref. 32) had no effect on noise.

Many of the above tests were conducted at small scale (chords of several inches). Tests with an 18-in. chord uncambered airfoil in grid-generated turbulence were reported in Ref. 13. Porous leading and trailing edge regions, interchangeable with hard surfaces, had perforated sheet metal surfaces backed by a bulk acoustic absorber. This nonlifting airfoil represented an engine internal strut. Lifting airfoils, representing trailing edge flap segments, would also need an impervious central plate within the bulk absorber to prevent airflow from the lower to the upper surface. Porous trailing edges were found to cause no reduction of incidence fluctuation noise. Porous leading edges, however, caused 6 to 10 dB noise reduction above a frequency that increased with increasing airspeed. The level and extent of this noise reduction was difficult to evaluate because the measured noise spectrum rapidly decayed into tunnel background noise. Reductions of at least 6 dB were achieved at 1000 Hz center frequency for 150 knots (80 m/sec) airspeed and 1250 Hz center frequency for 243 knots (125 m/sec) airspeed. Use of practical-construction porous leading edge regions of wing trailing edge flaps should therefore yield at least 6 dB noise reduction at approach airspeeds for frequencies which significantly affect perceived noise level. Perforated metal sheets with acoustically absorbing backing material, capable of withstanding strong acoustic pressure fluctuations without fatigue failure, are currently used in turbofan engine nacelles. Such material is somewhat heavier and more expensive than the conventional aluminum skins of wing trailing edge flaps, for the same structural reliability.

[34] Hayden, R. E.: USB Noise Reduction by Nozzle and Flap Modifications. Powered-Lift Aerodynamics and Acoustics, NASA SP-406, May 1976, pp 283-305.

Another possible method for reducing trailing edge flap noise is the use of screens (Refs. 28 and 13) extended below the wing lower surface ahead of the flaps. The screens generate turbulence which has a small integral length scale. If this length scale dominates the wing wake and does not couple effectively with the flap chord, the flap lift force fluctuations and therefore flap noise would be reduced. The screens themselves would generate high-frequency noise, but such noise would be attenuated by the atmosphere and has low annoyance. Noise reductions due to screens have generally been less than those from porous surfaces. However, retractable screens should impose negligible weight penalty.

6.3 Landing Gear

As shown by Heller (Ref. 18), landing gear noise is primarily bluff-body vortex shedding noise caused by the struts, dampers, axles, and other strut-mounted hardware. Noise from the wheels themselves was found to be small. Isolated landing gear cavities were noisy, but the presence of struts protruding from the open regions inhibited the organized cavity oscillation modes. Bluff-body wake fluctuations can be suppressed (Ref. 35) by use of a splitter plate extending about 2 diameters downstream. This concept has been used for reducing hydrodynamic drag of underwater cables. The splitter plate prevents formation of a Karman vortex street in the strut wake. It is not clear whether the altered strut wake would continue to reduce cavity noise. Cavity noise was shown in Ref. 36 to be eliminated or reduced by air injection within the cavity base. As the injected air is convected out of the cavity, it shields the cavity downstream edge from flow disturbances within the shear layer. Flow disturbances otherwise would impinge against the downstream edge to produce inflow to the cavity which generates additional periodic shear-layer disturbances. With flow injection, these oscillations of the shear layer and cavity internal flow are suppressed. A cavity tone which protruded about 25 dB above background noise was shown in Figure 10 of Ref. 36 to be eliminated by air injection. The required flow rate for arbitrarily chosen uniform injection was about 1/8 the product of cavity planform area and free stream density and velocity. Other concepts for decreasing cavity noise were

[35]Sallett, D. W.: Splitter Plate for Prevention of Vortex Shedding Behind Finite Circular Cylinders in Uniform Cross Flow. Naval Ordnance Lab. NOLTR 69-31, July 1967.

[36]Sarohia, V. and Massier, P. F.: Control of Cavity Noise. AIAA Paper 76-528, July 1976.

discussed in Ref. 37. Cavity noise generally occurs at such low frequencies that its contribution to perceived noise is small. High Reynolds number bluff-body noise, which is broadband and decays slowly at moderate and high frequencies, should be greatly reduced by use of lightweight inexpensive splitter plates.

6.4 Clean Aerodynamic Surfaces and Leading Edge Devices

Airframe noise from slats, leading edge flaps, and clean aerodynamic surfaces has been shown to be trailing edge noise caused by the turbulent boundary layer. One concept for decreasing trailing edge noise, described in Ref. 38, is the use of sawtooth trailing edges to take advantage of the edge sweepback effect. Depending on whether sweepback is assumed to affect the spanwise correlation length, the ratio of acoustic energy is predicted to vary between cosine and cosine squared of edge sweep angle. Model data were presented in Ref. 38 for two different sized sawtooth trailing edges, both having 60° sweep. Noise reductions ranged from about 3 to 6 dB, in agreement with prediction. Effects of a sawtooth trailing edge on weight and aerodynamic performance are not known.

Porous trailing edge regions have been extensively tested (e.g., Refs. 28, 29, and 34) for decreasing trailing edge noise from upper-surface-blowing externally blown flaps. Tests have indicated up to 10 dB maximum reductions and about 5 dB reduction over a fairly wide frequency range. Methods for tailoring the perforated material acoustic resistance and streamwise extent for the required noise attenuation properties were given in Ref. 39. As with porous leading edges for wing flaps, a central impervious structure would be needed to sustain aerodynamic lift. A very small increase of wing profile drag would be caused by the small chordwise extent of perforated material. This passive noise reduction concept seems to have no other disadvantages except the need to provide drains for rainwater collected within the acoustic absorber.

[37]Heller, H. H. and Bliss, D. B.: Flow-Induced Pressure Fluctuations in Cavities and Concepts for Their Suppression. Aeroacoustics: STOL Noise; Airframe and Airfoil Noise, Vol. 45, Progress in Aeronautics and Astronautics, M.I.T. Press, Cambridge, Mass., pp 281-296. Also, AIAA Paper 75-491, Mar. 1975.

[38]Filler, L.: Swept Edge to Reduce the Noise Generated by Turbulent Flow Over the Edge. J. Acoust. Soc. Am., Vol. 59, No. 3, Mar. 1976, pp 697-699.

[39]Bohn, A. J.: Edge Noise Attenuation by Porous-Edge Extensions. AIAA Paper 76-80, Jan. 1976.

Use of trailing edge blowing to interpose a layer of low-turbulence air between a trailing edge and a turbulent flow has also been examined (Refs. 27 through 31, and 34). This concept has not worked consistently for externally blown flaps, possibly because the blown air must have a very low turbulence level. The need to obtain engine bleed air, and provide ducts and control valves, causes increased weight, increased cost, and decreased reliability. Use of a passive device such as porous trailing edges appears preferable.

Data are not openly available for the noise radiated by a clean airfoil or wing in low-turbulence airflow at Reynolds numbers large enough to provide turbulent boundary layers on both surfaces. This noise level of trailing edge noise caused by the wing turbulent boundary layer is less than acoustic open jet or wind tunnel background noise. Trailing edge noise of clean airfoils has been measured in a small number of unpublished tests with directional microphones rather than conventional microphones. A directional microphone uses a single microphone placed in a physical reflector, or an array of conventional microphones with electronic signal addition at appropriate time delays. The resulting output contains an enhanced acoustic signal from the geometric region being scanned and an attenuated signal from other regions which produce background noise. Such microphones had originally been developed for studies of jet exhaust noise source location. Measurement of airframe noise from clean wing surfaces and leading edge devices is within the current state of the art for directional microphones. Accurate measurement of large reductions in such noise for much of the frequency range of interest may be beyond current state of the art.

7.0 CONCLUSIONS

1. The noise component method developed in this report correctly predicts the amplitudes and spectrum shapes of noise due to extended landing gear and trailing edge flaps. Measured noise of clean jet aircraft is correctly predicted at relatively low frequencies but is underpredicted at higher frequencies where engine noise probably occurs. Measured noise of clean propeller-driven aircraft and a sailplane was correctly predicted.

2. The NASA-recommended drag element method correctly predicts the general level but not the spectrum shape of trailing edge flap noise at small deflections, and overestimates the overall level at large flap deflections. It poorly predicts noise from extended landing gear but correctly predicts clean-airframe noise.

3. The NASA-recommended total aircraft noise method for clean aircraft gave poor predictions of spectra and annoyance-weighted noise levels.

4. It is likely that trailing edge flap noise, at frequencies which are highly weighted for annoyance, can be reduced 8 dB by porous leading edge regions on all flap segments.

5. Landing-gear noise can be reduced by use of splitter plates downstream of struts and axles to inhibit bluff-body vortex shedding. Additional devices such as cavity bleed may then be needed to reduce landing-gear cavity noise, which generally is decreased by the strut flow field.

6. Trailing-edge noise of clean wing and horizontal tail surfaces can be reduced up to 6 dB by porous trailing edges.

7. Directional microphones will be needed to measure basic trailing-edge noise levels of clean wing models in acoustic wind tunnels.

8.0 REFERENCES

1. Brines, G. L.: Studies for Determining the Optimum Propulsive System Characteristics for Use in a Long Range Transport Aircraft. NASA CR-120950, July 1972.

2. Sofrin, T. G. and Riloff, N. Jr.: Two-Stage, Low-Noise Advanced Technology Fan. V. Acoustic Final Report. NASA CR-134831, Sept. 1975.

3. Morgan, H. G. and Hardin, J. C.: Airframe Noise - The Next Aircraft Noise Barrier. J. of Aircraft, Vol. 12, No. 7, July 1975, pp 622-624.

4. Hardin, J. C., Fratello, D. J., Hayden, R. E., Kadman, Y., and Africk, S.: Prediction of Airframe Noise. NASA TN D-7821, Feb. 1975.

5. Fink, M. R.: Approximate Prediction of Airframe Noise. J. of Aircraft, Vol. 13, No. 11, Nov. 1976, pp 833-834. Also, AIAA Paper 76-526, July 1976.

6. Ffowcs Williams, J. and Hall, L. H.: Aerodynamic Sound Generation by Turbulent Flow in the Vicinity of a Scattering Half Plane. J. of Fluid Mechanics, Vol. 40, Part 4, Mar. 1970, pp 657-670.

7. Chase, D. M.: Sound Radiated by Turbulent Flow off a Rigid Half Plane as Obtained From a Wavevector Spectrum of Hydrodynamic Pressure. J. of the Acoustical Society of America, Vol. 52, No. 3, Part 2, Sept. 1972, pp 1011-1023.

8. Fink, M. R.: Experimental Evaluation of Theories for Trailing Edge and Incidence Fluctuation Noise. AIAA Journal, Vol. 13, No. 11, Nov. 1975.

9. Healy, G. J.: Measurement and Analysis of Aircraft Far-Field Aerodynamic Noise. NASA CR-2377, Dec. 1974.

10. Fink, M. R.: Prediction of Airfoil Tone Frequencies. J. of Aircraft, Vol. 12, No. 2, Feb. 1975, pp 118-120.

11. Putnam, T. W., Lasagna, P. L., and White, K. C.: Measurements and Analyses of Aircraft Airframe Noise. Aeroacoustics: STOL Noise; Airframe and Airfoil Noise, Vol. 45, Progress in Aeronautics and Astronautics, M.I.T. Press, Cambridge, Mass., 1976, pp 363-378. Also, AIAA Paper 75-510, Mar. 1975.

12. Fethney, P.: An Experimental Study of Airframe Self-Noise. Aeroacoustics: STOL Noise; Airframe and Airfoil Noise, Vol. 45, Progress in Aeronautics and Astronautics, M.I.T. Press, Cambridge, Mass., 1976, pp 379-403. Also, AIAA Paper 75-511, Mar. 1975.

13. Fink, M. R.: Prediction of Externally Blown Flap Noise and Turbomachinery Strut Noise. NASA CR-134883, Aug. 1975.

14. Revell, J. D., Healy, G. J., and Gibson, J. S.: Methods for the Prediction of Airframe Aerodynamic Noise. Aeroacoustics: Acoustic Wake Propagation; Aircraft Noise Prediction; Aeroacoustics Instrumentation, Vol. 46, Progress in Aeronautics and Astronautics, M.I.T. Press, Cambridge, Mass., 1976, pp 139-154. Also, AIAA Paper 75-539, Mar. 1975.

15. Munson, A. G.: A Modeling Approach to Nonpropulsive Noise. AIAA Paper 76-525, July 1976.

16. Pendley, R. E.: Recent Advances in the Technology of Aircraft Noise Control. J. of Aircraft, Vol. 13, No. 7, July 1976, pp 513-519.

17. Lasagna, P. L. and Putnam, T. W.: Preliminary Measurements of Aircraft Aerodynamic Noise. AIAA Paper 74-572, June 1974.

18. Heller, H. H. and Dobrzynski, W. M.: Sound Radiation From Aircraft Wheel-Well/Landing Gear Configurations. AIAA Paper 76-552, July 1976.

19. Shearin, J. G., Fratello, D. J., Bohn, A. J., and Burggraf, W. D.: Model and Full-Scale Large Transport Airframe Noise. AIAA Paper 76-550, July 1976.

20. Perkins, C. D. and Hage, R. E.: Aircraft Performance, Stability and Control. John Wiley & Sons, Inc., New York, 1949.

21. Abbott, I. H. and von Doenhoff, A. E.: Theory of Wing Sections, Including a Summary of Airfoil Data. Dover Publications, Inc., New York, 1959.

22. Hersh, A. S., Putnam, T. W., Lasagna, P. L., and Burcham, F. W., Jr.: Semi-Empirical Airframe Noise Prediction Model. AIAA Paper 76-527, July 1976.

23. Burley, R. R.: Preliminary Measurement of the Airframe Noise From an F-106B Delta Wing Aircraft at Low Flyover Speeds. NASA TM X-71527, Mar. 1974.

24. Burley, R. R.: Suppressor Nozzle and Airframe Noise Measurements During Flyover of a Modified F-106B Aircraft With Underwing Nacelles. ASME Paper 74-WA/Aero-1, Nov. 1974.

25. Gibson, J. S.: Nonengine Aerodynamic Noise Investigation of a Large Aircraft. NASA CR-2378, Oct. 1974.

26. White, K. C., Lasagna, P. L., and Putnam, T. C.: Preliminary Measurements of Aircraft Airframe Noise With the NASA CV-990 Aircraft. NASA TM X-73116, Jan. 1976.

27. Potter, R. C.: An Experiment to Examine the Effect of Porous Trailing Edges on the Sound Generated by Blades in an Airflow. NASA CR-66565, Mar. 1968.

28. Hayden, R. E., Kadman, Y., and Chanaud, R. C.: A Study of the Variable Impedance Surface Concept as a Means for Reducing Noise from Jet Interaction with Deployed Lift-Augmenting Flaps. NASA CR-112166, July 1972.

29. Hayden, R. E., et al.: A Preliminary Evaluation of Noise Reduction Potential for the Upper Surface Blown Flap. NASA CR-112246, 1972.

30. McKinzie, D. J. and Burns, R. J.: Externally Blown Flap Trailing Edge Noise Reduction by Slot Blowing - Preliminary Study. AIAA Paper 73-245, Jan. 1973.

31. Scharton, T. D., et al.: A Study of Trailing Edge Blowing as a Means of Reducing Noise Cenerated by the Interaction of Flow With a Surface. NASA CR-132270, Sept. 1973.

32. Pennock, A. P., Swift, G., and Marbert, J. A.: Static and Wind Tunnel Tests for the Development of Externally Blown Flap Noise Reduction Techniques. NASA CR-134675, Feb. 1975.

33. Hersh, A. S., Hayden, R. E., and Soderman, P.: Investigation of Acoustic Effects of Leading-Edge Serrations on Airfoils. J. Aircraft, Vol. 11, No. 4, April 1974, pp 197-202.

34. Hayden, R. E.: USB Noise Reduction by Nozzle and Flap Modifications. Powered-Lift Aerodynamics and Acoustics, NASA SP-406, May 1976, pp 283-305.

35. Sallett, D. W.: Splitter Plate for Prevention of Vortex Shedding Behind Finite Circular Cylinders in Uniform Cross Flow. Naval Ordnance Lab. NOLTR 69-31, July 1967.

36. Sarohia, V. and Massier, P. F.: Control of Cavity Noise. AIAA Paper 76-528, July 1976.

37. Heller, H. H. and Bliss, D. B.: Flow-Induced Pressure Fluctuations in Cavities and Concepts for Their Suppression. Aeroacoustics: STOL Noise; Airframe and Airfoil Noise, Vol. 45, Progress in Aeronautics and Astronautics, M.I.T. Press, Cambridge, Mass., 1976, pp 281-296. Also, AIAA Paper 75-491, Mar. 1975.

38. Filler, L.: Swept Edge to Reduce the Noise Generated by Turbulent Flow Over the Edge. J. Acoust. Soc. Am., Vol. 59, No. 3, Mar. 1976, pp 697-699.

39. Bohn, A. J.: Edge Noise Attenuation by Porous-Edge Extensions. AIAA Paper 76-80, Jan. 1976.

9.0 APPENDIX I: MATHEMATICAL CONVENTIONS FOR COMPUTER PROGRAM

As with the NASA ANOPP method for airframe noise, the acoustic field is represented in spherical coordinates r, θ, ϕ. The polar angle θ is measured from the aircraft forward direction, which for calculation of airframe noise can be taken as the forward horizontal direction. The azimuth angle ϕ is measured from a reference plane containing the flight direction and the vertical direction. It is assumed that the distance from the airframe is large enough so that acoustic pressure varies as the inverse of the radius.

The Fourier transform of the acoustic pressure is

$$p_\omega = \frac{1}{2\pi} \int_{-\infty}^{\infty} P(t) e^{i\omega t} dt \qquad (A\text{-}1)$$

so that the mean-squared acoustic pressure is

$$\overline{p^2} = 2\int_0^{\infty} |p_\omega|^2 d\omega \qquad (A\text{-}2)$$

The integral in Eq. (A-2) may be expressed as a sum of integrals over all frequency bands. For one-third octave bands, the mean-squared acoustic pressure in any band is

$$\overline{p_f^2} = 2\int_{\omega_\ell}^{\omega_u} |p_\omega|^2 d\omega \qquad (A\text{-}3)$$

where ω_ℓ and ω_u are the lower and upper limits of the frequency band.

Since the acoustic pressure varies inversely with radius, the intensity I may be given as

$$I(r,\theta,\Phi) = \frac{1}{\rho_0 c_0} \frac{A}{r^2} p_F^2(\theta,\phi) \qquad (A\text{-}4)$$

where A is a representative area of the noise source. The acoustic power which is within this frequency band and is radiated through a solid angle $d\Omega$ is

$$P(\theta,\phi) = r^2 I = \frac{A}{\rho_0 c_0} p_f^2(\theta,\phi) \tag{A-5}$$

Neglecting acoustic absorption, the acoustic power is thus independent of radius and is a convenient quantity to represent each acoustic source. Equation (A-5) may be written in terms of dimensionless ratios by dividing the acoustic pressure by $\rho_a c_a^2$ to obtain

$$\frac{P(\theta,\phi)}{\rho_0 c_0^3 A} = \left(\frac{p_f(\theta,\phi)}{\rho_0 c_0^2}\right)^2 \tag{A-6}$$

The term on the left of Eq. (A-6) is a dimensionless acoustic power which is equal to the square of the dimensionless pressure on the right of the equation. That is,

$$P(\theta,\phi) = p_f^2(\theta,\phi) \tag{A-7}$$

in dimensionless notation. As with the NASA ANOPP noise prediction programs, this computer program is written entirely in terms of dimensionless variables so that they will be valid for any system of units.

All subroutines follow the same computation sequence. The dimensionless total acoustic power for each noise source is calculated first. The power $P(\theta,\phi)$ radiated in any direction is then found by multiplying the total power by a directivity factor $D(\theta,\phi)/4\pi$, where $D(\theta,\phi)$ has been normalized by the condition

$$\int_0^{2\pi} \int_0^{\pi} \sin\theta \; D(\theta,\phi)\, d\phi\, d\theta = 4\pi \tag{A-8}$$

In other words, $D(\theta,\phi)$ is defined such that its average value is equal to one.

The power within any one-third octave band may be found by multiplying the power by a spectrum function $S(f_n)$ which satisfies the normalization condition

$$\sum_{n=1}^{\infty} S(f_n) = 1 \tag{A-9}$$

Thus the total acoustic power produced by a noise source in a one-third octave band is

$$P(f_n) = PS(f_n) \tag{A-10}$$

and the power within a band and radiated in a given direction is

$$P(\theta,\phi,f_n) = P\left(\frac{D(\theta,\phi)}{4\pi}\right) S(f_n,\theta,\phi) \tag{A-11}$$

The mean-squared acoustic pressure at a given distance in a given direction is found from the power by multiplying by the factor A/r^2; that is,

$$p_f^2(r,\theta,\phi) = P(A/r^2)\ \frac{D(\theta,\phi)}{4\pi}\ S(f_n,\theta,\phi) \tag{A-12}$$

These mathematical conventions are identical to those of the NASA ANOPP computer program for airframe noise. Differences occur in the specific noise mechanisms assumed for noise produced by various airframe components. These mechanisms can have directivity functions $D(\theta,\phi)$, convective amplification function (not described in the preceding analysis), and spectrum functions $S(f_n)$ which differ from those used in the NASA ANOPP method for airframe noise.

All airframe noise radiation was represented in the NASA ANOPP method as being produced by lift dipoles. In a coordinate system moving with the airframe, the directivity factor would be proportional to $\sin^2\theta\cos^2\phi$. Motion of this acoustic field past a fixed observer causes the frequency and amplitude measured by the fixed observer to differ from those of the moving coordinate system. A frequency f in the ground-fixed system corresponds to a frequency

$(1-M\cos\theta)f$ in the moving system. This Doppler shift occurs for all types of noise sources. For a lift dipole, the directivity factor in ground-fixed coordinates is

$$D_L(\theta,\phi) = \sin^2\theta\cos^2\phi/\left[A(M)(1-M\cos\theta)^4\right] \tag{A-13}$$

Here, the function A(M) is an average convective amplification factor caused by compressibility. It is defined by

$$A(M)=\frac{1}{4\pi}\int_0^{2\pi}\int_0^{\pi}\sin\theta\,\frac{\sin^2\theta\cos^2\phi}{(1-M\cos\theta)^4}\,d\phi\,d\theta=\frac{1}{3}(1-M^2)^{-2} \tag{A-14}$$

Convective amplification for wing and horizontal-tail trailing edge noise and leading edge slat noise was taken as

$$D_E(\theta,\phi)=\cos^2(\theta/2)\cos^2\phi/\left[A(M)(1-M\cos\theta)^4\right] \tag{A-15}$$

Edge noise from the vertical tail is rotated in orientation from that of the wing and horizontal tail. Its directivity function is

$$D_V(\theta,\phi)=\cos^2(\theta/2)\sin^2\phi/\left[A(M)(1-M\cos\theta)^4\right] \tag{A-16}$$

However, measured airframe noise directivity for clean airframes has been found (Ref. 15, and Figs. 5 and 6 herein) to be more closely given by neglecting the Mach number dependence in Eq. (A-15).

Landing-gear noise has been found experimentally (Ref. 18) to be approximately independent of azimuth angle. Variation of directivity with polar angle was not specified but is arbitrarily assumed to be that for a lift dipole as in Ref. 4. Sound radiation from the wheel-well cavity would be expected (Ref. 4, p 44) to be that for a monopole source in an infinite baffle. However, cavity noise is not specifically represented in the method developed here. The directivity function for landing-gear noise then is

$$D_G(\theta,\phi) = \sin^2\theta \Big/ \left[A_G(M)\,(1-M\cos\theta)^4\right] \qquad \text{(A-17)}$$

where

$$A_G(M) = \frac{1}{4\pi}\int_0^{2\pi}\int_0^{\pi} \frac{\sin^3\theta}{(1-M\cos\theta)^4}\, d\phi\, d\theta = 2A(M) \qquad \text{(A-18)}$$

The equations used in the method developed herein for calculating noise radiation from various airframe components are listed below.

Airframe Component	Directivity	Convective Amplification
Wing	(A-15),M=0	A(M)=1/3
Horizontal Tail	(A-15),M=0	A(M)=1/3
Vertical Tail	(A-16),M=0	A(M)=1/3
Trailing Edge Flaps	(A-14)	(A-14)
Leading Edge Slats, Flaps	(A-15),M=0	A(M)=1/3
Landing Gear	(A-17)	(A-18)

Although the mathematical conventions used in this noise prediction method are the same as those of the NASA ANOPP method for airframe noise, there is a difference in viewpoint. The NASA ANOPP method starts with a basic acoustic quantity (sound power) for a basic well-understood noise source (lift dipole). Calculated sound power is distributed in space by use of readily available solutions for directivity in compressible flow. Empiricism occurs only in choosing equations for maximum amplitude and normalized spectrum shape. In contrast, calculation of noise from landing gears and trailing-edge flaps as given herein has started with empirical correlations of acoustic-pressure spectra. These spectra were integrated numerically to obtain maximum OASPL. Directivity functions had to be assumed arbitrarily, and compressibility effects caused by relative motion had to be picked, to allow back-calculation of acoustic power. That is, acoustic power is the most fundamental quantity from an analytical viewpoint but the least readily obtained quantity from empirical correlations of airframe noise data.

10.0 APPENDIX B: COMPUTER PROGRAM FOR CALCULATING AIRFRAME NOISE

10.1 General Description

This digital computer program, written in FORTRAN IV, predicts airframe noise that would be measured by microphones mounted on posts or tripods above the ground, in lines parallel to the flight path, at input-designated azimuth and sideline angles. If the atmospheric properties are not specified as input but allowed to remain at their default values, and the input integer UNITS is specified as 1, the aircraft altitude and linear dimensions should have the dimensions of feet, areas square feet, and airspeed knots. If UNITS is not equal to 1, and the atmospheric properties are not specified, airspeed should be input as feet per second. Input values of atmospheric properties for use with input dimensions and airspeed in the metric system (meters, square meters, meters per second) are given in the first set of comments within the program listing. Comment statements are placed throughout the program listing to describe the purpose of each portion of the program and to define the program variables.

The program consists of a main control program, four subroutines which calculate noise radiated from seven airframe components, a subroutine NOYS which calculates perceived noise level (PNL) of the combined noise spectrum, and an output subroutine OUTP which organizes the printout. Subroutine OPT123 calculates trailing edge noise from the wing, horizontal tail, and vertical tail, respectively. Subroutine OPT4 calculates trailing edge flap noise and subroutine OPT5 calculates leading edge slat noise. Subroutine OPT67 calculates landing gear noise from the main landing gear and nose landing gear, respectively. Each of these last four subroutines follows the same flow path. Normalized acoustic power is computed first. This quantity is multiplied by the appropriate directivity factor, and by the ratio of reference area to far-field distance squared, to obtain the ratio of overall mean square acoustic pressure to reference pressure squared. Finally, the one-third octave spectrum for that noise component is computed. The main program calculates the resulting OASPL and one-third octave band SPL for each component. It also adds the acoustic pressure ratios to obtain the sum of noise from all designated components. These airframe acoustic pressure ratios are utilized to calculate complete airframe OASPL, one-third octave band SPL, A-weighted noise level dB(A), and perceived noise level (PNL) at each designated position.

The following is a list and definition of the input variables and their default values. Wherever possible, the program symbols and default values are equal to those of the NASA ANOPP airframe noise digital computer program JCHARFM. However, numerical default values correspond to use of English-system units rather than metric-system units.

Program Symbol	Definition	Default Value
CA	Atmospheric speed of sound	1116.44
RHOA	Atmospheric mass density	0.002377
NUA	Atmospheric kinematic viscosity	1.576E-4
PREF	Acoustic reference pressure	4.1773E-7
FL	Lower limit for one-third octave center frequency, Hz	50.
FU	Upper limit for one-third octave center frequency, Hz	10000.
THL	Lower limit for polar angle, deg	10.
THU	Upper limit for polar angle, deg	170.
DELTH	Increment between successive polar angles, deg	10.
PHIL	Lower limit for azimuth (sideline) angle, deg	-80.
PHIU	Upper limit for azimuth angle, deg	80.
DELPHI	Increment between successive azimuth angles, deg	10.
H	Altitude	3.281
UNITS	Equal to 1 if velocity is in knots and any other integer if ft/sec (integer)	0
V	Velocity	100.
AW	Wing area	10.765
BW	Wing span	3.281
AT	Horizontal tail area	10.765
BT	Horizontal tail span	3.281
AV	Vertical tail area	10.765
BV	Vertial tail span	3.281
NF	Number of trailing edge flap chordwise segments (integer)	2
AF	Trailing edge flap area	1.615
CF	Trailing edge flap total chord	0.82
DELF	Trailing edge flap aft-segment deflection, deg	30.
NS1	Number of main landing gear units (integer)	2
NS2	Number of nose landing gear units (integer)	1
ND	Equal to 0. if wing is aerodynamically very clean or 1. for typical low subsonic speed aircraft and for extended leading edge slats or flaps	0.

Program Symbol	Definition	Default Value
N1	Number of main landing gear wheels per unit (integer)	2
N2	Number of nose landing gear wheels per unit (integer)	1
D1	Diameter of main landing gear wheels	1.
D2	Diameter of nose landing gear	1.
L1	Ratio of main landing gear strut length to wheel diameter	2.94
L2	Ratio of nose landing gear strut length to wheel diameter	2.94

All input lengths (altitude, span, chord, diameter) and areas must have the dimensions ft and ft^2 if the first four quantities on this list are kept in English units (ft/sec, slugs/ft^3, ft^2/sec, and lb/ft^2). The default values correspond to flight in sea-level standard atmosphere. Input quantities can be given in metric units (m and m^2, with velocity m/sec) if these first four quantities are supplied as metric-system input. For sea-level standard atmosphere, these are CA=340.3, RHOA=1.225, NUA=1.464E-5, and the metric-system acoustic reference pressure PREF=2.E-5.

This program has been run on a UNIVAC 1110 large digital computer but should operate on all machines of generally similar capability. Each execution and output cycle (one aircraft configuration and flight condition, for the full range of polar angles at one sideline angle) requires only several tens of seconds of central processing unit time.

10.2 Program Input Format

The input for each case comprises (1) a title card which provides an identification label in the printed output, (2) the calculation frequency range, angular positions, flight condition, and airframe geometry, (3) the specific program options (noise components) to be used, and (4) an indication that all required program options have been called, so that noise of the complete configuration can be determined. Data input is done using the NAMELIST format. A sample input is given on the next page for calculating airframe flyover noise of the Lockheed JetStar aircraft with trailing edge flaps extended and landing gear retracted (NASA Flight Research Center Flight 7A). Because the vertical tail does not radiate noise directly beneath the aircraft, subroutine OPT3 and its input quantities for vertical tail noise are not used. Each line denotes a separate input card. The range of polar angle TH has been decreased from the default range but 10^o increments have been

retained. Specifying zero sideline angle for both PHIL and PHIU causes calculations to be held to the flyover line. Default values for frequency range and atmosphere properties are retained. UNITS is input as 1 so that velocity can be input in knots.

```
JETSTAR, FLAPS DOWN, GEAR UP, RUN 7A

$INPUT

THL=30., THU=90.,  PHIL=0., PHIU=0.,

AW=542.5, BW=53.67, AT=149., BT=24.75, ND=0.,

AF=53.67, CF=2.28, DELF=50.,

H=500., UNITS=1, V=170., IOPT=1,

$END

$INPUT

IOPT=2

$END

$INPUT

IOPT=4

$END

$INPUT

IEND=1

$END
```

This sequence of cards can be followed by another title card and calculation case or by a termination card. All of the above cards start in column 2. Output for this case is given after the program listing.

```
      REAL L1,L2,NUA,L1D
      INTEGER UNITS
C*****************************************************************************
C **  INPUT DATA.
C **  CA, RHO , NUA, PREF ARE ATMOSPHERIC SPEED OF SOUND, MASS DENSITY, AND
C **  KINEMATIC VISCOSITY, AND ACOUSTIC REFERENCE PRESSURE. DEFAULT VALUES ARE
C **  FOR SEA LEVEL STANDARD ATMOSPHERE IN ENGLISH UNITS. FL, FU ARE UPPER AND
C **  LOWER 1/3 OCTAVE CENTER FREQUENCIES OF SPECTRUM. THU, THL, DELTH, PHIU,
C **  PHIL, DELPHI ARE UPPER AND LOWER LIMITS, AND ANGLE STEP, FOR POLAR ANGLE
C **  THETA AND AZIMUTH ANGLE PHI. FLIGHT CONDITIONS ARE ALTITUDE H, FT AND
C **  VELOCITY V (KNOTS IF UNITS = 1 (INTEGER), FT/SEC IF UNITS NOT EQUAL TO ONE
C **  AND DEFAULT ATMOSPHERIC CONDITIONS ARE USED). BW, AW, BT, AT, BV, AV ARE
C **  SPAN (B) AND AREA (A) OF WING (W), HORIZONTAL TAIL (T), AND VERTICAL TAIL
C **  (V). NO = 0. FOR AERODYNAMICALLY CLEAN AIRCRAFT AND 1. FOR TYPICAL LOW
C **  SUBSONIC SPEED AIRCRAFT. CF AND DELF ARE TRAILING EDGE FLAP CHORD AND
C **  DEFLECTION (DEG). FOR LANDING GEAR, THE SUBSCRIPT 1 IS MAIN GEAR AND 2 IS
C **  NOSE GEAR. NS1 AND NS2 ARE THE NUMBER OF UNITS OF EACH TYPE; N1 AND N2 ARE
C **  THE NUMBER OF WHEELS ON EACH UNIT (1, 2 OR 4). THE QUANTITIES N1, N2, NS1,
C **  NS2, AND UNITS ARE THE ONLY INTEGER DATA. D1 AND D2 ARE WHEEL DIAMETERS,
C **  AND L1 AND L2 ARE RATIOS OF STRUT LENGTH TO WHEEL DIAMETER. LENGTHS AND
C **  AREAS ARE FT. AND SQ. FT. IF DEFAULT ATMOSPHERIC CONDITIONS ARE USED. THE
C **  USER CAN INPUT DATA IN THE MKS METRIC SYSTEM OF UNITS BY INPUTTING CA =
C **  340.3, RHOA = 1.225, NUA = 1.464E-5, PREF = 2.E-5, AND UNITS = ANY INTEGER
C **  BUT ONE. CALCULATED SPECTRA ARE 3 DB ABOVE FREE FIELD, CORRESPONDING TO
C **  UNCORRECTED MEASUREMENTS WITH MICROPHONES ON POSTS.
C **     NF  S NUMBER OF TRAILING EDGE FLAP CHORDWISE SEGMENTS(INTEGER).
C*****************************************************************************
      DIMENSION PRINTG(34),TITLE(7,4),HEADNG(13)
      COMMON/AFNIN/ IOPT,CA,FL,FU,PREF,H,V,RHOA,NUA,THL,THU,DELTH,
     1              PHIU,PHIL,DELPHI,BW,AW,BT,AT,BV,AV,N1,D1,L1,N2,D2,
     2              L2,ND,AF,DELF,NS1,NS2,UNITS,CF,LOOP2,C,CC,CCC,NFEP1,
     3              FB(40),S(43,34),SUM(43,34),THETA,PHI,IF,LF,NFBMAX
      DATA CA,FL,FU,PREF,H,   PHOA,NUA,THL,THU,DELTH,PHIU,PHIL,DELPHI,
     1     BW,AW,BT,AT,BV,AV,N1,D1,L1,N2,D2,L2,ND,AF,
     2     NS1,NS2,CF,NF /
     3     1116.44, 50., 10000., 4.1773E-07, 3.281,          0.002377,
     4  1.57 E-04,10., 170., 10., 80., -80., 10., 3.261, 10.765,
     5  3.281, 10.765, 3.281, 10.765, 2, 1., 2.94, 1, 1., 2.94,
     6  0, 1.615,  2, 1,  0.62,2/
      DATA ((TITLE(I,J),J=1,4),I=1,7)/
     1     'CLEAN ','WING N','OISE  ','     ',
     2     'HORIZO','NTAL T','AIL NO','ISE  ',
     3     'VERTIC','AL TAI','L NOIS','E    ',
     4     'TRAILI','NG EDG','E FLAP',' NOISE',
     5     'LEADIN','G EDGE',' SLAT ','NOISE ',
     6     'MAIN L','ANDING',' GEAR ','NOISE ',
     7     'NOSE L','ANDING',' GEAR ','NOISE '/
      NAMELIST/INPUT/ IOPT, CA,FL,FU,PREF,H,V,RHOA,NUA,THL,THU,DELTH,
     1                PHIU,PHIL,DELPHI,BW,AW,BT,AT,BV,AV,N1,D1,L1,N2,D2,
     2                L2,ND,AF,DELF,NS1,NS2,UNITS,CF,IEND,NF
      DATA NFBMAX,NTHPH/40,34/
      NHALF = NTHPH/2
```

```
      NFBP1=NFBMAX+1
      DEGRAD =.01745329
      RADDEG =  57.2957795
      IEND=0
      IDONE=0
      READ(5,700) IDONE,  (HEADNG(I),I=1,13)
      IF(IDONE.NE.0) GO TO 4000
      DELF = 0.
      V=0.
      UNITS=0
      ISKIP = 0
      FB(1)=1.25
      FB(2)=1.6
      FB(3)=2.
      FB(4)=2.5
      FB(5)=3.15
      FB(6)=4.
      FB(7)=5.
      FB(8)=6.3
      FB(9)=8.
      FB(10) = 10.
      DO 2 I=1,NFBP1
      DO 2 J = 1,NTHPH
      S(I,J)=0.0
    2 SUM(I,J) = 0.0
      DO 4 I = 1,10
      FB(I+10) = 10.  * FB(I)
      FB(I+20) = 100.  * FB(I)
    4 FB(I+30) = 1000. * FB(I)
C*****************************************************************************
C **  READ AND PRINT INPUT
C*****************************************************************************
    6 READ(5,INPUT)
      WRITE(6,800)
      IF(IEND.NE.0) GO TO 2000
      WRITE(6,INPUT)
      WRITE(6,805) (HEADNG(I),I=1,13)
      IF(NF.GE.1.AND.NF.LE.3) GO TO 3001
      WRITE(6,3002)
 3002 FORMAT(' INADMISSIBLE NUMBER OF TRAILING EDGE FLAPS, SETTING NF=2)')
      NF=2
 3001 CONTINUE
      IF(ISKIP.EQ.0.AND.UNITS.EQ.1)  V = 1.6889*V
      IF(UNITS.EQ.1) ISKIP = 1
C*****************************************************************************
C **  OBTAIN FREQUENCY RANGE
C*****************************************************************************
      IF=1
      DO 10 I=1,NFBMAX
      IF(FL.LT.FB(I)) GO TO 20
      IF=I
   10 CONTINUE
   20 LF= NFBMAX
      DO 30 I=1,NFBMAX
      J= NTHPH-I
      IF(FU.GT.FB(J)) GO TO 40
      LF=J
```

```
   30   CONTINUE
   40   IF(IF.LT.LF) GO TO 50
        WRITE(6,810)
        LF=IF
   50   CONTINUE
C*****************************************************************************
C ** CHECKING VARIOUS RANGES OF SEVERAL VARIABLES
C*****************************************************************************
        IF(THL.GT.0..AND.THL.LT.180.) GO TO 60
        WRITE(6,820)
        GO TO 1000
   60   IF(THU.GT.0..AND.THU.LT.180.) GO TO 70
        WRITE(6,830)
        GO TO 1000
   70   IF(THL.LE.THU) GO TO 80
        WRITE(6,840)
        GO TO 1000
   80   IF(PHIL.GT.-80..AND.PHIL.LT.80.) GO TO 90
        WRITE(6,850)
        GO TO 1000
   90   IF(PHIU.GT.-80..AND.PHIU.LT.80.) GO TO 100
        WRITE(6,860)
        GO TO 1000
  100   IF(PHIL.LE.PHIU) GO TO 110
        WRITE(6,870)
        GO TO 1000
  110   IF(DELTH.GT.0..AND.DELPHI.GT.0.) GO TO 120
        WRITE(6,880)
        GO TO 1000
  120   IF(NS1.GT.0) GO TO 130
        WRITE(6,890)
        GO TO 1000
  130   IF(NS2.GT.0) GO TO 140
        WRITE(6,900)
        GO TO 1000
  140   IF(N1.EQ.1.OR.N1.EQ.2.OR.N1.EQ.4) GO TO 150
        WRITE(6,910)
        GO TO 1000
  150   IF(N2.EQ.1.OR.N2.EQ.2.OR.N2.EQ.4) GO TO 160
        WRITE(6,920)
        GO TO 1000
C*****************************************************************************
C **   COMPUTING NUMBER OF PHI'S AND THETA'S. MAXIMUM ALLOWABLE NUMBER OF EITHER
C **   IS 34.
C*****************************************************************************
  160   NTHETA =(THU-THL)/DELTH +1.0001
        NPHI   =(PHIU-PHIL)/DELPHI + 1.00001
        IF(NTHETA.LE.34.OR.NPHI.LE.34) GO TO 170
        WRITE(6,930) NTHPH
        GO TO 1000
  170   IUP = NPHI
        MUP   =NTHETA
        IF(NTHETA.NE.1) GO TO 180
        IUP   =NTHETA
        THETA= THL*DEGRAD
        MUP   =NPHI
```

```
 180  CONTINUE
C*****************************************************************************
C ** PRINTING OPTION TITLE
C*****************************************************************************
      WRITE(6,940) (TITLE(IOPT,J),J=1,4)
C*****************************************************************************
C ** MAJOR LOOPING WHERE
C **                 IF NTHETA = 1 OUTER LOOP IS THETA, INNER IS PHI
C **                 IF NTHETA NOT = 1 OUTER LOOP IS PHI, INNER THETA
C*****************************************************************************
      DO 500 LOOP1=1,IUP
      IF(NTHETA.NE.1) PHI =(PHIL+(LOOP1-1)*DELPHI)*DEGRAD
      DPHI = PHI*RADDEG
      IF(NTHETA.EQ.1) DTHETA = THETA*RADDEG
      IF(NTHETA.NE.1) WRITE(6,950) DPHI
      IF(NTHETA.EQ.1) WRITE(6,960) DTHETA
      DO 400 LOOP2=1,MUP
      IF(NTHETA.NE.1) THETA=(THL+(LOOP2-1)*DELTH)*DEGRAD
      IF(NTHETA.EQ.1) PHI=(PHIL+(LOOP2-1)*DELPHI)*DEGRAD
      PRINTG(LOOP2) = THETA * RADDEG +.0001
      IF(NTHETA.EQ.1) PRINTG(LOOP2) = PHI* RADDEG +.0001
      GO TO (200,210,220,230,240,250,260),IOPT
 200  C  = AW/BW
      CC = COS(PHI)
      CCC = BW
      CALL OPT123
      GO TO 270
 210  C  = AT/BT
      CC = COS(PHI)
      CCC = BT
      CALL OPT123
      GO TO 270
 220  C  = AV/BV
      CC = SIN(PHI)
      CALL OPT123
      CCC = BV
      GO TO 270
 230  IF(LOOP1.EQ.1.AND.LOOP2.EQ.1) DELF=DELF*DEGRAD
      CALL OPT4(NF)
      GO TO 270
 240  C = AW/BW
      CC = COS(PHI)
      CCC = BW
      CALL OPT5
      GO TO 270
 250  N12 = N1
      NS12 = NS1
      D12 = D1
      L12 = L1
      CALL OPT67(N12,NS12,D12,L12)
      GO TO 270
 260  N12 = N2
      NS12 = NS2
      D12 = D2
      L12 = L2
      CALL OPT67(N12,NS12,D12,L12)
```

```
 270  CONTINUE
 400  CONTINUE
      CALL OUTP(IF,LF,NHALF,MUP,NFBP1,PRINTG,FB,S,1)
 500  CONTINUE
      GO TO 6
 700  FORMAT(I1,13A6)
 800  FORMAT(1H1)
 805  FORMAT(//,2X,13A6)
 810  FORMAT(//' ERROR IN FREQUENCY RANGE INPUT')
 820  FORMAT(//' THL IS OUTSIDE THE BOUNDS (0,180) ' )
 830  FORMAT(//' THU IS OUTSIDE THE BOUNDS (0,180) ' )
 840  FORMAT(//' THL IS GREATER THAN THU ' )
 850  FORMAT(//' PHIL IS OUTSIDE THE BOUNDS (-80,80) ' )
 860  FORMAT(//' PHIU IS OUTSIDE THE BOUNDS (-80,80) ' )
 870  FORMAT(//' PHIL IS GREATER THAN PHIU ' )
 880  FORMAT(//' DELPHI AND/OR DELTH ARE(IS) NEGATIVE OR ZERO ' )
 890  FORMAT(//' UNALLOWABLE NUMBER OF NOSE LANDING GEAR STRUTS ' )
 900  FORMAT(//' UNALLOWABLE NUMBER OF MAIN LANDING GEAR STRUTS ' )
 910  FORMAT(//' UNALLOWABLE NUMBER OF MAIN WHEELS ' )
 920  FORMAT(//' UNALLOWABLE NUMBER OF NOSE WHEELS ' )
 930  FORMAT(//' THE NUMBER OF THETAS OR PHIS EXCEED ',I2)
 940  FORMAT(///,20X,4A6)
 950  FORMAT(//,2X,'AZIMUTH ANGLE, PHI =',F7.0,' DEGREES')
 960  FORMAT(//,2X,'SIDELINE ANGLE, THETA =', F7.0, 'DEGREES' )
 970  FORMAT( ///,20X,'SUMMARY' )
1000  CONTINUE
      GO TO 3000
2000  WRITE(6,970)
      CALL OUTP(1, 40,NHALF,MUP,NFBP1,PRINTG,FB,SUM,2)
3000  CONTINUE
      GO TO 1
4000  CONTINUE
      STOP
      END
```

```
      SUBROUTINE NOYS(ASPL,PN,  II,NANG)
      DIMENSION SUM3(43),ZPMX(43),ASPL(43,25),ZPR(43,25),PNDB(43),
     1 L1(24),L2(24),L3(24),LC(24),L4(24),M1(24),M2(24),M3(24),M4(24)
      REAL L1,L2,L3,LC,L4,M1,M2,M3,M4
      DATA L1 / 49.,44.,39.,34.,30.,27.,24.,21.,18.,5*16.,
     115.,12.,9.,5.,4.,5.,6.,10.,17.,21. /
      DATA L2 / 55.,51.,46.,42.,39.,36.,33.,30.,27.,5*25.,
     123.,21.,18.,15.,2*14.,15.,17.,23.,29. /
      DATA L3 / 64.,60.,56.,53.,51.,48.,46.,44.,42.,5*40.,
     138.,34.,32.,30.,2*29.,30.,31.,37.,41. /
      DATA LC / 91.01,85.88,87.32,79.85,79.76,75.96,73.96,
     174.91,94.63,13*100.,44.29,50.72 /
      DATA L4 / 52.,51.,49.,47.,46.,45.,43.,42.,41.,5*40.,
     138.,34.,32.,30.,2*29.,30.,31.,34.,37. /
      DATA M1 / 0.07952,2*0.06816,0.05964,10*0.053013,
     10.05964,2*0.053013,2*0.047712,2*0.053013,0.068160,0.07952,
     20.0596401 /
      DATA M2 / 2*0.058098,0.052288,0.047534,2*0.043573,
     10.040221,0.037349,7*0.034859,0.040221,0.037349,4*0.034859,
     22*0.037349,0.043573 /
      DATA M3 / 0.043478,0.04057,2*0.036831,0.035336,
     12*0.03333,0.032051,0.030675,6*0.030103,7*0.02996,2*0.042285 /
      DATA M4 / 15*0.030103,9*0.02996 /
      DO 720 J=II,NANG
      SUM3(J)=0.0
      ZPMX(J)=0.0
      DO 710 K2=1,24
      IF (ASPL(J,K2)-L1(K2))600,610,610
  600 ZPR(J,K2)=.1
      GO TO 700
  610 IF(ASPL(J,K2) - L2(K2)) 620,630,630
  620 ZPR(J,K2)=0.1*10.**(M1(K2)*(ASPL(J,K2)-L1(K2)))
      GO TO 700
  630 IF (ASPL(J,K2)-L3(K2))640,650,650
  640 ZPR(J,K2)=10.**(M2(K2)*(ASPL(J,K2)-L3(K2)))
      GO TO 700
  650 IF (ASPL(J,K2)-LC(K2))660,670,670
  660 ZPR(J,K2)=10.**(M3(K2)*(ASPL(J,K2)-L3(K2)))
      GO TO 700
  670 IF (ASPL(J,K2)-150.)690,690,680
  680 ASPL(J,K2)=150.
  690 ZPR(J,K2)=10.**(M4(K2)*(ASPL(J,K2)-L4(K2)))
  700 IF(ZPR(J,K2) .LT. .1) GO TO 710
      IF(ZPR(J,K2) .GT. ZPMX(J)) ZPMX(J)=ZPR(J,K2)
      SUM3(J)=SUM3(J)+ZPR(J,K2)
  710 CONTINUE
  720 CONTINUE
      DO 730 J=II,NANG
      PND=ZPMX(J)+.15*(SUM3(J)-ZPMX(J))
      PNDB(J)=0.0
      IF(PND .GT. .048) PNDB(J)=33.22*ALOG10(PND)+40.
      PN= PNDB(J)
  730 CONTINUE
      RETURN
      END
```

```
      SUBROUTINE OPT123
C *****************************************************************************
C **   THIS SUBROUTINE CALCULATES TRAILING EDGE NOISE FOR WING W,
C **   HORIZONTAL TAIL T, AND VERTICAL TAIL V.
C *****************************************************************************
      REAL M,L1,L2,NUA
      COMMON/AFNIN/ IOPT,CA,FL,FU,PREF,H,V,RHOA,NUA,THL,THU,DELTH,
     1              PHIU,PHIL,DELPHI,BW,AW,BT,AT,BV,AV,N1,D1,L1,N2,D2,
     2              L2,ND,AF,DELF,NS1,NS2,UNITS,CF,LOOP2,C,CC,CCC,NFBP1,
     3              FB(40),S(43,34),SUM(43,34),THETA,PHI,IF,LF,NFBMAX
      II = NFBP1
      M= V/CA
      CR = AW/BW
      XJA = (PREF/(RHOA*CA*CA))**2.
      DL = .37*C *(V*C /NUA)**(-0.2)
      DR = .37*CR*(V*CR/NUA)**(-0.2)
C *****************************************************************************
C **   DL IS BOUNDARY LAYER THICKNESS FOR WING OR TAIL SURFACE. DR IS WING
C **   BOUNDARY LAYER THICKNESS, USED IN APPROXIMATION FOR ATMOSPHERIC
C **   ATTENUATION TO 500 FEET.
C *****************************************************************************
      P = 6.3**ND*4.7165*XJA*10.**(14.18+5.*ALOG10(M))
C *****************************************************************************
C **   P IS NORMALIZED ACOUSTIC POWER, WHERE REFERENCE AREA IS PRODUCT OF SPAN
C **   AND BOUNDARY LAYER THICKNESS.
C *****************************************************************************
      AE = .25
      DE =(COS(THETA*.5)*CC)**2./(AE)
      R = H/(SIN(THETA) * COS(PHI))
      STR       =.10*M*CA/(DL *(1.-M*COS(THETA)))
C *****************************************************************************
C **   STR IS STROUHAL NUMBER AT PEAK 1/3 OCTAVE AMPLITUDE.
C *****************************************************************************
      S(II,LOOP2) =(P/XJA) *(CCC*DL/R**2.) * DE/12.5664
C *****************************************************************************
C **   GENERATES NORMALIZED OVERALL MEAN SQUARE ACOUSTIC PRESSURE.
C *****************************************************************************
      DO 10 I=IF,LF
      ST  = FB(I)/STR
      SR = FB(I) *DP/(.10*V)
      S(I,LOOP2)=S(II,LOOP2)*.613*ST**4.*(.5+ST**1.5)**(-4.)*
     1           EXP(-.007*ABS(SR-1.)**1.5)
C *****************************************************************************
C **   GENERATES NORMALIZED 1/3 OCTAVE MEAN SQUARE ACOUSTIC PRESSURE.
C *****************************************************************************
 10   SUM(I,LOOP2)=S(I,LOOP2) + SUM(I,LOOP2)
      SUM(II,LOOP2)= S(II,LOOP2) + SUM(II,LOOP2)
C *****************************************************************************
C **   THESE ARE SUMS OF NORMALIZED OVERALL AND 1/3 OCTAVE MEAN SQUARE ACOUSTIC
C **   PRESSURE FOR ALL SUBROUTINES USED.
C *****************************************************************************
      RETURN
      END
```

```
      SUBROUTINE OPT4(NF)
C *****************************************************************
C **   THIS SUBROUTINE GENERATES TRAILING EDGE FLAP NOISE AS A FLUCTUATING
C **   LIFT DIPOLE NORMAL TO THE LAST FLAP SEGMENT.
C *****************************************************************
      REAL M,L1,L2,NUA
      COMMON/AFNIN/ IOPT,CA,FL,FU,PREF,H,V,RHOA,NUA,THL,THU,DELTH,
     1              PHIU,PHIL,DELPHI,BW,AW,BT,AT,BV,AV,N1,D1,L1,N2,D2,
     2              L2,ND,AF,DELF,NS1,NS2,UNITS,CF,LOOP2,C,CC,CCC,NFBP1,
     3              FB(40),S(43,34),SUM(43,34),THETA,PHI,IF,LF,NFBMAX
      II = NFBP1
      M= V/CA
      XJA = (PREF/(RHOA*CA*CA))**2.
      PF = XJA*10.**10.9*4.1888*(6.61*M)**6.
C *****************************************************************
C **   PF IS NORMALIZED ACOUSTIC POWER REFERENCED TO FLAP AREA.
C *****************************************************************
      AL = .333
      DF = (SIN(THETA*DELF)*COS(PHI))**2./(AL)
      R = H/(SIN(THETA) * COS(PHI))
      S(II,LOOP2)=(PF/XJA) *(AF/(R*R))*DF/12.5664*SIN(DELF)**2.
C *****************************************************************
C **   GENERATES NORMALIZED OVERALL MEAN SQUARE ACOUSTIC PRESSURE.
C *****************************************************************
      DO 10 I=IF,LF
      SF = FB(I)*CF/(V*(1.-M*COS(THETA)))
      IF(SF.LE.2.) S(I,LOOP2)=S(II,LOOP2) * .05*SF
      IF(SF.GT.2..AND.SF.LE.20.) S(I,LOOP2)=S(II,LOOP2)*.1516*SF**(
     X   -.6)
      IF(SF.GT.20.) S(I,LOOP2) = S(II,LOOP2)* 201.*SF**(-3.)
        IF(NF.NE.3) GO TO 2000
        IF(SF.GT.2..AND.SF.LE.75.) S(I,LOOP2)=S(II,LOOP2)*.115*SF**(-.2)
        IF(SF.GT.75.) S(I,LOOP2)=S(II,LOOP2)*20460.*SF**(-3.)
2000  CONTINUE
C *****************************************************************
C **   GENERATES NORMALIZED 1/3 OCTAVE MEAN SQUARE ACOUSTIC PRESSURE FOR EACH OF
C **   3 REGIMES OF STROUHAL NUMBERS.
C *****************************************************************
   10 SUM(I,LOOP2)=S(I,LOOP2) + SUM(I,LOOP2)
      SUM(II,LOOP2)= S(II,LOOP2) + SUM(II,LOOP2)
      RETURN
      END
```

```
      SUBROUTINE OPTS
C *****************************************************************************
C **   THIS SUBROUTINE CALCULATES LEADING EDGE SLAT NOISE AS A SUM OF INCREASED
C **   WING TRAILING  EDGE NOISE AND A HIGHER-FREQUENCY EDGE NOISE.
C *****************************************************************************
      REAL M,L1,L2,NUA
      COMMON/AFNIN/ IOPT,CA,FL,FU,PREF,H,V,RHOA,NUA,THL,THU,DELTH,
     1              PHIU,PHIL,DELPHI,BW,AW,BT,AT,BV,AV,N1,D1,L1,N2,D2,
     2              L2,ND,AF,DELF,NS1,NS2,UNITS,CF,LOOP2,C,CC,CCC,NFBP1,
     3              FB(40),S(43,34),SUM(43,34),THETA,PHI,IF,LF,NFBMAX
      II = NFBP1
      M= V/CA
      CR = AW/BW
      XJA = (PREF/(RHOA*CA*CA))**2.
      DL = .37*C *(V*C /NUA)**(-0.2)
      DR = .37*CR*(V*CR/NUA)**(-0.2)
      P = 6.3**ND*4.7165*XJA*10.**(14.18+5.*ALOG10(M))
      AE = .25
      DE =(COS(THETA*.5)*CC)**2./(AE)
      R = H/(SIN(THETA) * COS(PHI))
      STR       =.10*M*CA/(DL *(1.-M*COS(THETA)))
      OPRW        =(P/XJA) *(CCC*DL/R**2.) * DE/12.5664
      S(II,LOOP2) = 4. * OPRW
C *****************************************************************************
C **   NORMALIZED OVERALL MEAN SQUARE ACOUSTIC PRESSURE FOR SLAT.
C *****************************************************************************
      DO 10 I=IF,LF
      STL =  FB(I) * DR*(1.-M*COS(THETA))/(.4562*V)
C *****************************************************************************
C **   STROUHAL NUMBER FOR SLAT-RADIATED EDGE NOISE.
C *****************************************************************************
      ST  = FB(I)/STR
      SR = FB(I) *DR/(.10*V)
      PRW=OPRW     *.613*ST**4.*(.5+ST**1.5)**(-4.)*
     1          EXP(-.007*ABS(SR-1.)**1.5)
C *****************************************************************************
C **   GENERATES NORMALIZED 1/3 OCTAVE MEAN SQUARE ACOUSTIC PRESSURE FOR WING.
C *****************************************************************************
      S(I,LOOP2)=2.*PRW+2.*OPRW*.613*STL**4.*(.5+STL**1.5)**(-4.)*
     1          EXP(-.007*ABS(SR-1.)**1.5)
C *****************************************************************************
C **   GENERATES NORMALIZED 1/3 OCTAVE MEAN SQUARE ACOUSTIC PRESSURE FOR SLAT.
C *****************************************************************************
 10   SUM(I,LOOP2)=S(I,LOOP2) + SUM(I,LOOP2)
      SUM(II,LOOP2)= S(II,LOOP2) + SUM(II,LOOP2)
      RETURN
      END
```

```
      SUBROUTINE OPT67(N12,NS12,D12,L12)
C ***************************************************************************
C **   THIS SUBROUTINE CALCULATES LANDING GEAR NOISE FOR 1,2, OR 4 WHEEL GEARS.
C **   INPUT SUBSCRIPT 1 IS CALLED MAIN GEAR, 2 IS CALLED NOSE GEAR.
C ***************************************************************************
      REAL M,L1,L2,NUA,L12
      COMMON/AFNIN/ IOPT,CA,FL,FU,PREF,H,V,RHOA,NUA,THL,THU,DELTH,
     1              PHIU,PHIL,DELPHI,BW,AW,BT,AT,BV,AV,N1,D1,L1,N2,D2,
     2              L2,ND,AF,DELF,NS1,NS2,UNITS,CF,LOOP2,C,CC,CCC,NFBP1,
     3              FB(40),S(43,34),SUM(43,34),THETA,PHI,IF,LF,NFBMAX
      II = NFBP1
      CR = AW/BW
      DR = .37*CR*(V*CR/NUA)**(-.2)
      R = H/(SIN(THETA)*COS(PHI))
      CONST=12.52
      M = V/CA
      XJA = (PREF/(RHOA*CA*CA))**2.
      IF(N12.NE.4) GO TO 10
      CONST=12.42
   10 PCG=XJA*10.**CONST*8.3776*N12*NS12*(3.404*M)**6.
C ***************************************************************************
C **   PCG IS NORMALIZED ACOUSTIC POWER WHICH DOES NOT VARY WITH SIDELINE
C **   ANGLE PHI.
C ***************************************************************************
      AL = .3333
      DG = SIN(THETA)**2./(2.*AL)
      OPRCG= (PCG/XJA)*(D12/R)**2.*DG/12.5664
C ***************************************************************************
C **   OPRCG IS NORMALIZED OVERALL MEAN SQUARE ACOUSTIC PRESSURE WHICH DOES NOT
C **   VARY WITH PHI.
C ***************************************************************************
      PSG = XJA*10.**CONST *8.3776*NS12*.34*L12*(3.404*M)**6.
C ***************************************************************************
C **   PSG IS NORMALIZED ACOUSTIC POWER CAUSED BY FLUCTUATING SIDE FORCE ON
C **   LANDING GEAR STRUT.
C ***************************************************************************
      DS = (SIN(THETA)*SIN(PHI))**2./(AL)
      OPRSG= (PSG/XJA)*(D12/R)**2.*DS/12.5664
C ***************************************************************************
C **   OPRSG IS NORMALIZED OVERALL MEAN SQUARE ACOUSTIC PRESSURE CAUSED BY
C **   FLUCTUATING SIDE FORCE.
C ***************************************************************************
      DO 40 I=IF,LF
      SG = FB(I)*D12/(V*(1.-M*COS(THETA)))
      SR = FB(I)*DR/(.10*V)
      IF(N12.EQ.4) GO TO 20
      PRCG= OPRCG*13.59*SG*SG*(12.5*SG*SG)**(-2.25)
      PRSG= OPRSG*3.244*SG*SG/(30.+SG**8.)
C ***************************************************************************
C **   GENERATES NORMALIZED 1/3 OCTAVE MEAN SQUARE ACOUSTIC PRESSURES FOR BOTH
C **   COMPONENTS OF 1-WHEEL AND 2-WHEEL LANDING GEAR NOISE.
C ***************************************************************************
      GO TO 30
   20 PRCG = OPRCG *.0572*SG*SG*(1.+.25*SG*SG)**(-1.5)
      PRSG = OPRSG * 1.274 * SG**3. *(1.06+SG*SG)**(-3.)
C ***************************************************************************
```

```
C **   GENERATES NORMALIZED 1/3 OCTAVE MEAN SQUARE ACOUSTIC PRESSURES FOR BOTH
C **   COMPONENTS OF 4-WHEEL LANDING GEAR NOISE.
C ***********************************************************************
 30   S(I,LOOP2) = (PRCG+PRSG)*EXP(-.007*ABS(SR-1.)**1.5)
      S(II,LOOP2) = OPRCG +OPRSG
C ***********************************************************************
C **   COMBINES BOTH COMPONENTS OF LANDING GEAR NOISE.
C ***********************************************************************
 40   SUM(I,LOOP2) = SUM(I,LOOP2) + S(I,LOOP2)
      SUM(II,LOOP2) = SUM(II,LOOP2) + S(II,LOOP2)
      RETURN
      END
```

```
      SUBROUTINE OUTP(IF,LF,NHALF,MUP,NFBP1,PRINTG,FB,S,ISUM)
      DIMENSION PRINTG(1),FB(1),S(43,1),SPL(24),ASPL(43,25)
      IF(ISUM.EQ.1) GO TO 7
      DO 5 I = 1,MUP
      DBA1=   .0002 * (   S(14,I) + S(15,I) + S(16,I))
     1      +.00347 * (   S(17,I) + S(18,I) + S(19,I))
     2      + .0309 * (   S(20,I) + S(21,I) + S(22,I))
     3      + .1585 * (   S(23,I) + S(24,I) + S(25,I))
     4      + .5130 * (   S(26,I) + S(27,I) + S(28,I))
     5      + 1.000 * (   S(29,I) + S(30,I) + S(31,I))
     6      + 1.318 * (   S(32,I) + S(33,I) + S(34,I))
     7      + 1.230 * (   S(35,I) + S(36,I) + S(37,I))
     8      + .7244 * (   S(38,I) + S(39,I) + S(40,I))
  5   S(NFBP1+1,I)=10.*ALOG10(DBA1)
C ***********************************************************************
C **   THIS PROCESS CALCULATES A-WEIGHTED SOUND LEVEL, DB(A).
C ***********************************************************************
  7   CONTINUE
      DO 20 I=IF,LF
      DO 10 L = 1,MUP
      ARG = S(I,L)
      IF(ARG.EQ.0.) ARG = 1.
      S(I,L) = 10.*ALOG10(ARG)
 10   CONTINUE
 20   CONTINUE
      IF(ISUM.EQ.1) GO TO 29
      DO 28 K=1,MUP
      I=0
      DO 25 J=17,40
      I=I+1
 25   ASPL(K,I)=S(J,K)
      CALL NOYS(ASPL,PN,K,K)
 28   S(NFBP1+2,K) = PN
 29   CONTINUE
      DO 30 L = 1,MUP
      ARG = S(NFBP1,L)
      IF(ARG.EQ.0.) ARG = 1.
      S(NFBP1,L) = 10.*ALOG10(ARG)
```

```
   30   CONTINUE
        WRITE(6,800)
        IPG = 0
   40   IT = 1+ IPG*NHALF
        LT = MIN0(MUP,IT +NHALF -1)
        WRITE(6,810) ( PRINTG(I),I=IT,LT)
        DO 50 I = IF,LF
        WRITE(6,820) FB(I), (S(I,J),J=IT,LT)
   50   CONTINUE
        WRITE(6,830)  (S(NFBP1,J),J=IT,LT)
        IF(ISUM.EQ.2)  WRITE(6,840)(S(NFBP1+1,J),J=IT,LT)
        IF(ISUM.EQ.2)  WRITE(6,850)(S(NFBP1+2,J),J=IT,LT)
        IPG = IPG +1
        IF(LT-MUP) 40,60,60
   60   RETURN
  800 FORMAT(///' TABLE OF VALUES OF SOUND PRESSURE LEVEL (DECIBELS) FOR
     1   ',/, 15X,'CONSTANT ALTITUDE FLIGHT.')
  810 FORMAT(//  ' 1/3 OB    DIRECTIVITY ANGLE (DEGREES)',/,' CTR FREQ:',
     1   /,' (HERTZ)  ',17F7.0,///)
  820 FORMAT(2X,F9.2,17F7.2)
  830 FORMAT(4X, 'OVERALL',17F7.2)
  840 FORMAT(/4X,'  DB(A)',17F7.2)
  850 FORMAT(4X,' PNL,DB',17F7.2)
      END
```

10.4 Sample Program Output

Program output for the sample input given in the preceding section is shown here. The output table for each of the three airframe noise components is preceded by a table of all the NAMELIST variables and their numerical values, not reproduced here.

JETSTAR,FLAPS DOWN,RUN7A

CLEAN WING NOISE

AZIMUTH ANGLE, PHI = 0. DEGREES

TABLE OF VALUES OF SOUND PRESSURE LEVEL (DECIBELS) FOR CONSTANT ALTITUDE FLIGHT

1/3 OB CTR FREQ: (HERTZ)	DIRECTIVITY ANGLE (DEGREES) 30.	40.	50.	60.	70.	80.	90.
50.00	39.78	42.18	43.92	45.17	46.00	46.43	46.45
63.00	42.88	45.24	46.93	48.13	48.90	49.26	49.22
80.00	45.77	48.07	49.70	50.83	51.52	51.81	51.68
100.00	48.10	50.35	51.92	52.97	53.57	53.77	53.56
125.00	50.03	52.22	53.71	54.67	55.18	55.28	54.97
160.00	51.64	53.75	55.14	56.00	56.41	56.40	55.98
200.00	52.58	54.62	55.93	56.70	57.01	56.90	56.38
250.00	53.04	55.01	56.24	56.92	57.14	56.94	56.33
315.00	53.03	54.94	56.10	56.69	56.83	56.54	55.85
400.00	52.56	54.41	55.50	56.03	56.09	55.73	54.97
500.00	51.76	53.57	54.61	55.08	55.08	54.67	53.86
630.00	50.63	52.40	53.39	53.82	53.77	53.32	52.47
800.00	49.19	50.93	51.89	52.28	52.20	51.71	50.83
1000.00	47.65	49.36	50.30	50.67	50.57	50.05	49.15
1250.00	45.95	47.65	48.57	48.92	48.79	48.26	47.35
1600.00	43.90	45.59	46.50	46.83	46.70	46.15	45.22
2000.00	41.92	43.60	44.49	44.82	44.67	44.12	43.18
2500.00	39.79	41.46	42.35	42.67	42.51	41.95	41.01
3150.00	37.40	39.07	39.96	40.27	40.11	39.54	38.60
4000.00	34.70	36.36	37.25	37.55	37.39	36.82	35.87
5000.00	31.88	33.54	34.42	34.73	34.56	33.99	33.04
6300.00	28.55	30.21	31.09	31.39	31.22	30.65	29.69
8000.00	24.49	26.15	27.03	27.33	27.16	26.59	25.63
10000.00	19.91	21.57	22.45	22.75	22.58	22.00	21.05
OVERALL	62.27	64.21	65.42	66.09	66.32	66.14	65.58

JETSTAR,FLAPS DOWN,RUN7A

HORIZONTAL TAIL NOISE

AZIMUTH ANGLE, PHI = 0. DEGREES

TABLE OF VALUES OF SOUND PRESSURE LEVEL (DECIBELS) FOR CONSTANT ALTITUDE FLIGHT

1/3 OB CTR FREQ: (HERTZ)	DIRECTIVITY ANGLE (DEGREES) 30.	40.	50.	60.	70.	80.	90.
50.00	28.50	30.95	32.75	34.07	34.99	35.50	35.60
63.00	31.99	34.41	36.18	37.47	38.34	38.81	38.88
80.00	35.39	37.78	39.51	40.75	41.57	41.98	41.99
100.00	38.32	40.67	42.35	43.54	44.30	44.65	44.59
125.00	40.96	43.26	44.89	46.00	46.69	46.96	46.82
160.00	43.47	45.70	47.25	48.28	48.86	49.04	48.80
200.00	45.29	47.46	48.92	49.86	50.36	50.43	50.09
250.00	46.64	48.74	50.12	50.97	51.36	51.34	50.90
315.00	47.53	49.56	50.85	51.60	51.69	51.77	51.23
400.00	47.90	49.86	51.07	51.73	51.92	51.70	51.07
500.00	47.78	49.67	50.82	51.40	51.51	51.21	50.51
630.00	47.23	49.07	50.15	50.66	50.71	50.34	49.58
800.00	46.27	48.07	49.10	49.55	49.54	49.12	48.31
1000.00	45.08	46.84	47.83	48.25	48.20	47.73	46.88
1250.00	43.65	45.38	46.34	46.72	46.64	46.15	45.27
1600.00	41.82	43.53	44.47	44.83	44.72	44.20	43.30
2000.00	39.98	41.67	42.59	42.93	42.81	42.27	41.36
2500.00	37.95	39.64	40.54	40.87	40.74	40.19	39.26
3150.00	35.65	37.33	38.22	38.54	38.39	37.84	36.90
4000.00	33.00	34.67	35.56	35.88	35.72	35.16	34.22
5000.00	30.22	31.89	32.77	33.08	32.92	32.36	31.41
6300.00	26.91	28.58	29.46	29.77	29.61	29.04	28.09
8000.00	22.88	24.54	25.42	25.73	25.56	24.99	24.04
10000.00	18.32	19.98	20.86	21.16	20.99	20.42	19.46
OVERALL	57.11	59.05	60.26	60.93	61.16	60.98	60.42

JETSTAR,FLAPS DOWN,RUN7A

TRAILING EDGE FLAP NOISE

AZIMUTH ANGLE, PHI = 0. DEGREES

TABLE OF VALUES OF SOUND PRESSURE LEVEL (DECIBELS) FOR CONSTANT ALTITUDE FLIGHT

1/3 OB CTR FREQ: (HERTZ)	DIRECTIVITY ANGLE (DEGREES) 30.	40.	50.	60.	70.	80.	90.
50.00	62.42	64.59	65.82	66.29	66.09	65.23	63.64
63.00	63.42	65.60	66.82	67.29	67.09	66.23	64.64
80.00	64.46	66.63	67.86	68.33	68.13	67.27	65.68
100.00	65.43	67.63	68.83	69.30	69.10	68.24	66.65
125.00	66.40	68.57	69.80	70.27	70.07	69.21	67.62
160.00	67.47	69.64	70.87	71.34	71.14	70.28	68.69
200.00	68.29	70.61	71.84	72.31	72.11	71.25	69.66
250.00	67.71	70.11	71.60	72.37	72.49	71.95	70.63
315.00	67.11	69.51	71.00	71.77	71.89	71.35	70.08
400.00	66.49	68.89	70.38	71.15	71.27	70.73	69.46
500.00	65.90	68.30	69.80	70.57	70.69	70.15	68.88
630.00	65.30	67.70	69.19	69.96	70.08	69.55	68.27
800.00	64.68	67.08	68.57	69.34	69.46	68.92	67.65
1000.00	64.10	66.50	67.99	68.76	68.88	68.34	67.07
1250.00	63.52	65.92	67.41	68.18	68.30	67.76	66.49
1600.00	62.87	65.27	66.77	67.54	67.65	67.12	65.85
2000.00	62.07	64.69	66.18	66.95	67.07	66.54	65.26
2500.00	59.16	61.90	63.80	65.02	65.61	65.56	64.68
3150.00	56.15	58.89	60.79	62.00	62.60	62.54	61.75
4000.00	53.04	55.78	57.67	58.89	59.49	59.43	58.64
5000.00	50.13	52.87	54.77	55.98	56.58	56.52	55.73
6300.00	47.12	49.86	51.75	52.97	53.57	53.51	52.72
8000.00	44.01	46.75	48.64	49.86	50.45	50.40	49.61
10000.00	41.10	43.84	45.73	46.95	47.55	47.49	46.70
OVERALL	78.35	80.66	82.05	82.71	82.71	82.05	80.66

SUMMARY

TABLE OF VALUES OF SOUND PRESSURE LEVEL (DECIBELS) FOR CONSTANT ALTITUDE FLIGHT

1/3 OB CTR FREQ: (HERTZ)	DIRECTIVITY ANGLE (DEGREES) 30.	40.	50.	60.	70.	80.	90.
1.25	.00	.00	.00	.00	.00	.00	.00
1.60	.00	.00	.00	.00	.00	.00	.00
2.00	.00	.00	.00	.00	.00	.00	.00
2.50	.00	.00	.00	.00	.00	.00	.00
3.15	.00	.00	.00	.00	.00	.00	.00
4.00	.00	.00	.00	.00	.00	.00	.00
5.00	.00	.00	.00	.00	.00	.00	.00
6.30	.00	.00	.00	.00	.00	.00	.00
8.00	.00	.00	.00	.00	.00	.00	.00
10.00	.00	.00	.00	.00	.00	.00	.00
12.50	.00	.00	.00	.00	.00	.00	.00
16.00	.00	.00	.00	.00	.00	.00	.00
20.00	.00	.00	.00	.00	.00	.00	.00
25.00	.00	.00	.00	.00	.00	.00	.00
31.50	.00	.00	.00	.00	.00	.00	.00
40.00	.00	.00	.00	.00	.00	.00	.00
50.00	62.45	64.62	65.85	66.32	66.13	65.29	63.73
63.00	63.46	65.64	66.87	67.35	67.16	66.33	64.78
80.00	64.52	66.70	67.93	68.41	68.23	67.41	65.87
100.00	65.52	67.69	68.92	69.41	69.23	68.41	66.88
125.00	66.51	68.68	69.91	70.40	70.23	69.41	67.88
160.00	67.60	69.77	71.00	71.48	71.31	70.49	68.96
200.00	68.43	70.74	71.97	72.45	72.27	71.44	69.91
250.00	67.89	70.27	71.76	72.53	72.65	72.13	70.83
315.00	67.32	69.70	71.18	71.94	72.06	71.54	70.30
400.00	66.72	69.09	70.57	71.33	71.45	70.92	69.67
500.00	66.13	68.51	69.98	70.74	70.85	70.32	69.07
630.00	65.51	67.89	69.36	70.12	70.23	69.70	68.44
800.00	64.86	67.24	68.71	69.47	69.58	69.05	67.79
1000.00	64.25	66.63	68.10	68.86	68.98	68.44	67.18
1250.00	63.64	66.02	67.50	68.26	68.38	67.84	66.57
1600.00	62.96	65.35	66.83	67.60	67.71	67.17	65.91
2000.00	62.14	64.75	66.23	67.00	67.11	66.58	65.31
2500.00	59.24	61.97	63.85	65.06	65.64	65.59	64.71
3150.00	56.25	58.96	60.84	62.05	62.64	62.58	61.78
4000.00	53.14	55.86	57.74	58.94	59.53	59.47	58.67
5000.00	50.24	52.95	54.83	56.04	56.62	56.56	55.77
6300.00	47.22	49.94	51.82	53.02	53.61	53.55	52.75
8000.00	44.09	46.81	48.69	49.90	50.49	50.43	49.63
10000.00	41.16	43.88	45.77	46.98	47.57	47.51	46.72
OVERALL	78.48	80.79	82.17	82.83	82.64	82.20	80.83
OB(A)	73.91	76.33	77.83	78.62	78.78	78.29	77.08
PNL,DB	85.67	88.23	89.79	90.63	90.94	90.59	89.47

11.0 APPENDIX III: TABULATED AIRFRAME FLYOVER NOISE SPECTRA

Flyover noise one-third octave spectra, at the measurement time that produced maximum OASPL, were plotted in Refs. 11, 17, and 26 for tests conducted at NASA Dryden Flight Research Center. The aircraft tested were the Aero Commander Shrike, Lockheed JetStar, Convair 990, and Boeing 747. Values of OASPL, flight speed (m/sec), and mass (Newtons) were given in Table 2 of Ref. 22 for ten flights of the Lockheed JetStar, four flights of the Convair 990, and five flights of the Boeing 747. The aircraft configurations comprise the clean aircraft, trailing edge flaps extended to one deflection for each aircraft, landing gear extended and flaps retracted (for the Lockheed JetStar and Boeing 747), and both the landing gear and flaps extended. Spectra were supplied for the Aero Commander Shrike at two airspeeds with landing gear extended and flaps retracted, and at one airspeed with landing gear and trailing edge flaps extended.

These data were measured using a microphone installed flush with a large ground board. The resulting one-third octave band sound pressure levels (SPL) should be regarded as 6 dB above free field because of in-phase reflection of acoustic waves at the microphone. In contrast, noise certification measurements generally are obtained with microphones mounted 4 ft above a hard surface. The resulting measured sum of directly radiated and randomly-phased reflected acoustic waves is 3 dB above free field at greater than several hundred Hz center frequencies.

Measured flyover noise spectra were corrected by NASA for differences between measured and 500 ft flight altitude. Two adjustments were applied. Amplitude at all frequencies was adjusted for the altitude difference by use of an inverse squared variation with altitude. The spectra were further corrected for the atmospheric attenuation over a path length equal to the difference between 500 ft and the actual altitude. This frequency-dependent correction was calculated for the attenuation properties of standard-atmosphere temperature and humidity. Therefore the tabulated spectra correspond to the direction for peak OASPL of a flyover at 500 ft altitude. They include the effects of atmospheric attenuation between that altitude and the ground. Both OASPL and preceived noise level (PNL) of the resulting adjusted spectra were generally calculated by NASA. These spectra and integrated levels for the four aircraft types are listed in Tables 3 through 6 herein. Velocity (knots) and gross weight (lb) were taken from NASA-supplied data sheets for most runs. For other runs, they were calculated from Table 2 of Ref. 22 which provides flight information in metric-system units.

Spectra for the Vickers VC 10 in the clean configuration and with several individual components deflected were obtained by the Royal Aircraft Establishment (RAE) and reported in Ref. 12. These flyover peak-OASPL spectra also were measured with a flush-mounted microphone and are 6 dB above free field. All of the eight spectra supplied by RAE were obtained at 160 knots nominal airspeed and 600 ft nominal altitude. These spectra, which include whatever atmospheric attenuation was present, are given in Table 7. Values of OASPL for these spectra were given in Ref. 12 only for the frequency range from 40 to 1600 Hz because engine tone noise dominated the spectra at higher frequencies. Those values are not tabulated herein.

Airframe noise spectra were measured by Lockheed-California Co. for the Douglas DC-3, Convair 240, Aero Commander Shrike, Prue-2, and Cessna 150. These measurements used microphones mounted on tripods 4 ft above the ground. Tabulated spectra are readily available from Table A-1 of Ref. 9 and are not repeated herein.

These spectra are being published to facilitate the evaluation of other methods for predicting airframe noise. Geometric properties are given in Table 8 for the five airframes for which spectra are listed in Tables 3 through 7.

TABLE 3

AERO COMMANDER SHRIKE, 500 FT ALTITUDE

1/3 Octave freq., Hz	Run 4, gear down, flaps down, 113 kt, 6566 lb, SPL, dB	Run 6, gear down, flaps up, 112 kt, 6475 lb, SPL, dB	Run 7, gear down, flaps up, 153 kt, 6440 lb, SPL, dB
50	63	66	68.9
63	62	66.5	70.4
80	61	65.5	69.9
100	60	65.5	69.4
125	59.5	63.5	69.4
160	59	61	66.4
200	59.5	60.5	66.9
250	59.5	58.5	64.9
315	59.5	58	66.4
400	60	58	65.4
500	60.5	57.5	65.8
630	61	58.5	66.7
800	61	59	66.6
1000	59.5	58	65.5
1250	57.5	56	64.9
1600	54	52.5	60.7
2000	53.5	51.5	60.4
2500	50	48.5	58.0
3150	46	43.5	53.1
4000	46.5	40.5	48.1
5000	-	34	44.4
6300	-	-	39.4
8000	-	-	34.3
10000	-	-	-
OASPL	72.3	74.1	79.5

TABLE 4

LOCKHEED JETSTAR , 500 FT ALTTTUDE

1/3 Octave freq., Hz	Run 2, clean, 247 kt, 36,186 lb	Run 3, clean, 297 kt, 35,586 lb	Run 4, clean, 342 kt, 34,986 lb	Run 4a, clean, 350 kt, 33,986 lb	Run 5, clean, 358 kt, 33,336 lb
50	58.0	61.1	63.8	65.0	63.8
63	65.3	64.1	66.5	65.8	63.4
80	66.9	69.3	72.0	69.9	71.1
100	69.2	70.9	73.2	71.9	72.7
125	70.6	71.7	74.3	72.9	73.5
160	68.5	71.5	75.5	75.2	74.3
200	69.5	72.3	77.9	75.2	75.4
250	71.8	73.5	77.8	78.7	76.1
315	72.3	74.6	78.7	77.2	77.2
400	70.6	72.8	77.2	75.3	76.3
500	69.7	71.8	76.4	74.9	76.1
630	72.1	74.6	78.2	78.3	79.0
800	73.0	76.2	78.6	79.1	80.2
1000	75.0	78.2	80.7	81.1	82.3
1250	75.3	78.8	80.9	82.3	82.9
1600	75.6	77.7	80.5	82.1	82.6
2000	74.3	75.2	78.3	79.5	79.8
2500	71.9	74.0	76.7	78.1	79.5
3150	65.6	70.7	73.0	74.7	75.5
4000	61.4	66.6	69.4	71.3	72.9
5000	58.9	62.4	65.7	67.7	69.3
6300	55.1	58.4	61.0	62.9	65.6
8000	52.3	54.3	56.7	58.5	60.9
10000	58.5	64.6	61.8	63.3	61.3
OASPL	84.5	87.1	90.2	90.4	91.0
PNL	95.0	97.5	100.4	101.2	101.8

TABLE 4 (Concluded)

LOCKHEED JETSTAR , 500 FT ALTITUDE

1/3 Octave freq., Hz	Run 7A, flaps 50°, gear up, 170 kt, 31,539, lb	Run 8, flaps up, gear down, 194 kt, 31,011 lb	Run 9, flaps up, gear down, 182 kt, 30,386 lb	Run 10, flaps 50°, gear down, 158 kt, 29,686 lb	Run 11, flaps up, gear down, 204 kt, 29,486 lb
50	71.6	68.8	65.7	70.8	66.1
63	72.6	69.7	68.5	72.5	67.8
80	75.0	72.6	71.5	72.3	70.7
100	76.4	74.4	74.1	75.0	72.8
125	76.4	73.8	75.9	74.6	73.5
160	73.5	75.9	77.1	73.0	75.4
200	73.6	73.7	77.7	74.7	76.3
250	74.9	75.0	77.8	74.6	76.1
315	75.0	75.5	76.6	75.3	75.7
400	71.7	74.4	75.0	73.0	74.7
500	71.6	72.2	75.2	72.0	72.5
630	75.6	75.7	77.5	72.0	76.1
800	75.3	76.5	78.0	75.0	77.4
1000	76.1	78.4	80.6	77.8	79.1
1250	76.9	77.8	80.5	76.2	78.8
1600	76.6	78.4	80.1	76.2	78.7
2000	73.7	76.2	77.0	73.4	77.4
2500	68.7	70.6	73.7	68.7	71.6
3150	64.8	65.6	69.3	64.1	66.3
4000	61.5	62.7	65.8	61.4	63.0
5000	58.8	60.3	61.6	58.2	60.3
6300	54.2	55.7	57.7	55.3	56.6
8000	-	-	-	51.4	49.2
10000	-	-	-	64.4	74.4
OASPL	87.3	87.3	89.6	86.5	88.4
PNL	96.3	97.4	96.3	96.3	98.4

TABLE 5

CONVAIR 990, 500 FT ALTITUDE

1/3 Octave freq, Hz	Run 3, Clean, 312 kt 182,000 lb	Run 17, Clean, 187 kt, 157,000 lb	Run 11, Flaps 36°, gear up, 189 kt, 166,000 lb	Run 10, Flaps 36°, gear down, 160 kt, 168,600 lb
50	68.5	68.1	77.7	76.1
63	69.1	66.5	77.6	76.9
80	74.1	70.3	79.7	79.3
100	77.2	74.7	82.2	81.0
125	80.1	74.0	82.7	81.7
160	80.0	73.9	82.2	81.2
200	79.4	71.5	81.8	80.2
250	79.3	71.6	80.7	80.9
315	79.4	71.3	81.5	80.9
400	78.2	72.3	83.3	82.9
500	79.2	73.0	84.4	82.4
630	79.4	74.4	84.6	81.6
800	80.2	74.0	82.5	79.9
1000	80.5	73.7	81.3	79.3
1250	81.3	77.6	80.4	79.0
1600	82.6	75.7	80.7	77.8
2000	82.6	73.1	77.7	76.1
2500	81.8	72.9	75.1	73.6
3150	81.1	69.2	72.0	70.0
4000	79.8	67.0	68.6	67.8
5000	79.6	63.5	65.2	64.0
6300	77.3	60.4	61.0	60.6
8000	75.2	56.3	58.2	58.5
10000	73.1	51.3	60.3	61.3
OASPL	93.9	86.1	94.1	92.7
PNL	106.5	96.5	102.2	100.4

TABLE 6

BOEING 747, 500 FT ALTITUDE

1/3 Octave freq, Hz	Run 2 Flaps 25°, gear down, 197 kt 512,000 lb	Run 3, Flaps 25°, gear up, 198 kt, 507,000 lb	Run 4, clean, 264 kt, 502,000 lb	Run 5, clean, 233 kt, 501,000 lb	Run 6, Flaps up, gear down, 215 kt, 497,000 lb
50	85.5	81.4	75.1	77.1	81.3
63	85.4	85.1	77.0	75.3	82.2
80	88.1	88.0	81.1	79.0	83.0
100	90.5	90.6	80.5	77.8	84.4
125	88.2	88.0	80.7	78.2	85.8
160	88.1	87.1	80.3	83.3	88.1
200	88.8	86.9	79.4	85.2	88.9
250	88.8	87.2	79.0	78.5	87.8
315	89.8	87.2	79.9	79.2	88.7
400	89.1	87.3	80.3	77.9	87.7
500	89.4	87.6	81.9	78.1	88.3
630	89.8	87.2	83.8	79.0	89.9
800	90.5	86.9	83.6	83.6	90.9
1000	90.4	87.1	85.5	83.8	90.5
1250	89.5	86.0	86.5	80.8	90.0
1600	88.6	87.0	82.7	80.9	89.8
2000	88.8	86.6	84.1	81.8	88.8
2500	88.4	86.4	84.1	80.2	88.1
3150	85.8	84.1	81.5	78.7	85.7
4000	83.7	82.0	80.4	77.3	84.2
5000	80.8	79.6	78.2	76.6	81.2
6300	77.2	76.5	74.0	73.0	75.9
8000	71.4	71.3	-	67.4	69.2
10000	-	59.1	-	63.6	59.8
OASPL	101.8	100.0	95.3	93.7	101.3
PNL	112.4	110.4	107.2	104.5	111.9

TABLE 7

VICKERS VC 10 FLYOVER SPECTRA
160 knots airspeed, 600 ft altitude, 195,000 lb

1/3 Octave Freq. Hz	Clean SPL, dB	Dirty SPL, dB	Gear Down, Doors Shut	Gear Down, Doors Open
40	70.0	84.5	74.5	84.0
50	71.5	83.0	75.0	82.0
63	70.0	83.0	74.5	80.5
80	71.0	82.0	75.0	81.0
100	74.5	83.0	77.0	82.0
125	72.5	83.5	77.0	83.5
160	72.5	83.0	77.5	83.0
200	73.5	83.5	80.0	82.0
250	74.0	84.0	81.5	82.5
315	73.5	82.0	80.0	81.0
400	74.0	81.0	77.5	79.0
500	74.5	80.0	76.5	78.5
630	73.5	81.0	77.0	79.0
800	74.0	81.5	77.0	79.5
1000	74.5	79.5	76.5	80.0
1250	74.0	78.5	76.0	78.0
1600	73.0	78.0	74.5	76.5
2000	74.0	79.0	75.5	79.5
2500	82.5	83.0	83.0	83.5
3150	75.0	81.5	77.0	78.0
4000	70.0	76.5	72.5	73.5
5000	68.5	73.0	70.5	72.5
6300	68.0	72.0	70.0	72.5
8000	67.0	69.5	68.5	70.5
10000	66.5	68.5	67.0	68.0

TABLE 7 (Concluded)

VICKERS VC 10 FLYOVER SPECTRA
160 knots airspeed, 600 ft altitude, 195,000 lb

1/3 Octave Freq. Hz	Slats Out SPL, dB	Flaps Extended, Angle = 20°, dB	35°, dB	45°, dB
40	73.0	72.5	79.3	84.6
50	74.5	74.0	80.0	83.1
63	73.5	74.6	80.3	82.1
80	75.5	75.5	80.6	81.8
100	76.0	77.7	80.5	82.0
125	77.0	77.3	80.3	81.0
160	77.5	77.8	79.6	80.8
200	78.5	77.0	79.6	81.0
250	79.5	77.4	79.2	81.0
315	78.0	76.1	77.8	80.3
400	77.5	76.3	77.7	80.0
500	78.0	76.3	77.2	79.0
630	77.5	76.0	78.3	79.6
800	77.5	77.4	77.4	80.3
1000	78.5	76.1	76.5	78.
1250	76.5	76.1	76.5	76.5
1600	74.5	74.1	75.7	76.4
2000	76.0	75.5	75.0	78.6
2500	83.5	83.5	81.7	83.5
3150	77.5	77.3	78.5	80.2
4000	72.5	72.5	73.1	75.0
5000	71.5	70.7	70.7	73.8
6300	71.5	69.0	69.3	71.7
8000	70.5	67.7	68.2	69.8
10000	70.0	66.8	67.2	68.4

TABLE 8

AIRFRAME GEOMETRIC PROPERTIES

Airframe Property	Aero Commander Shrike	Lockheed JetStar	Convair 990	Boeing 747	Vickers VC 10
Wing area, ft^2	255.	542.5	987.	5500.	2932.
Wing span, ft	49.0	53.67	95.	195.7	146.2
Horizontal tail area, ft^2	33.1	149.	185.	1470.	508.
Horizontal tail span, ft	16.75	24.75	25.67	72.75	43.83
Flap area, ft^2	21.2	62.6	337.5	847.	508.
Flap chord, ft	1.3	2.28	4.7	7.5	6.44
Flap angle, deg	22.	50.	36.	25.	20,35,45
Main gear/aircraft	2	2	2	4	2
Wheels/main gear	1	2	2	4	4
Main wheel diameter, ft	2.22	2.17	3.25	3.83	4.17
Wheels/nose gear	1	2	2	2	2
Nose wheel diameter, ft	1.46	1.5	2.42	3.83	3.25